

Modelling Gravitational Waveforms and Electromagnetic Signals from Neutron Star Binary Mergers

Kyohei Kawaguchi

ICRR, The University of Tokyo

Collaborator: Kenta Kiuchi, Koutarou Kyutoku, Tatsuya Narikawa,
Yuichiro Sekiguchi, Masaru Shibata, Hideyuki Tagoshi,
Masaomi Tanaka, Keisuke Taniguchi, Nami Uchikata

2018.7.27 @ ICRR seminar

My Introduction

- Kyohei Kawaguchi (川口 恭平)
- Institute for Cosmic Ray Research (ICRR),
Gravitational waves / High energy astrophysics group
- YITP (Kyoto Uni.) → AEI (MPI, Postdam) → ICRR
- Compact binary merger (NS binary merger),
numerical-relativity simulation,
gravitational waves, electromagnetic counterparts

Today's talk

- Introduction
- Gravitational waves from binary neutron stars
- Electromagnetic counterparts to binary neutron stars:
Kilonovae/Macronovae
- Future works

Introduction

Gravitational waves

- Gravitational waves (GW): the ripples of curvature that propagate with the speed of light
- GW sources for ground-based GW detectors
 - Compact binary mergers
 - Core collapse Super Novae
 - Rotating Neutron stars
 - Primordial GW (Inflation)
 - Cosmic Strings

Compact Binary: Binary composed of black-holes (BHs) and/or neutron stars (NSs)

advanced LIGO



advanced Virgo

<http://www.virgo-gw.eu/>

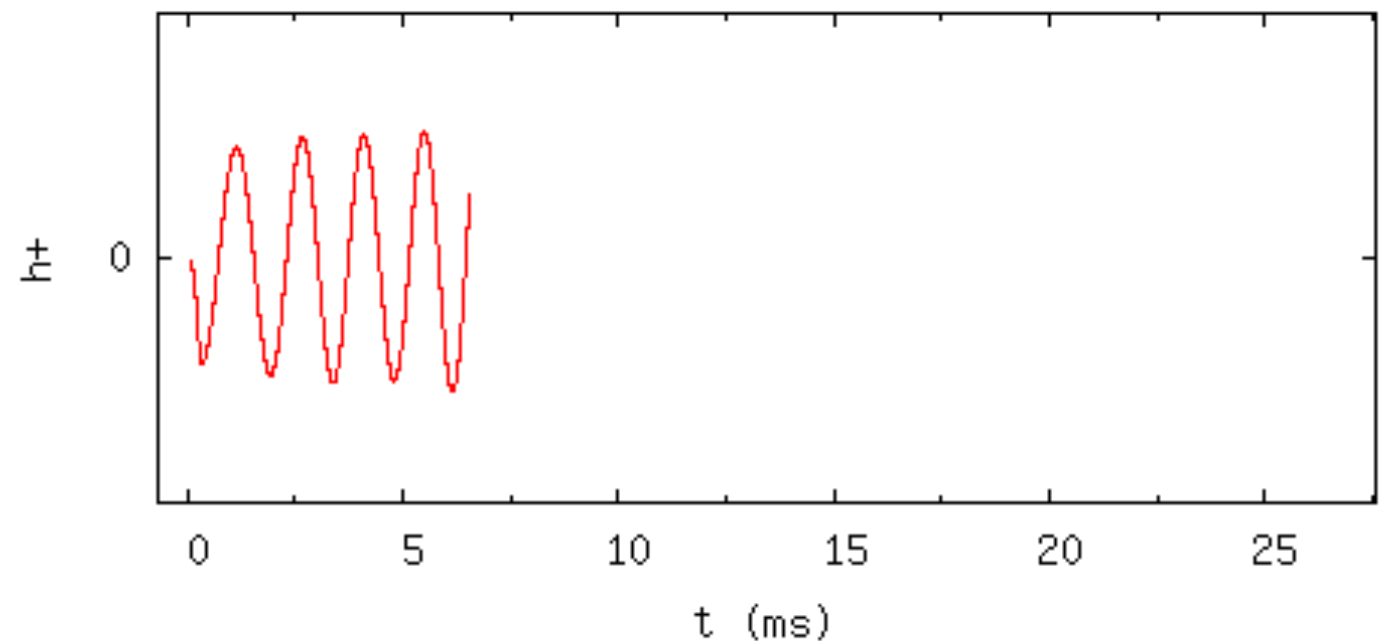
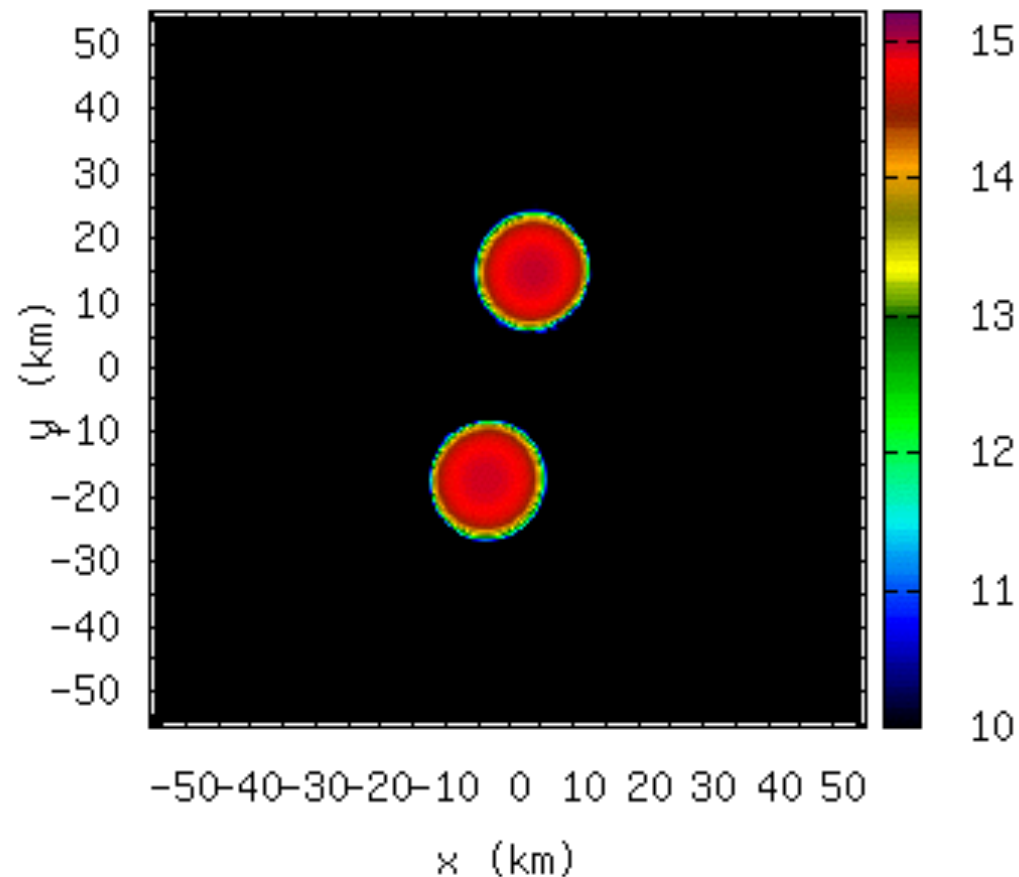
<http://gwcenter.icrr.u-tokyo.ac.jp/>



Compact binary mergers

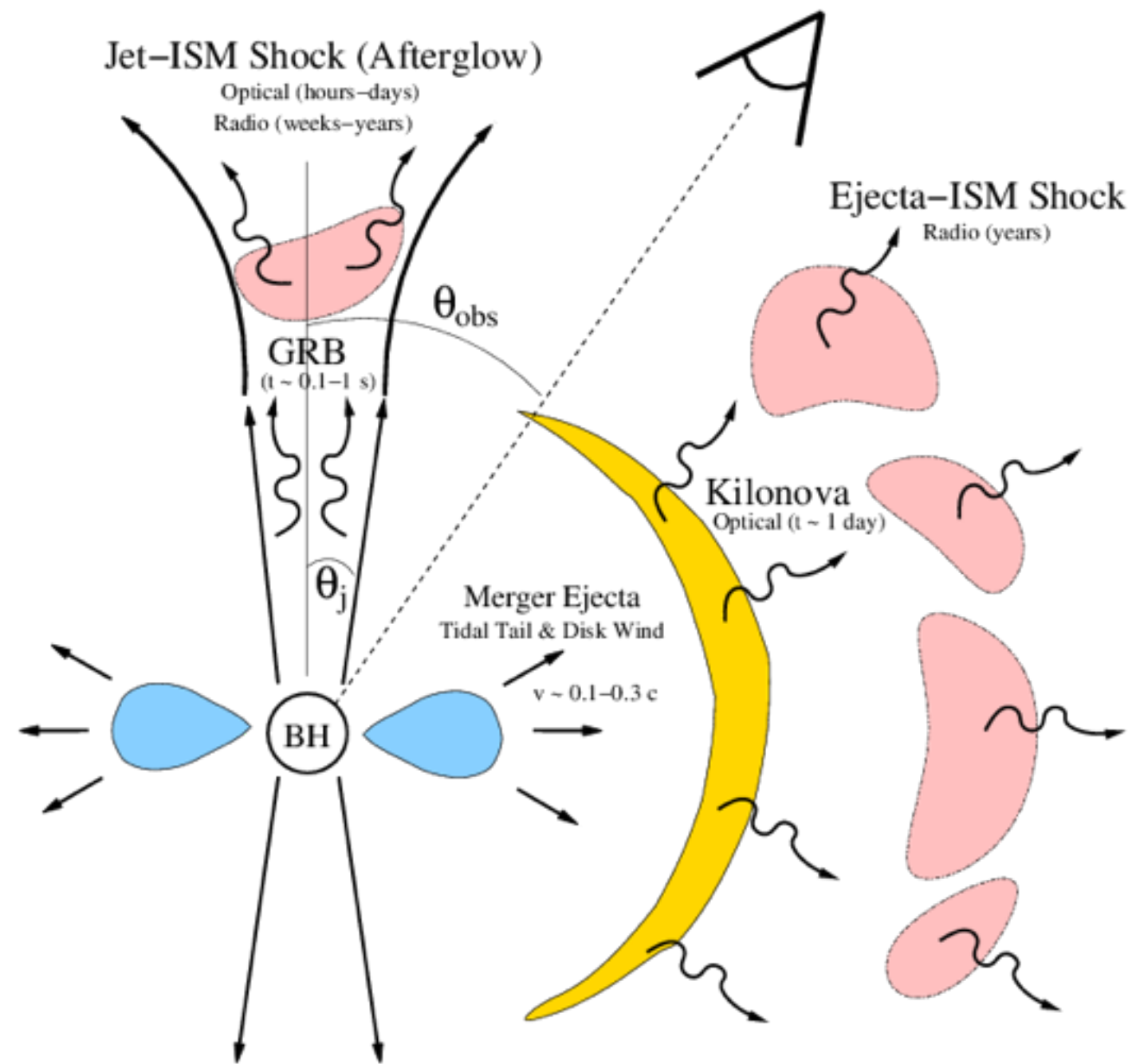
- Compact Binary—Binary composed of black-holes (BHs) and/or neutron stars (NSs)— efficiently emit gravitational waves shrinking their orbital separation, and the objects gradually merge
- Observation of gravitational waves provides us to the physical information of the binary (masses, spins, inclination...)

$t=6.2523$ ms



Electromagnetic Counterparts to NS binary mergers

- Various transient EM counterparts are proposed for NS binary mergers
- for example,
 - short-hard gamma-ray-burst
 - Afterglow
 - cocoon emission
 - kilonovae/macronovae
 - radio flare, etc.
- Host galaxy identification, remnant properties, environment
- Possible synthesis site of r-process nuclei



Ref: B. Metzger and E. Berger 2012

Gravitational-wave Astronomy

- GW150914 (The first GW event)

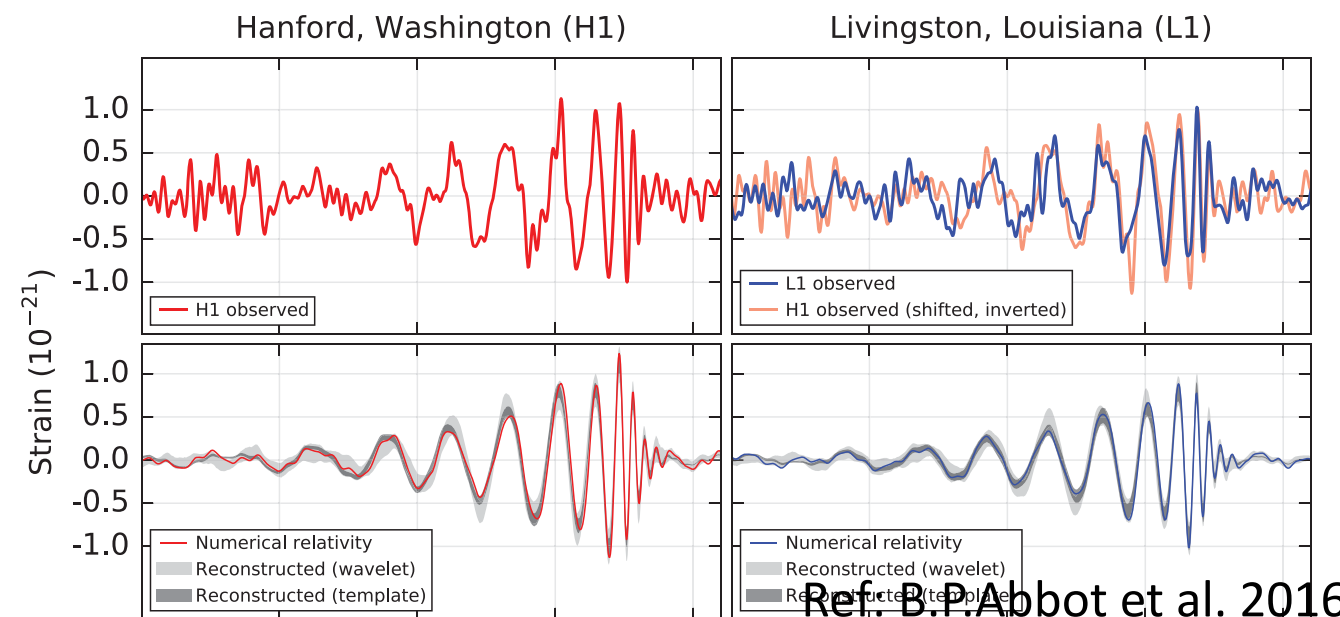
- Since 14th of September 2015, many GW events have been detected

- Binary BH (BBH; BH-BH)

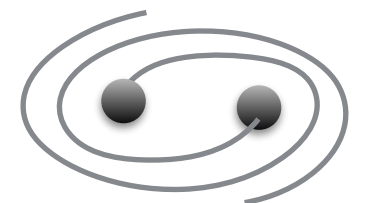
- GW150914, GW151226, GW170104, GW170608, GW170814

- Binary NS (BNS; NS-NS)
GW170817

→ Simultaneous detection of electromagnetic (EM) counterparts

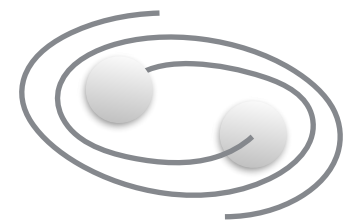
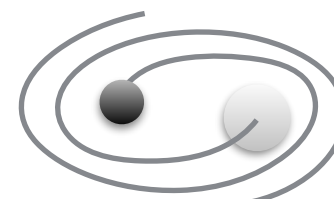


BH-BH



NS Binary

BH-NS



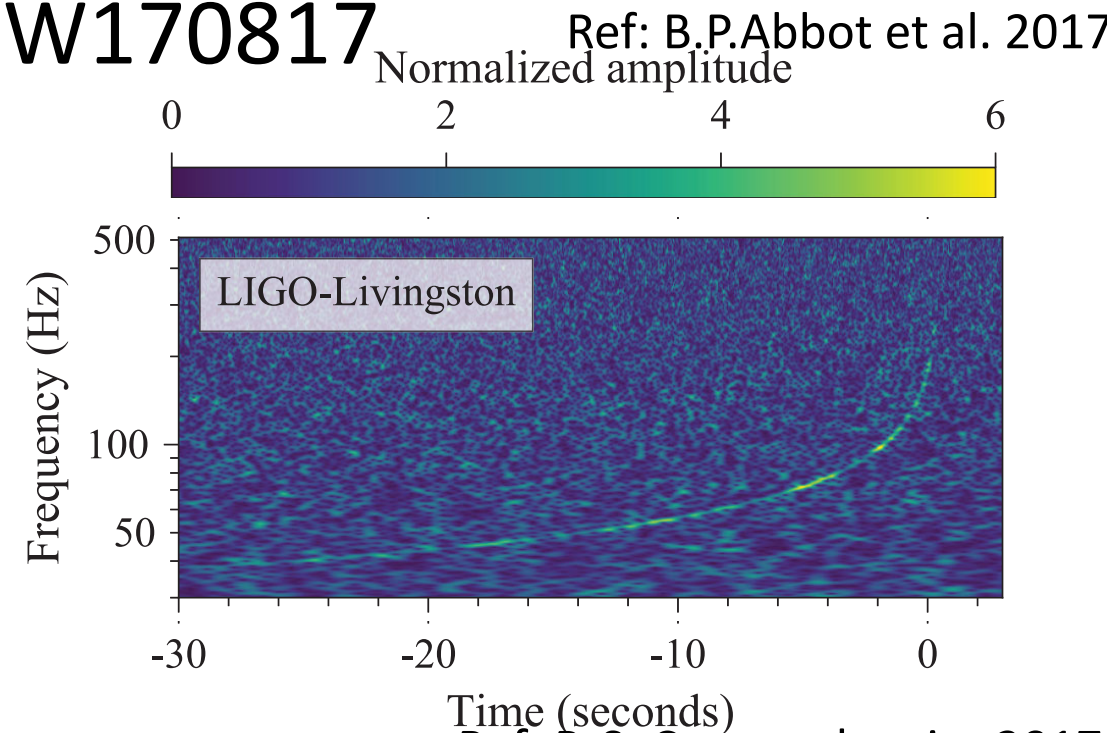
BNS (NS-NS)

GW170817:

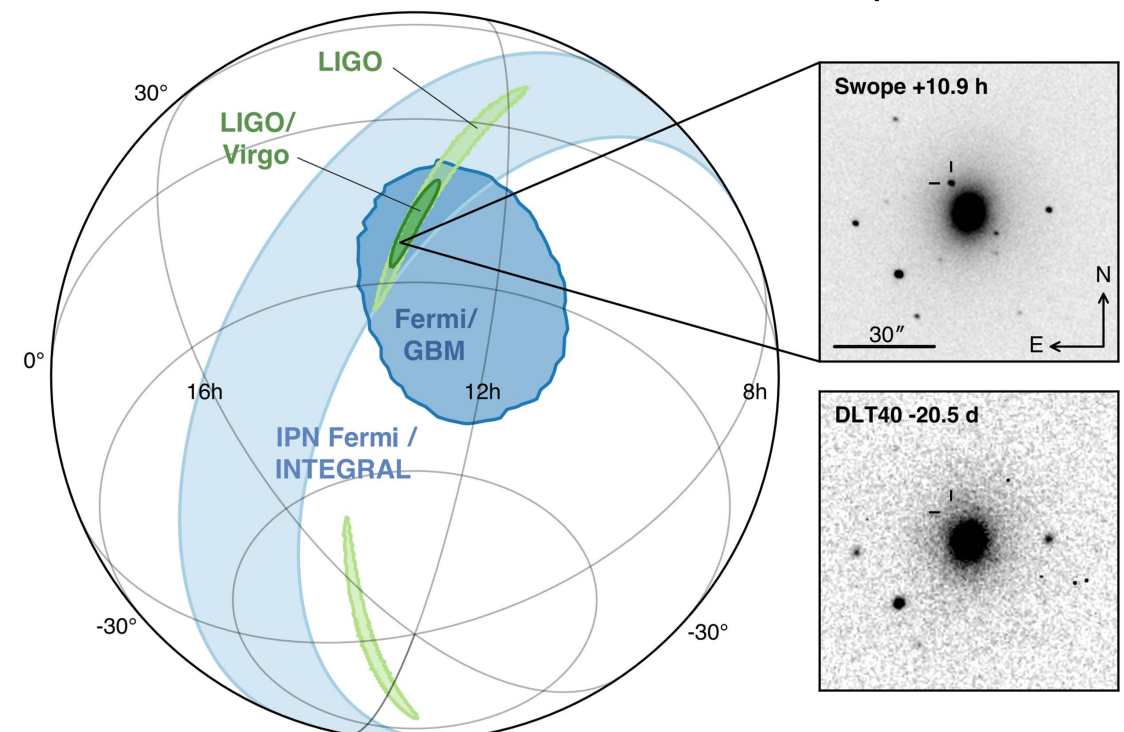
Binary Neutron star Merger

- On 17th of August 2017, advanced LIGO and advanced Virgo reported the first detection of gravitational waves from a binary BNS merger
- Electromagnetic (EM) counterparts to GW170817 were observed over the entire wavelength range (from radio to gamma wavelengths)

• GW170817



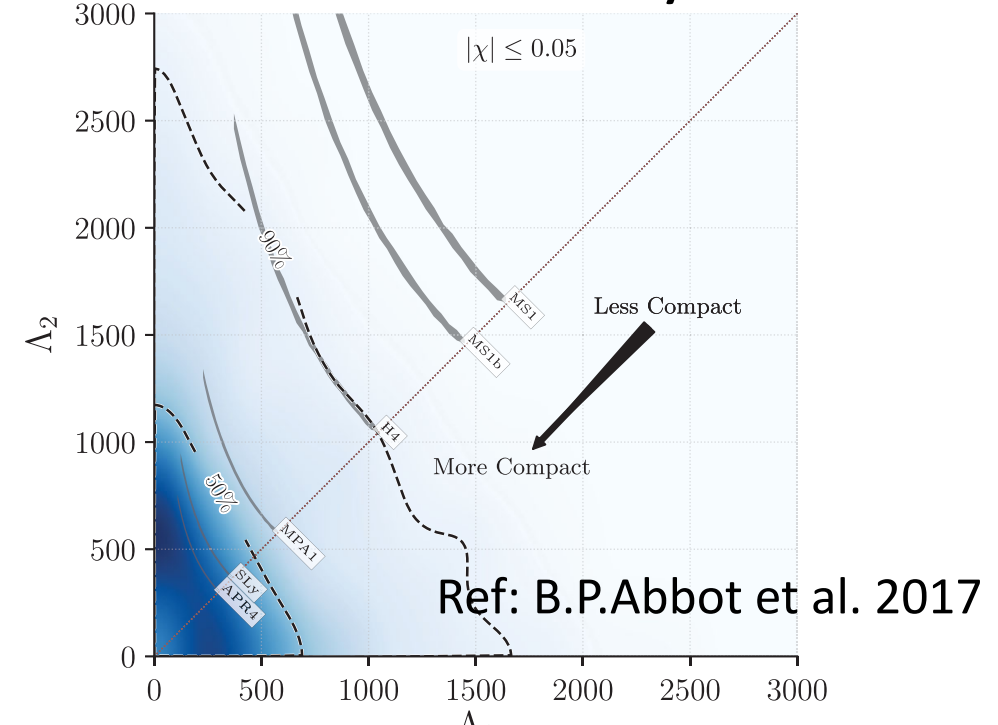
Ref: P. S. Cowperthwaite 2017



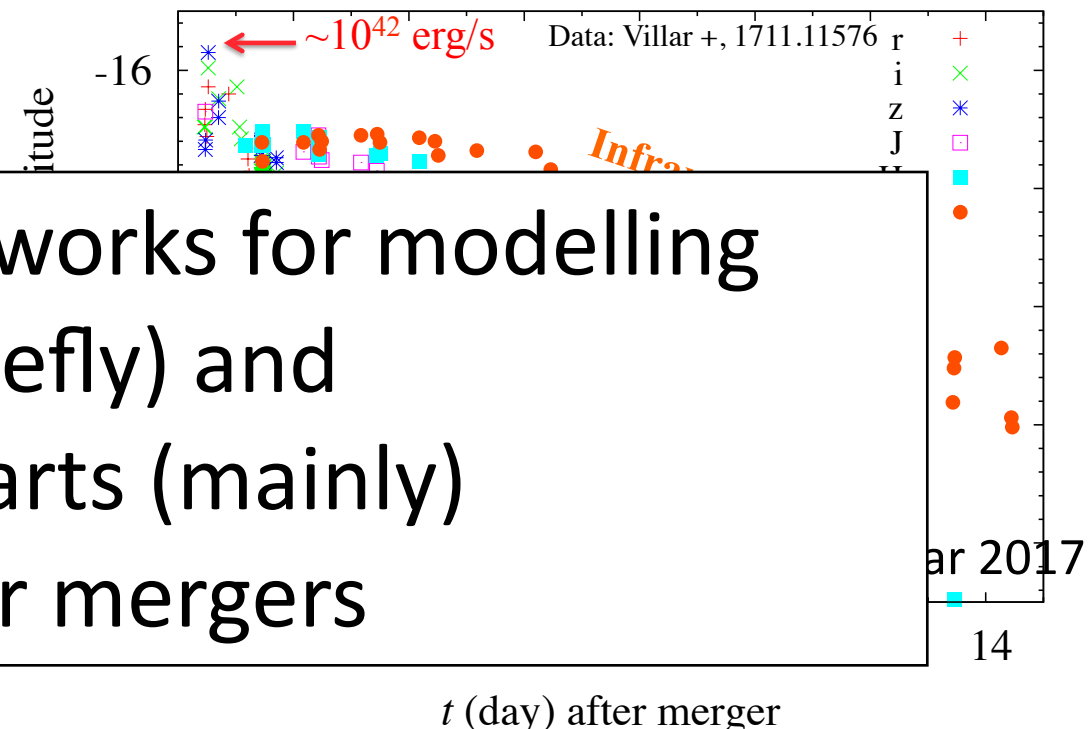
Multi-messenger Astronomy

- Single event, but many physics
 - Constraints on NS masses, spins, and NS equation of state (NS tidal deformability)
 - association of kilonova/macronova (?): mass ejection, r-process synthesis
 - Afterglow, radio flare: constraints on relativistic jet, environment of the event
 - Host galaxy: Hubble parameter, GW propagation speed
 - etc...

NS Tidal deformability



Optical-IR EM counterparts of GW170817



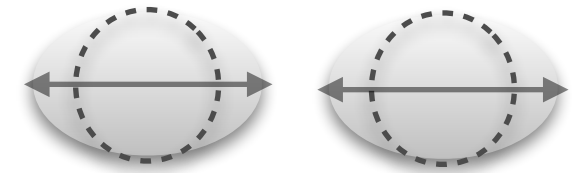
...and many tasks and problems

Today, I will talk about our recent works for modelling gravitational waves (briefly) and electromagnetic counterparts (mainly) from binary neutron star mergers

Gravitational waves from binary neutron star mergers

Neutron star binaries

- Gravitational waves contain the information of the binary (masses, spins, etc...) in its waveforms.
- In particular, if the binary contains a NS, we can extract the information of the internal structure of the NS
- During the inspiral, a NS is deformed by the tidal force of the companion object. Deformation of a NS (λ) accelerates the orbital shrinking, and modifies gravitational waveforms
- From the observed waveforms, *the tidal deformability* of a NS can be extracted
- The tidal deformability reflects the internal structure of a NS, and it can be used to constrain **the NS equation of state (EOS)**



Tidal deformation



$$\Delta\Phi_{\text{GW}}^{\text{Tidal}}(t)$$

Modification in the GW phase



$$\Lambda = G\lambda \left(\frac{c^2}{GM_{\text{NS}}} \right)^5 \sim \left(\frac{c^2 R_{\text{NS}}}{GM_{\text{NS}}} \right)^5$$

(dimensionless) tidal deformability

$$Q_{ij} = -\lambda \mathcal{E}_{ij} = -\lambda \partial_i \partial_j \Phi$$

Quadrupole

tidal field

Accuracy of gravitational waveform model

- Physical information is extracted from observed gravitational waves by the comparison with theoretical templates
→ **an accurate waveform templates are crucial for parameter estimation**
- Accurate waveform models for point-particle (no tidal effect) waveforms calibrated by numerical simulations are well developed (ex. EOB model, Phenom model)
- On the other hand, only a limited number of models (Dietrich et al. 2017) exist for the waveforms including NS tidal effects calibrated by numerical simulations

Analytic GW models for BNS

- The waveforms including the linear- order tidal effects are derived by post-Newtonian (PN) calculation (and the Effective-One-Body formalism)
 - Newtonian (Flanagan et al. 2008)
 - 1 PN (Vines et al. 2011)
 - 2.5 PN (Damour et al. 2012)
 - Self force (Bernuzzi et al. 2015)
 - Dynamical tide (Hinderer et al. 2016)
 - 2.5 PN tidal phase correction
- $$\Psi_{\text{tidal}}^{2.5\text{PN}} = \frac{3}{32} \left(-\frac{39}{2} \Lambda \right) x^{5/2} \times \left[1 + \frac{3115}{1248} x - \pi x^{3/2} + \frac{28024205}{3302208} x^2 - \frac{4283}{1092} \pi x^{5/2} \right]$$
- $$x := (\pi m_0 f)^{2/3} \approx \left(\frac{v}{c} \right)^2 : \text{PN parameter}$$
- **Tidal effects become significant in the last part of the inspiral. However, the model based on PN calculation would not be accurate just before the merger.**
Prediction by numerical simulations is important for BNS waveform modelling.
(at least needed to be checked)

Numerical Relativity Simulation

- **Numerical-relativity (NR) simulation** is the unique method to predict dynamics and gravitational waves in the merger phase—a regime where the non-linear effect of hydrodynamics should be taken into account in the framework of general relativity.
- We performed the simulations by using a numerical-relativity code, *SACRA* (Yamamoto et al. 2008), in which an adaptive-mesh-refinement (AMR) algorithm is implemented (Kiuchi et al. 2017, KK et al. 2018)

Einstein's equation

$$G_{\mu\nu} = \frac{8\pi G}{c^4} T_{\mu\nu}$$

Euler equation

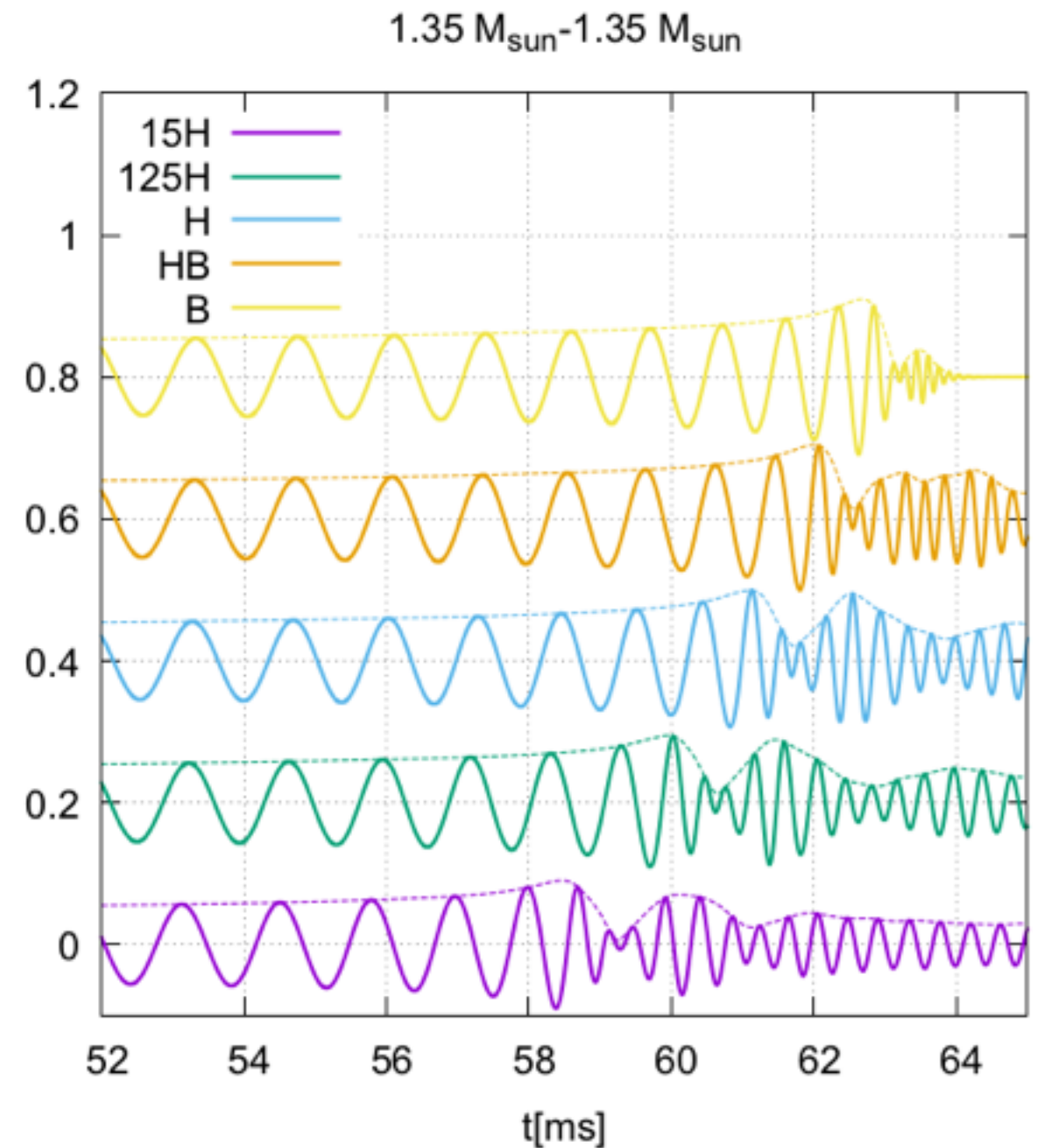
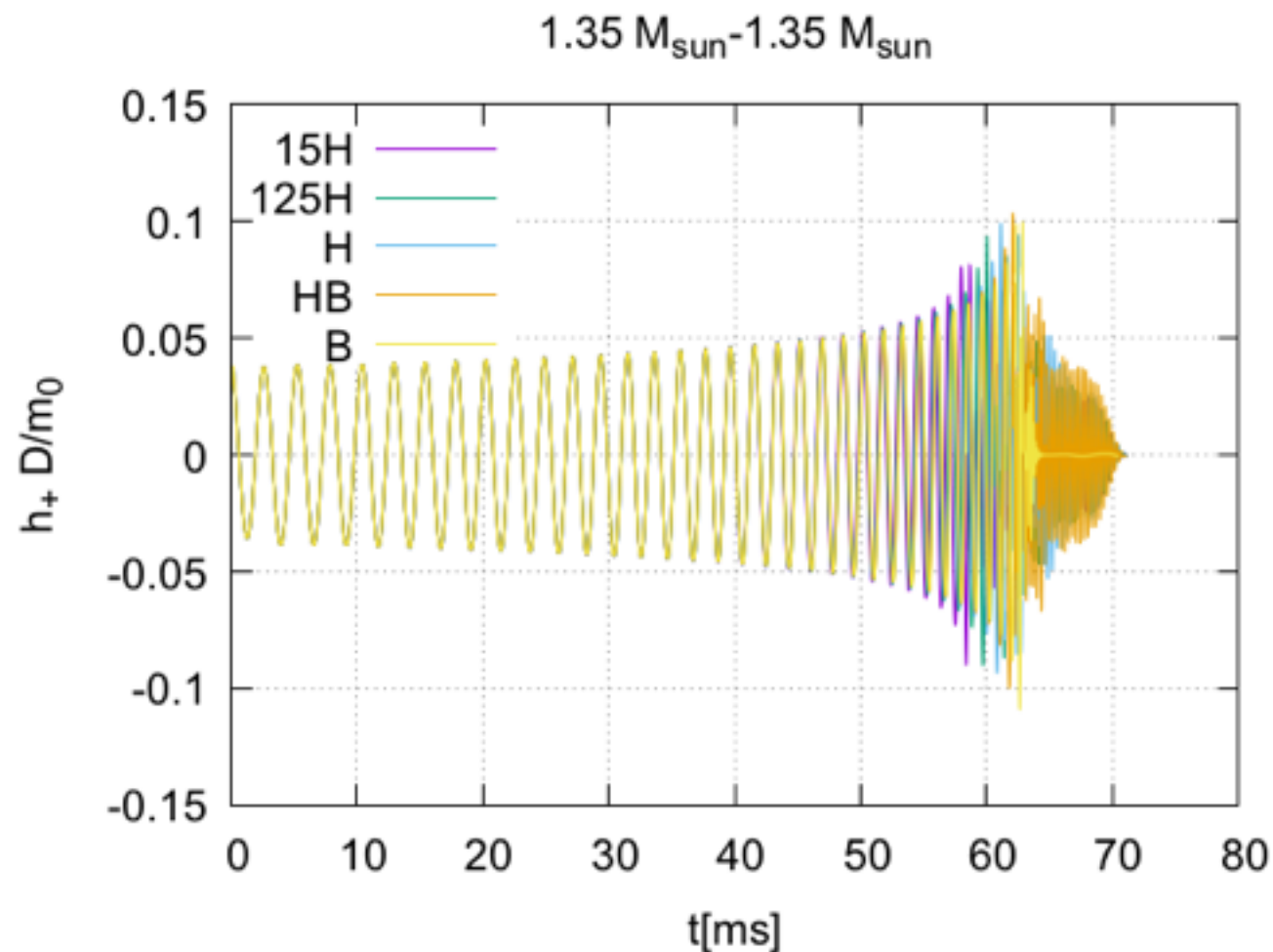
$$\nabla_{\mu} (\rho u^{\mu}) = 0 \quad \nabla_{\mu} T^{\mu\nu} = 0$$

Equation of state (EOS)

$$P = P(\rho), P(\rho, T, Y_e), \dots$$

(+MHD, viscosity, neutrino, etc.,)

Results (1.35-1.35M_sun)

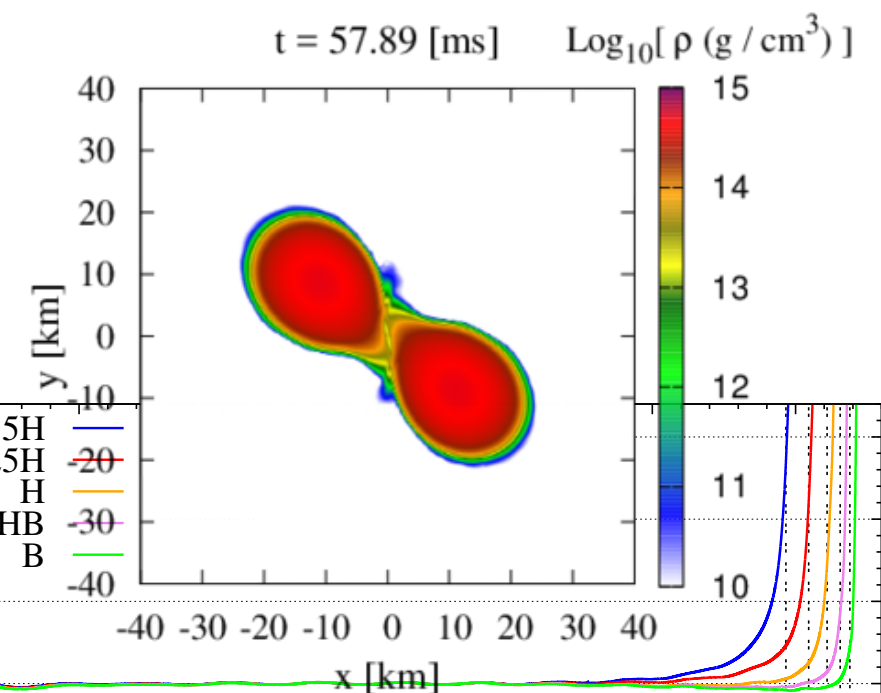
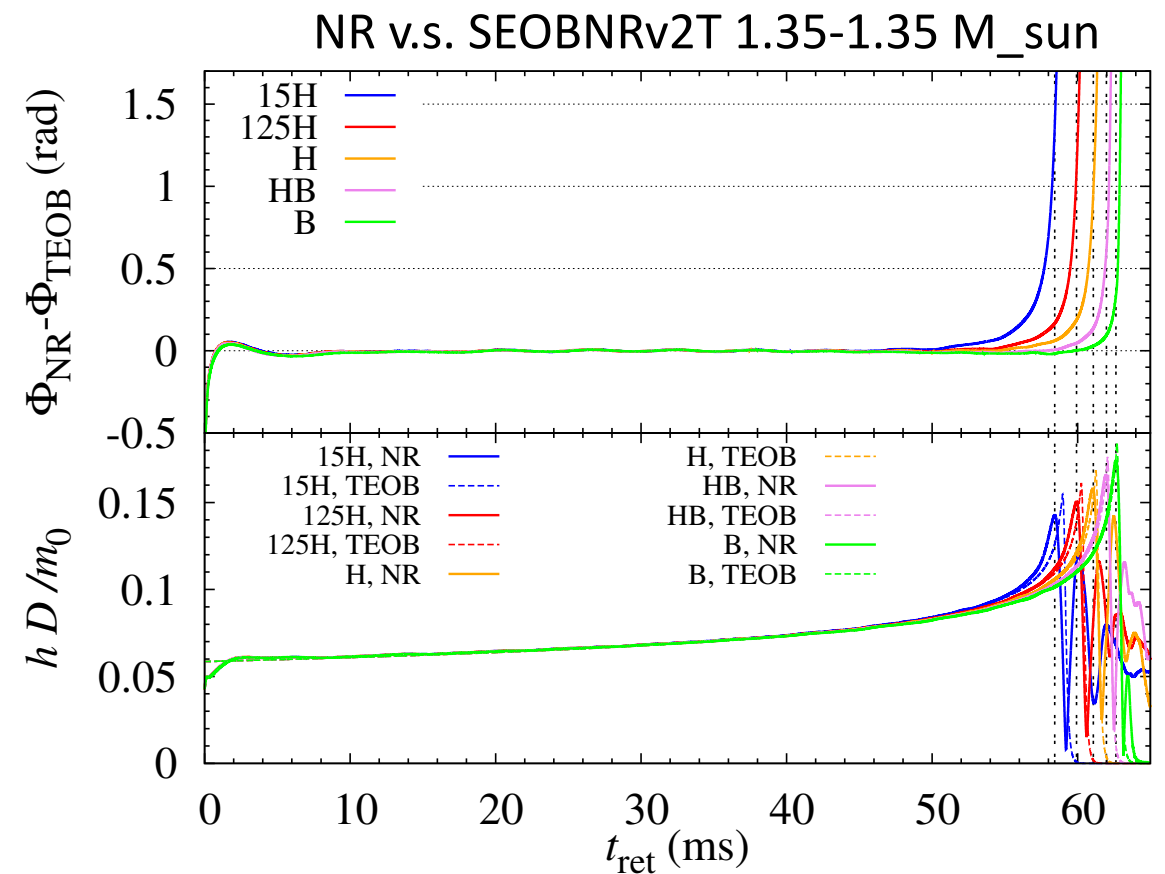


- Radius & Tidal deformability
15H > 125H > H > HB > B

Comparison with EOB model

- We compare our NR waveforms with the EOB waveforms considering dynamical tides (Hinderer et al. 2016)
- These latest tidal-EOB (SEOBNRv2T) waveforms can be accurate even up to ~ 3 ms before the onset of merger.
- The phase difference between the TEOB waveforms and the numerical-relativity results is still larger than ~ 1 rad after two NSs come into contact for the case that the NS radii are larger than 13 km ($\Lambda \sim 850$)

→ Further improvement of the waveform model may be needed to suppress the systematic error in the measurement of the tidal deformability.



Binary neutron star models

- 4 mass configuration (m_1+m_2)
 - 1.35 M_{sun} +1.35 M_{sun}
 - 1.21 M_{sun} +1.51 M_{sun} ($q=m_1/m_2=0.8$)
 - 1.16 M_{sun} +1.58 M_{sun} ($q=m_1/m_2=0.73$)
 - 1.25 M_{sun} +1.25 M_{sun}

$$\mathcal{M}_c = (m_1 + m_2)\eta^{3/5} : \text{chirp mass}$$

$$\eta = \frac{m_1 m_2}{m_1 + m_2} : \text{symmetric mass ratio}$$

- 5 equations of state (EOS)
 - 2 piecewise-polytropic EOS
 - (Read et al. 2009, Lackey et. al 2012)

$$10.8 \text{ km} \leq R_{\text{NS}} \leq 13.7 \text{ km}$$

Binary tidal deformability (e.g. Wade et al.)

$$300 \lesssim \tilde{\Lambda} \lesssim 1900$$

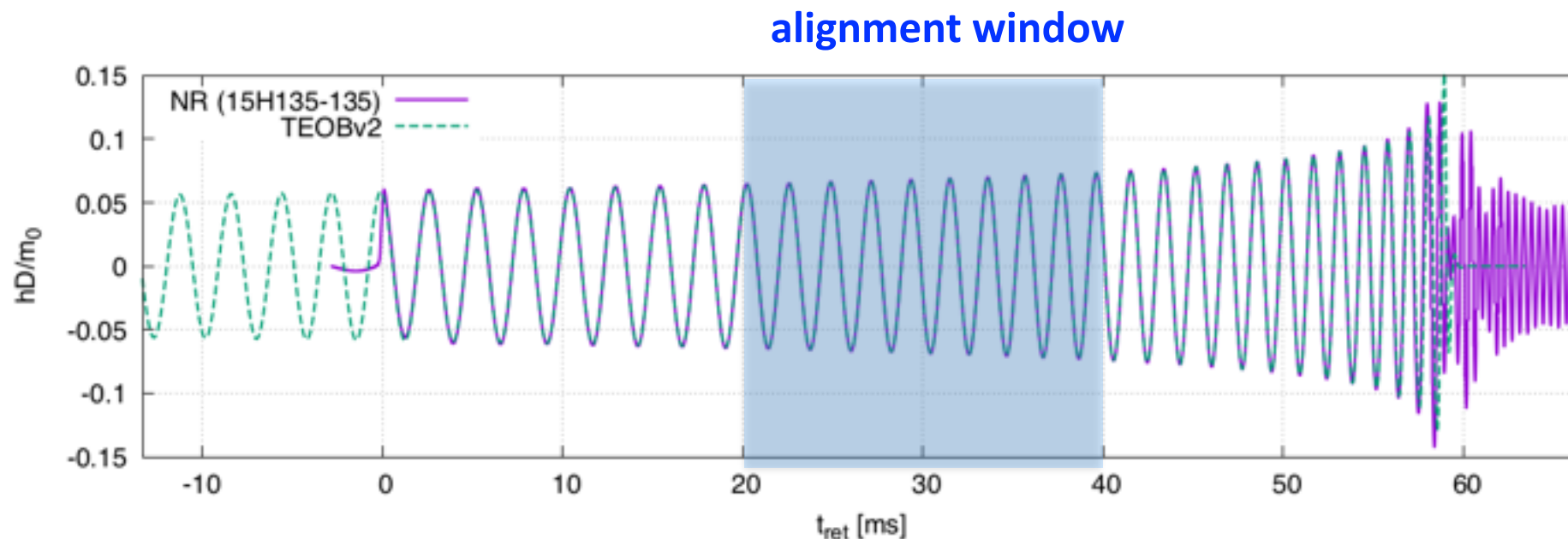
$$\tilde{\Lambda} = \frac{8}{13} \left[(1 + 7\eta - 31\eta^2) (\Lambda_1 + \Lambda_2) - \sqrt{1 - 4\eta} (1 + 9\eta - 11\eta^2) (\Lambda_1 - \Lambda_2) \right]$$

- We focus only on the case that the neutron-star spins are absent.

Model	m_1	m_2	EOS	\mathcal{M}_c	η	$\tilde{\Lambda}$
15H135-135	1.35	1.35	15H	1.17524	0.25	1211
125H135-135	1.35	1.35	125H	1.17524	0.25	863
H135-135	1.35	1.35	H	1.17524	0.25	607
HB135-135	1.35	1.35	HB	1.17524	0.25	422
B135-135	1.35	1.35	B	1.17524	0.25	289
15H121-151	1.21	1.51	15H	1.17524	0.247	1198
125H121-151	1.21	1.51	125H	1.17524	0.247	856
H121-151	1.21	1.51	H	1.17524	0.247	604
HB121-151	1.21	1.51	HB	1.17524	0.247	422
B121-151	1.21	1.51	B	1.17524	0.247	290
15H116-158	1.16	1.58	15H	1.17524	0.244	1185
125H116-158	1.16	1.58	125H	1.17524	0.244	848
H116-158	1.16	1.58	H	1.17524	0.244	601
HB116-158	1.16	1.58	HB	1.17524	0.244	421
B116-158	1.16	1.58	B	1.17524	0.244	291
15H125-125	1.25	1.25	15H	1.08819	0.25	1875
125H125-125	1.25	1.25	125H	1.08819	0.25	1352
H125-125	1.25	1.25	H	1.08819	0.25	966
HB125-125	1.25	1.25	HB	1.08819	0.25	683
B125-125	1.25	1.25	B	1.08819	0.25	476

Frequency-domain waveform model

- We derive a frequency domain waveform model based on the numerical-relativity waveforms, in particular, in the frequency domain for convenience in data analysis
- NR waveforms are still too short for the use of constructing an waveform model, so we construct hybrid waveforms composed of our latest numerical-relativity waveforms (>400 Hz) and the EOB (SEOBNRv2T) waveforms (<400 Hz) to calibrate the waveform model.
- Numerical-relativity waveforms ~ 30 gravitational cycles (>200 rad) 0.1–0.6 rad phase error up to the peak of the amplitude (less than 0.1 rad until $f < 1000$ Hz)
- The EOB (SEOBNRv2T) waveforms (Hinderer et al. 2016) Initial frequency: 10 Hz



Results

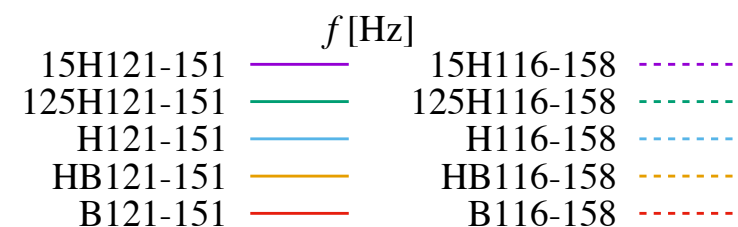
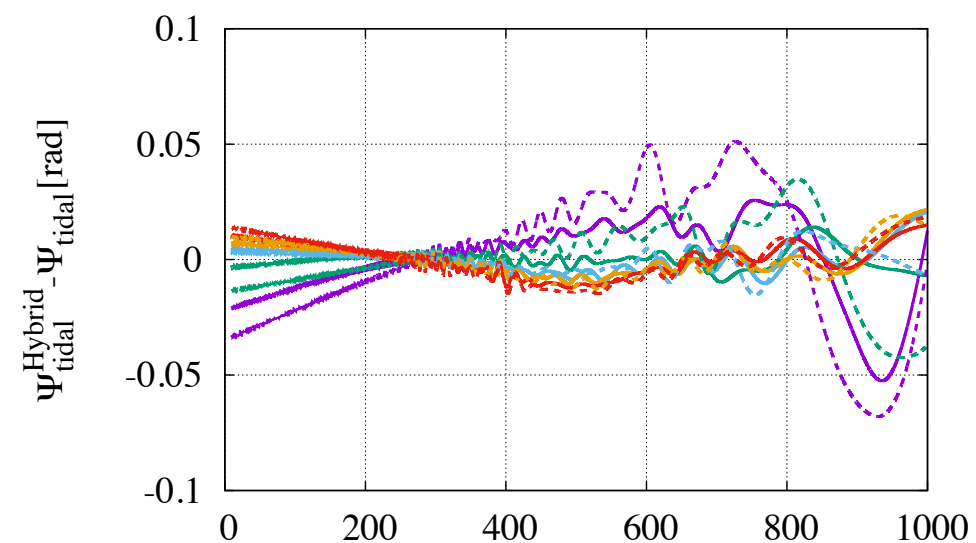
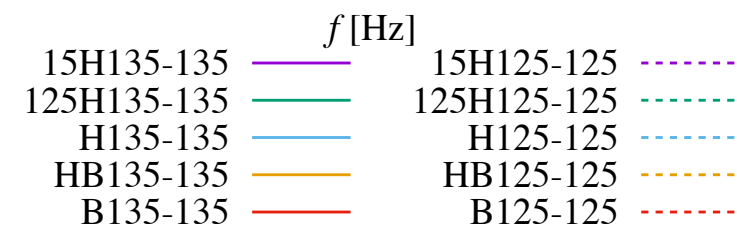
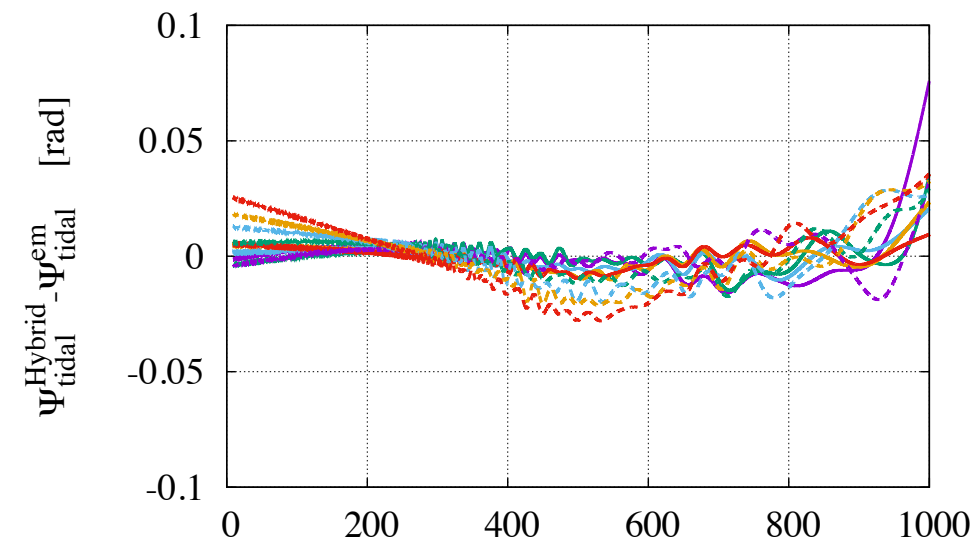
- The following phenomenological form of a fitting formula is employed:

$$\Psi_{\text{tidal}} = \frac{3}{128\eta} \left[-\frac{39}{2} \tilde{\Lambda} \left(1 + a\tilde{\Lambda}^{2/3} x^p \right) \right] x^{5/2} \\ \times \left[1 + \frac{3115}{1248} x - \pi x^{3/2} + \frac{28024205}{3302208} x^2 - \frac{4283}{1092} \pi x^{5/2} \right]$$

- Model parameters are determined by employing the hybrid waveform of 15H125-125, which has the largest value of Λ , and we obtained

$$a = 12.55, \\ p = 4.240.$$

- The phase difference between our waveform model and the hybrid waveforms is always smaller than 0.1 rad.
- There is only a small difference between the waveform models determined from different BNS hybrid waveforms



Validity check: Systematic error

Systematic error:

$$\Delta\theta = \theta_i - \theta_i^T$$

$$\min_{\{\theta_i\}_{i=1}^6} \left\| \tilde{h}_{\text{Hybrid}} \left[\{\theta_i^T\}_{i=1}^6 \right] - \tilde{h}_{\text{model}} \left[\{\theta_i\}_{i=1}^6 \right] \right\|$$

$$\left(\tilde{h}_1 | \tilde{h}_2 \right) = 4\text{Re} \left[\int_{f_{\min}}^{f_{\max}} \frac{\tilde{h}_1(f) \tilde{h}_2^*(f)}{S_n(f)} df \right] \quad \|\tilde{h}\| = \sqrt{(\tilde{h} | \tilde{h})}$$

$$\{\theta_i\}_{i=1}^6 = \left\{ \mathcal{M}_c, \eta, \tilde{\Lambda}, \phi_0, t_0, D_{\text{eff}} \right\}$$

$S_n(f)$: noise spectrum density

(the ZERO_DETUNED_HIGH_POWER configuration)

Ref. <https://dcc.ligo.org/LIGO-T0900288/public>

- The systematic error in the measurement of Λ with respect to the hybrid waveforms is always smaller than 20

Model	$\tilde{\Lambda}$	our waveform model		
		$\Delta\mathcal{M}_c [M_\odot]$	$\Delta\eta$	$\Delta\tilde{\Lambda}$
15H135-135	1211	1.1×10^{-7}	1.8×10^{-6}	2.1
125H135-135	863	1.9×10^{-7}	7.7×10^{-6}	2.8
H135-135	607	2.2×10^{-7}	9.0×10^{-6}	0.1
HB135-135	422	2.3×10^{-7}	8.8×10^{-6}	-2.4
B135-135	289	1.7×10^{-7}	6.0×10^{-6}	-3.7
15H121-151	1198	4.1×10^{-7}	2.4×10^{-5}	9.8
125H121-151	856	2.2×10^{-7}	1.0×10^{-5}	2.1
H121-151	604	1.8×10^{-7}	6.9×10^{-6}	-1.9
HB121-151	422	2.6×10^{-7}	1.1×10^{-5}	-2.6
B121-151	290	1.6×10^{-7}	5.3×10^{-6}	-6.1
15H116-158	1185	6.3×10^{-7}	4.0×10^{-5}	14.7
125H116-158	848	5.0×10^{-7}	2.9×10^{-5}	6.7
H116-158	601	2.8×10^{-7}	1.4×10^{-5}	-1.5
HB116-158	421	2.3×10^{-7}	9.7×10^{-6}	-5.0
B116-158	291	1.4×10^{-7}	2.9×10^{-6}	-9.1
15H125-125	1875	1.7×10^{-7}	4.3×10^{-6}	1.5
125H125-125	1352	7.1×10^{-8}	-3.2×10^{-6}	-3.6
H125-125	966	5.3×10^{-8}	-5.3×10^{-6}	-8.1
HB125-125	683	-4.5×10^{-8}	-6.9×10^{-6}	-13
B125-125	476	-4.3×10^{-8}	-1.5×10^{-5}	-20

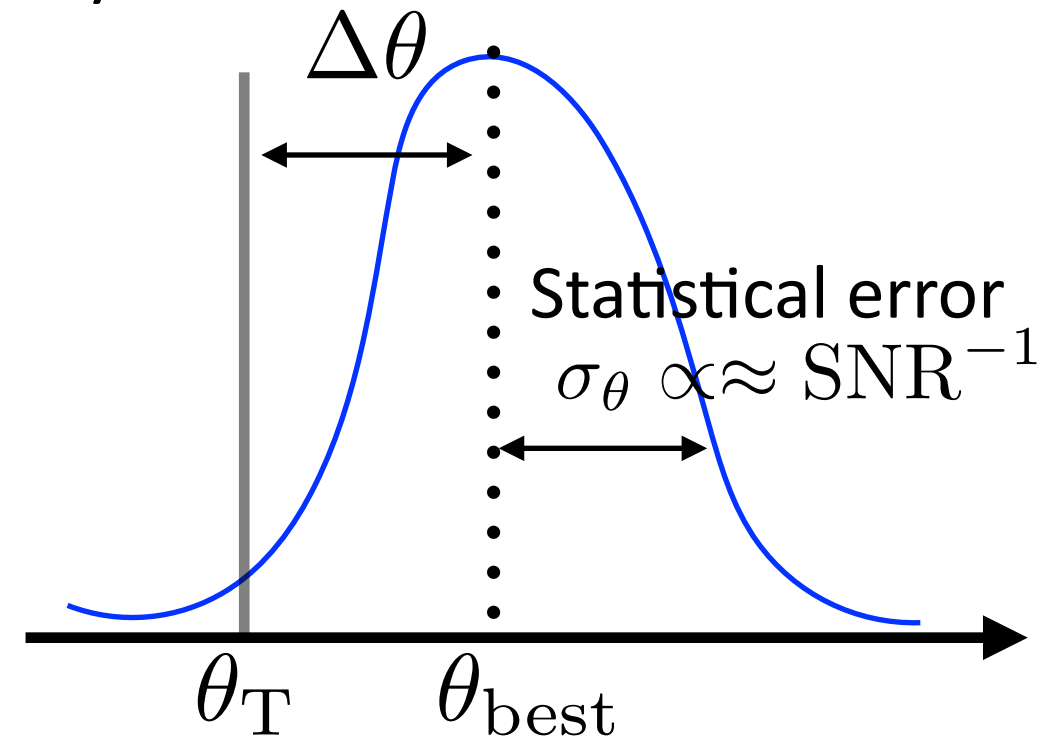
*used for the model calibration

Statistical error

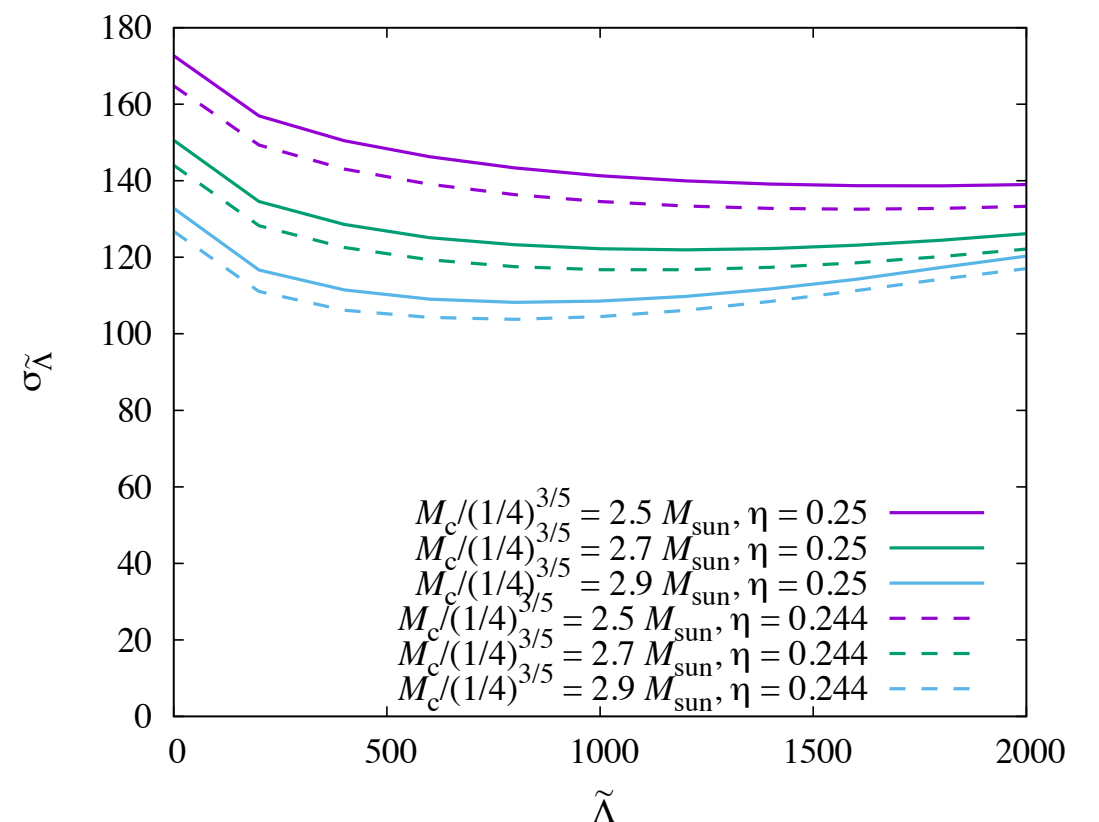
$$\text{SNR} \approx \sqrt{(\tilde{h}|\tilde{h})}$$

- Employing the standard Fisher-matrix analysis, we estimated the statistical error in the measurement of binary parameters
- Statistical error is always smaller than the systematic error of the model (against the hybrid waveforms) if SNR is smaller than ~ 100
- We obtained results consistent with the previous studies (Hinderer et al. 2010, Damour et al. 2012, Wade et al. 2014)

Systematic error



$f_{\min} = 10\text{Hz}, f_{\max} = 1000\text{Hz}, \rho = 50$



Now-going works

Preliminary

Ref: Narikawa et al. in prep.

- We apply the BNS waveform model for the analysis of GW170817 (with Narikawa-san, Uchikata-san, Tagoshi-san)
- We are also working for updating the waveform model by employing NR BNS waveforms in a wider parameter range (lower mass, higher mass ratio, NS spin)

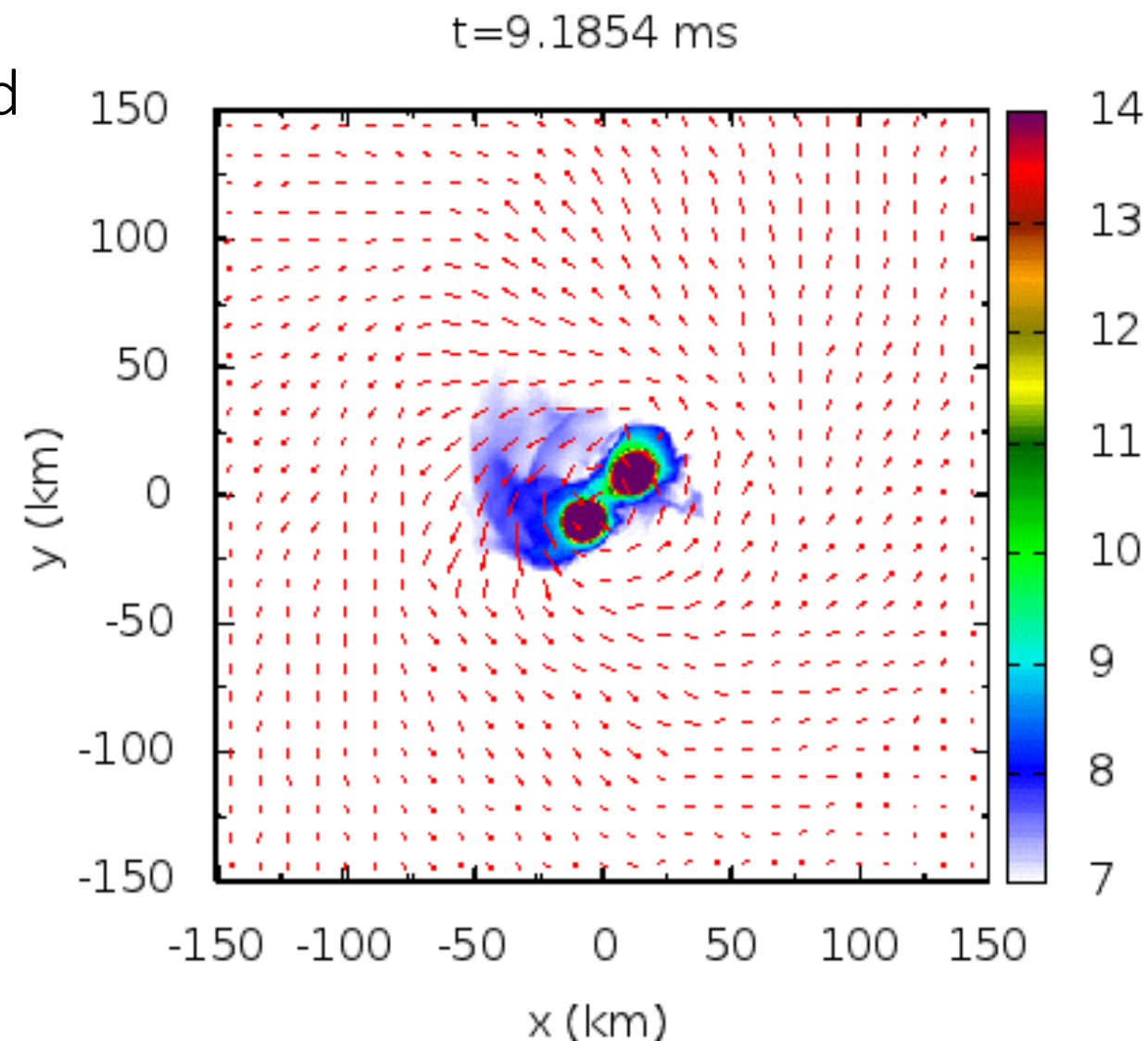
Electromagnetic counterparts
to binary neutron stars:
Kilonovae/Macronovae

Mass Ejection

- A fraction of NS material would be ejected from the system during the merger
- Ejected material is neutron-rich
→ heavy radioactive nuclei would be synthesised in the ejecta by the so-called r-process nucleosynthesis

→ EM emission in optical and NIR wavelengths could occur by radioactive decays of heavy elements
: kilonova/macronova (r-process nova)

Li & Paczyński 1998, Kulkarni 2005
, Metzger et al. 2010 ...



Ref: K. Hotokezaka et al. 2013

Properties of kilonovae / macronovae

Kilonova/macronova is expected to be nearly **isotropic** emission.

(cf. $\theta_{\text{jet}} \sim 10^\circ$ for sGRB)

The peak time of the emission will come in **~1—10 days**.

(cf. ~1 year for radio flare)

The most of the emission occurs in around **optical and infrared**.

The mass, velocity, morphology, and the composition (electron fraction) of the ejecta characterize the lightcurve of the kilonova/macronova.

Rough Estimation

$$t_{\text{peak}} \approx 3.3 \text{ days}$$

$$\times \left(\frac{M}{0.03 M_\odot} \right)^{1/2} \left(\frac{v}{0.2c} \right)^{-1/2} \left(\frac{\kappa}{1 \text{ cm}^2/\text{g}} \right)^{1/2}$$

$$L_{\text{peak}} \approx 2.0 \times 10^{41} \text{ ergs/s}$$

$$\times \left(\frac{f}{10^{-6}} \right) \left(\frac{M}{0.03 M_\odot} \right)^{1/2} \left(\frac{v}{0.2c} \right)^{1/2} \left(\frac{\kappa}{1 \text{ cm}^2/\text{g}} \right)^{-1/2}$$

$$T_{\text{peak}} \approx 3.1 \times 10^3 \text{ K}$$

$$\times \left(\frac{f}{10^{-6}} \right)^{1/4} \left(\frac{M}{0.03 M_\odot} \right)^{-1/8} \left(\frac{v}{0.2c} \right)^{-1/8} \left(\frac{\kappa}{1 \text{ cm}^2/\text{g}} \right)^{-3/8}$$

M_{eje} : ejecta mass

κ : opacity

v_{eje} : expanding velocity

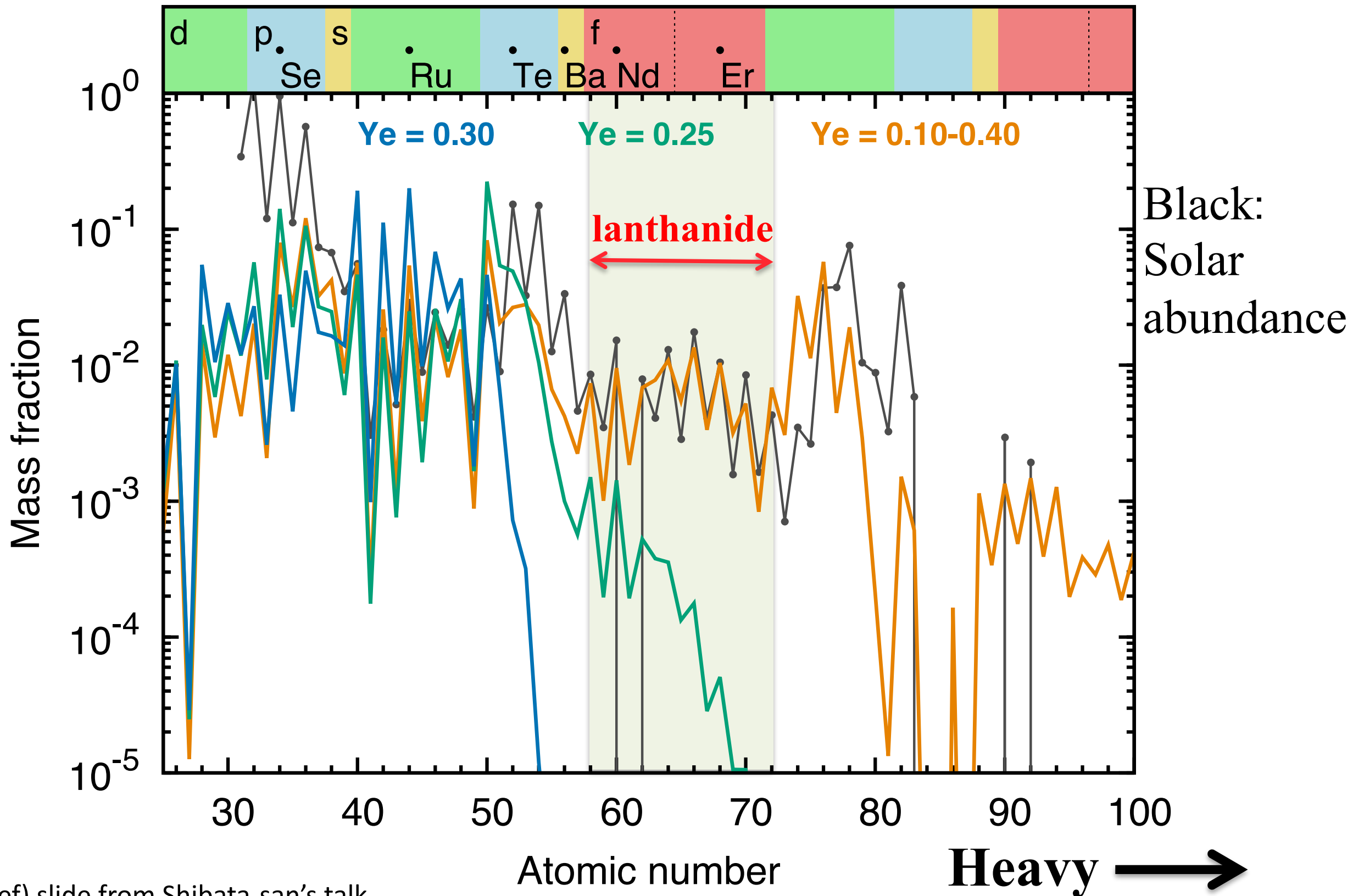
f : energy conversion rate

In particular the value of κ can vary significantly depending on the electron fraction Y_e of ejecta

$$\kappa = 0.1\text{—}10 \text{ cm}^2/\text{g}$$

R-proc. nucleosynthesis depends on Y_e ($=[p]/([p]+[n])$)

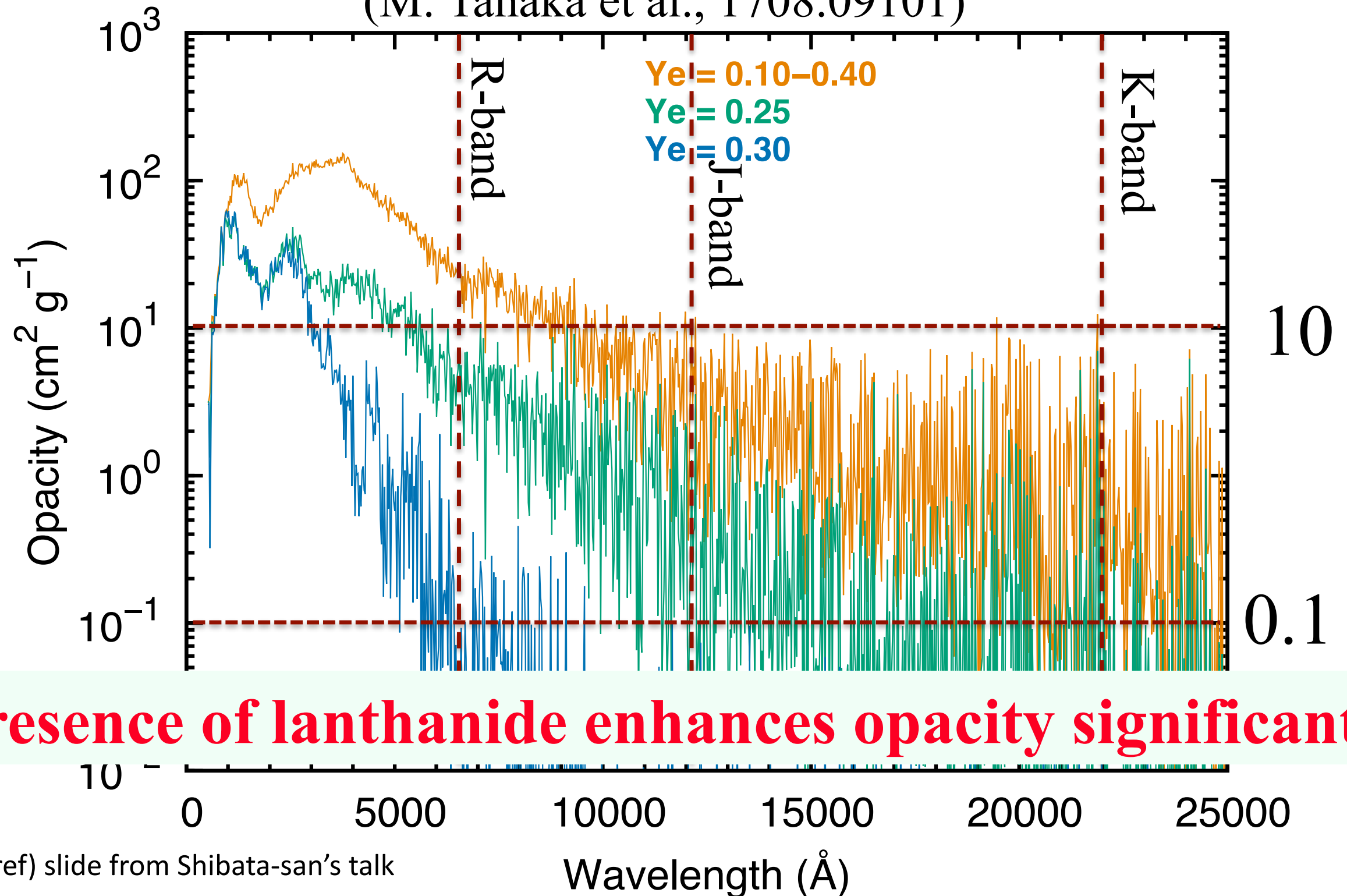
(M. Tanaka et al., 1708.09101)



ref) slide from Shibata-san's talk

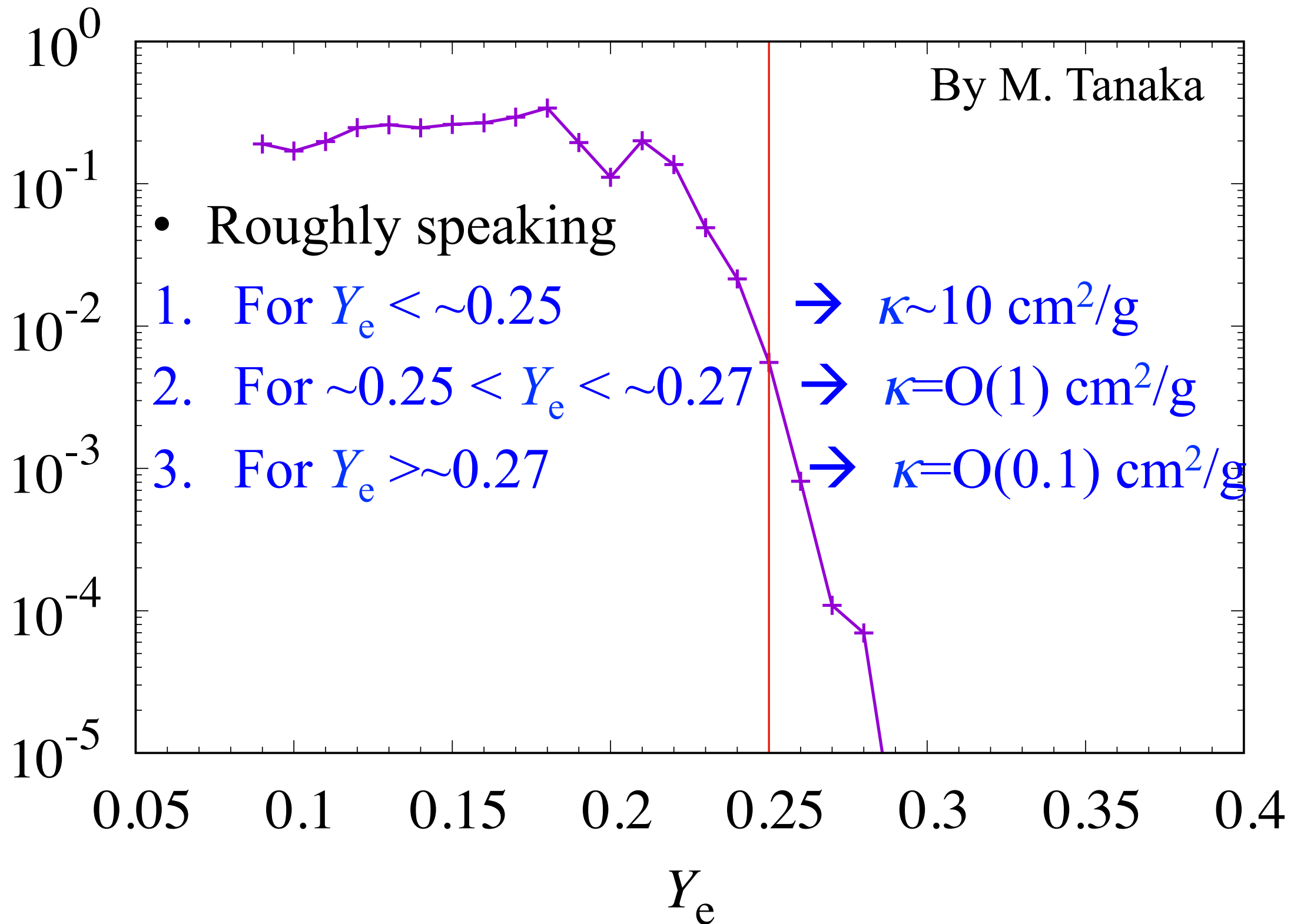
Opacity depends strongly on abundance, i.e., Y_e determined by lanthanide

(M. Tanaka et al., 1708.09101)



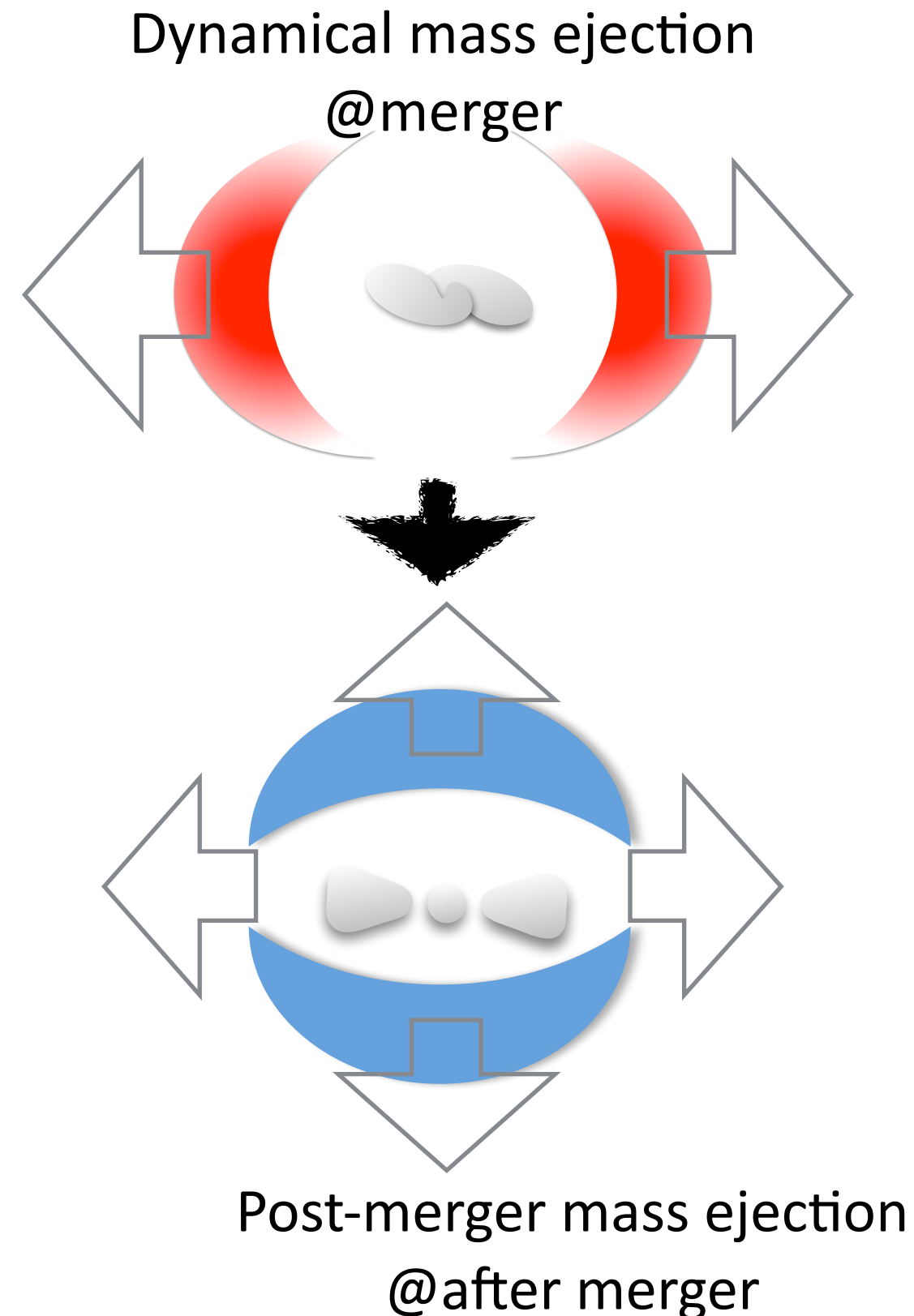
Fraction of lanthanides vs electron fraction

Mass fraction of Lanthanide (+ actinide)



Mass Ejection Mechanisms

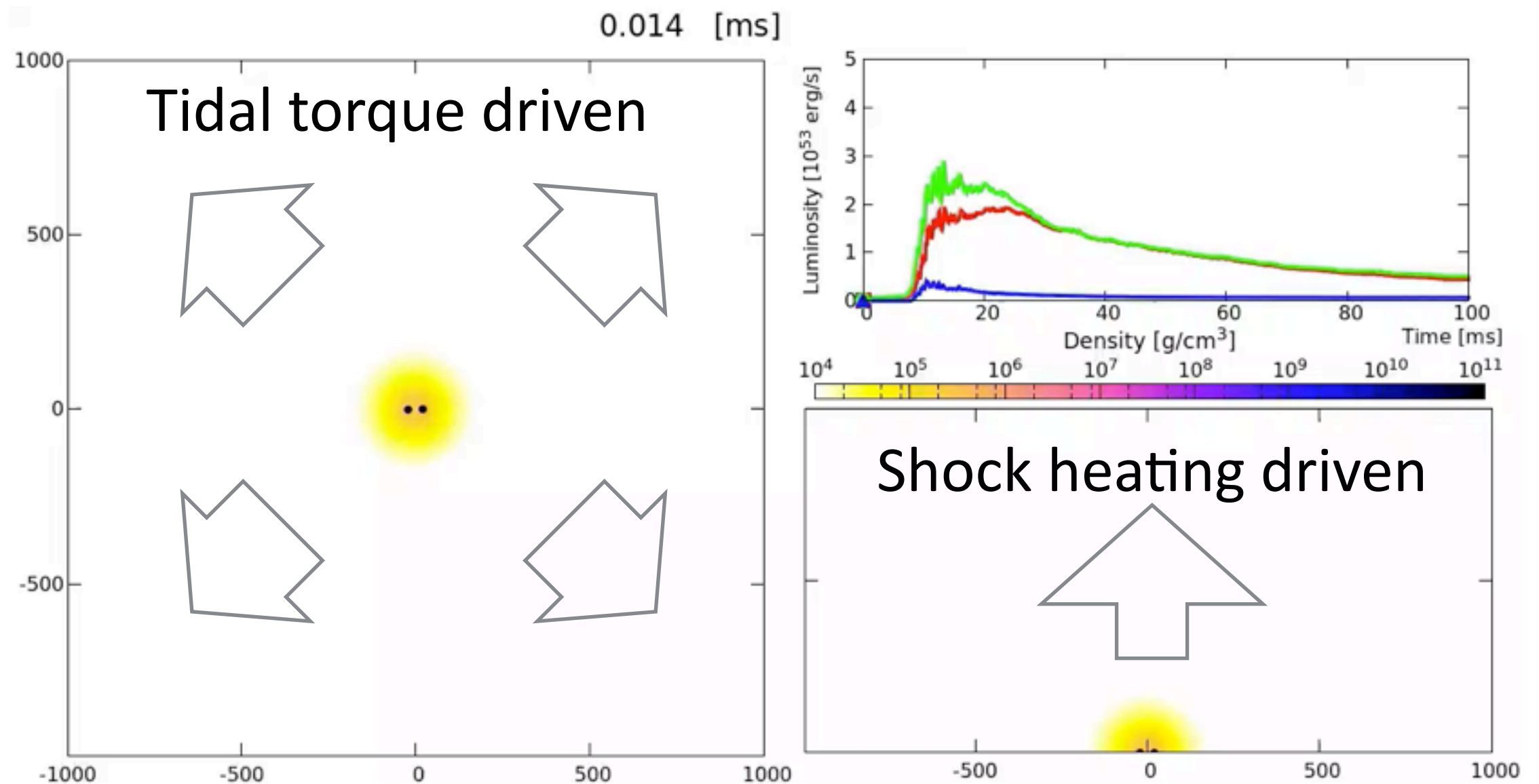
- Merger process and evolution of the merger remnant have been studied by NR simulations in the last decades revealing the mass ejection process
- **Dynamical mass ejection**
mass ejection driven by tidal interaction
or
shock heating during the collision
- **Post-merger mass ejection**
mass ejection from the merger remnant driven by viscous and neutrino heating



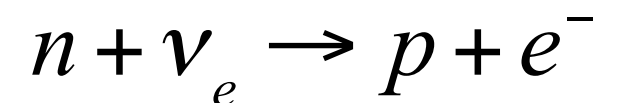
Dynamical mass ejection

Stiff EOS (DD2, $R \sim 13.2$ km): 1.30-1.40 M_{sun}

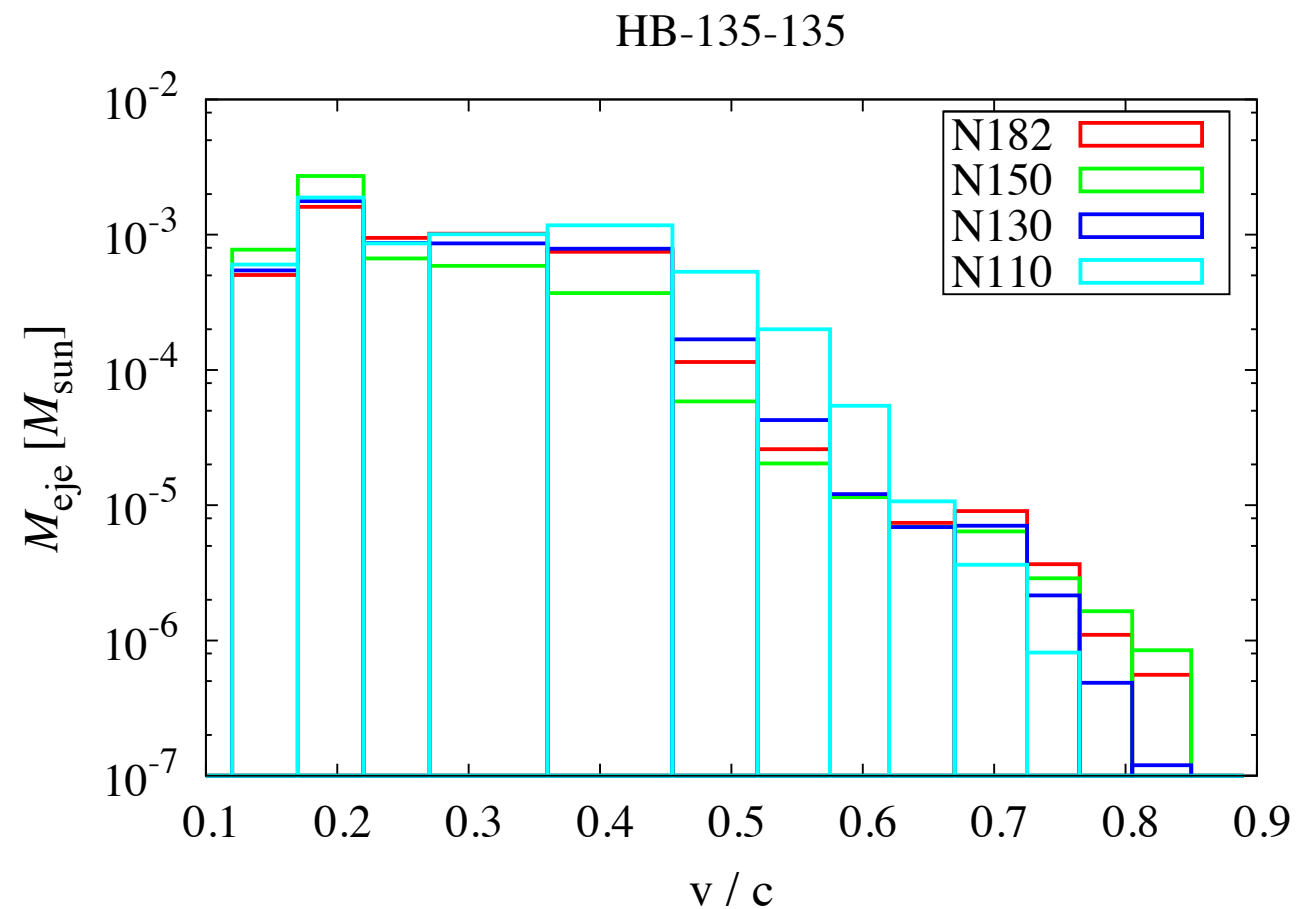
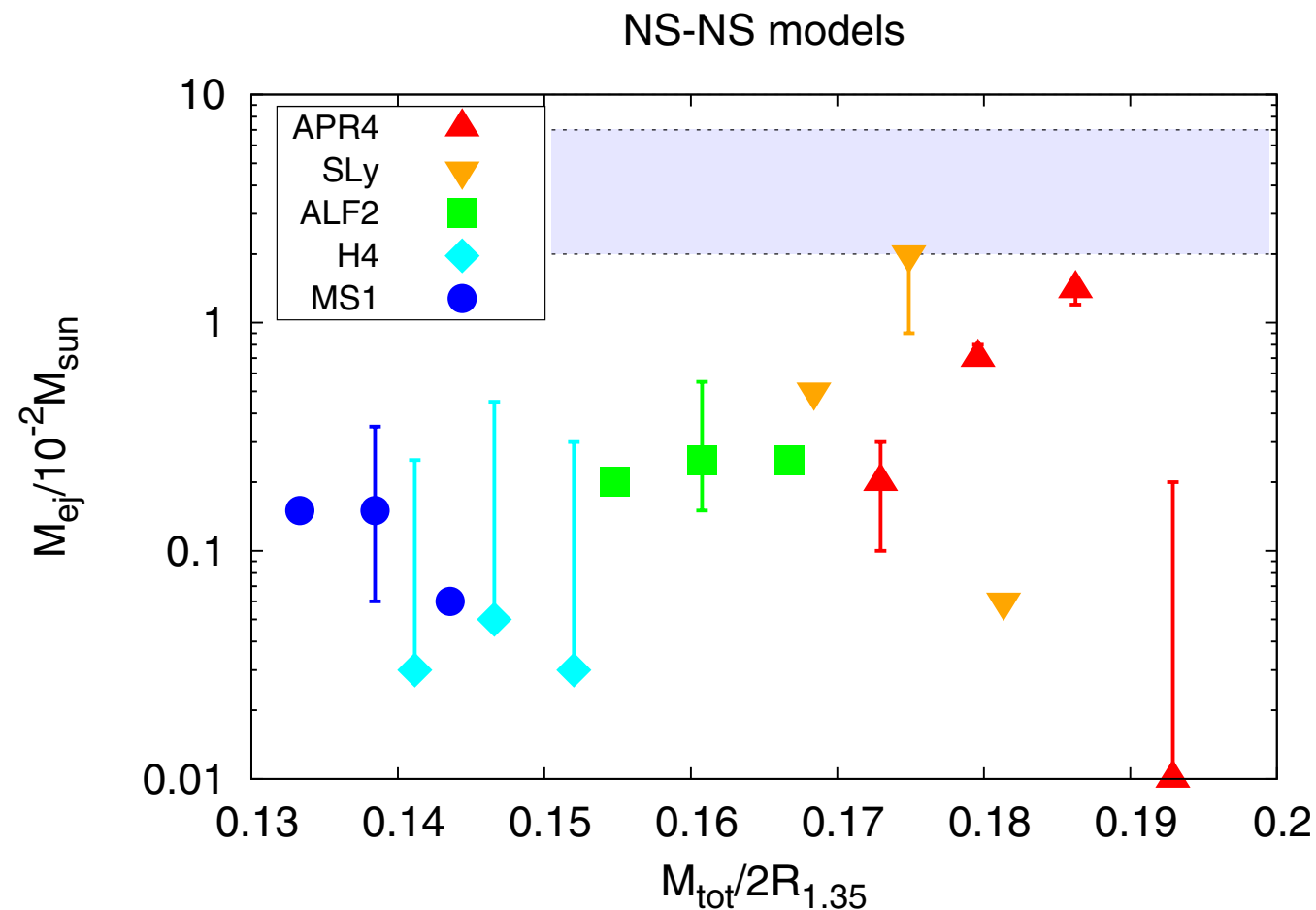
Ref: Y. Sekiguchi et al. 2016



NR simulation considering neutrino transport and its effect on the Ye



Dynamical mass ejection



Ref: K. Hotokezaka et al. 2013

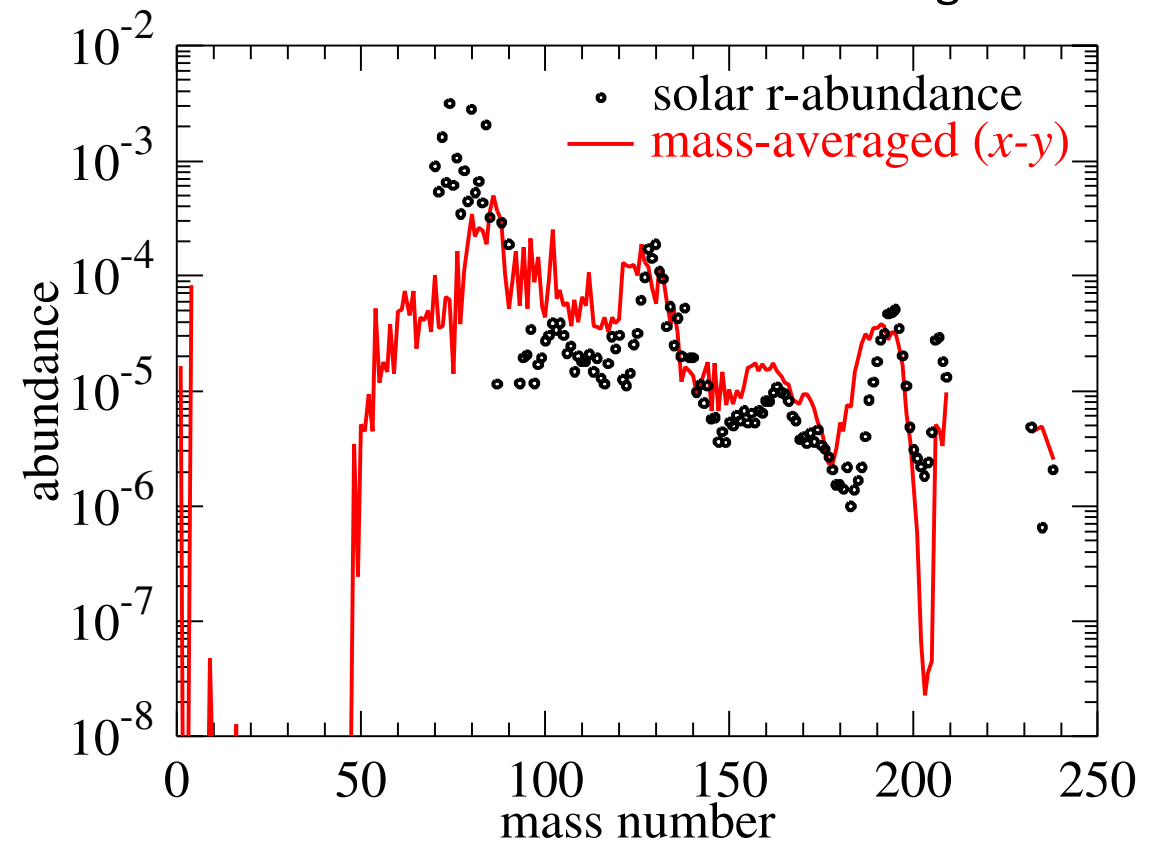
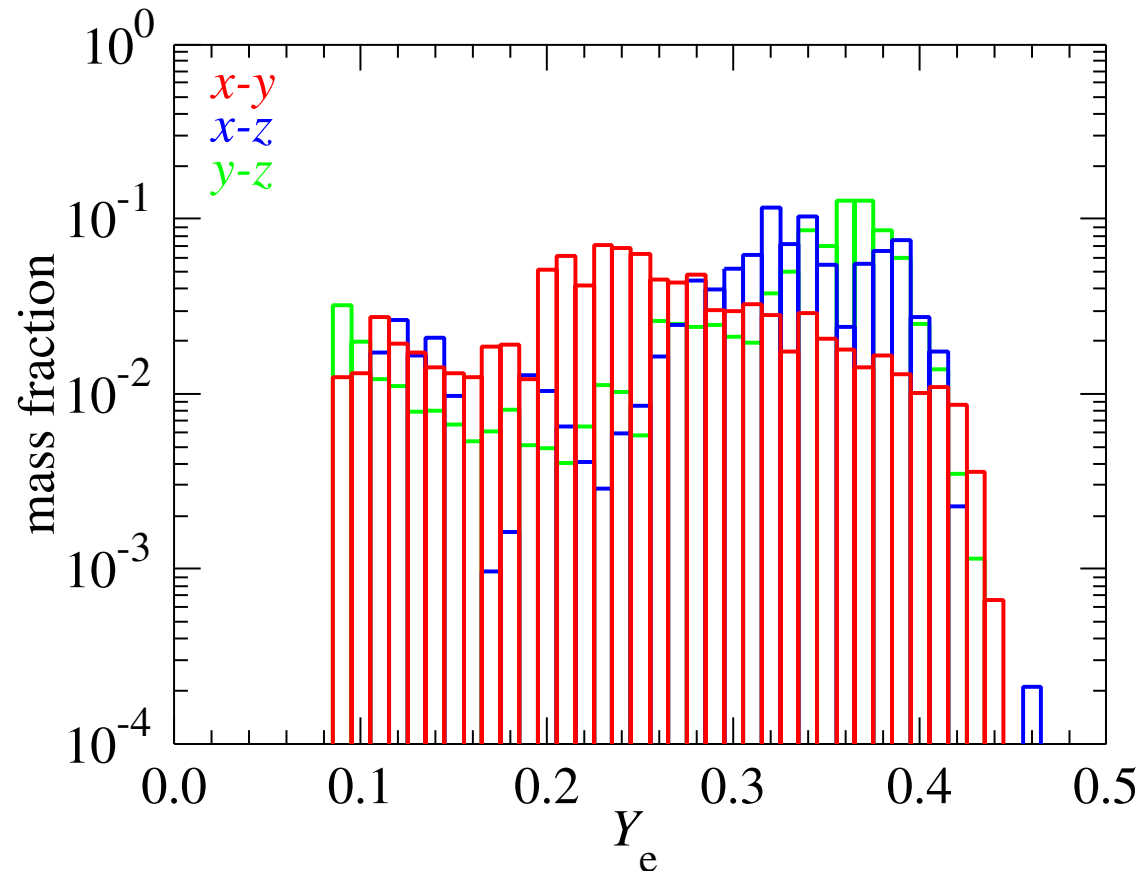
typical dynamical ejecta mass is 10^{-4} — 10^{-2} M_{sun}

depends on the NS mass and EOS

typical velocity ~ 0.1 - 0.3 c (some fraction has higher velocity)

Ye distribution

Ref: S. Wanajo et al. 2014
Y. Sekiguchi et al. 2015



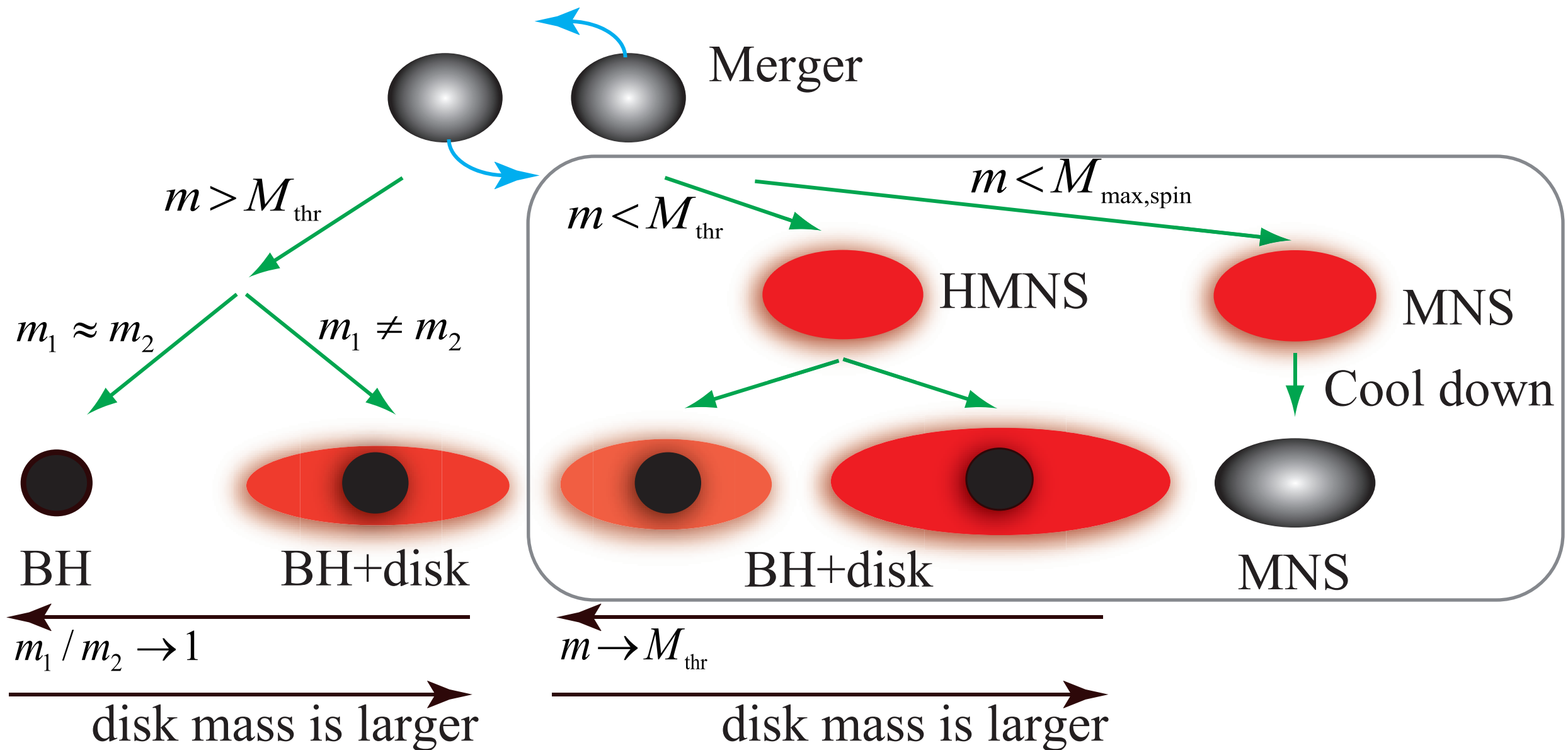
Ye partially becomes large due to shock heating and neutrino irradiation
(cf. NS $Y_e \sim < 0.1$) Yet, lanthanide is synthesised $\rightarrow \kappa \sim 10 \text{ cm}^2/\text{g}$

$$t_{\text{peak}} \approx 5.9 \text{ days} \left(\frac{M}{0.01 M_{\odot}} \right)^{1/2} \left(\frac{v}{0.2c} \right)^{-1/2} \left(\frac{\kappa}{10 \text{ cm}^2/\text{g}} \right)^{1/2}$$

$$L_{\text{peak}} \approx 3.4 \times 10^{40} \text{ ergs/s} \left(\frac{f}{10^{-6}} \right) \left(\frac{M}{0.01 M_{\odot}} \right)^{1/2} \left(\frac{v}{0.2c} \right)^{1/2} \left(\frac{\kappa}{10 \text{ cm}^2/\text{g}} \right)^{-1/2}$$

$$T_{\text{peak}} \approx 1.5 \times 10^3 \text{ K} \left(\frac{f}{10^{-6}} \right)^{1/4} \left(\frac{M}{0.01 M_{\odot}} \right)^{-1/8} \left(\frac{v}{0.2c} \right)^{-1/8} \left(\frac{\kappa}{10 \text{ cm}^2/\text{g}} \right)^{-3/8}$$

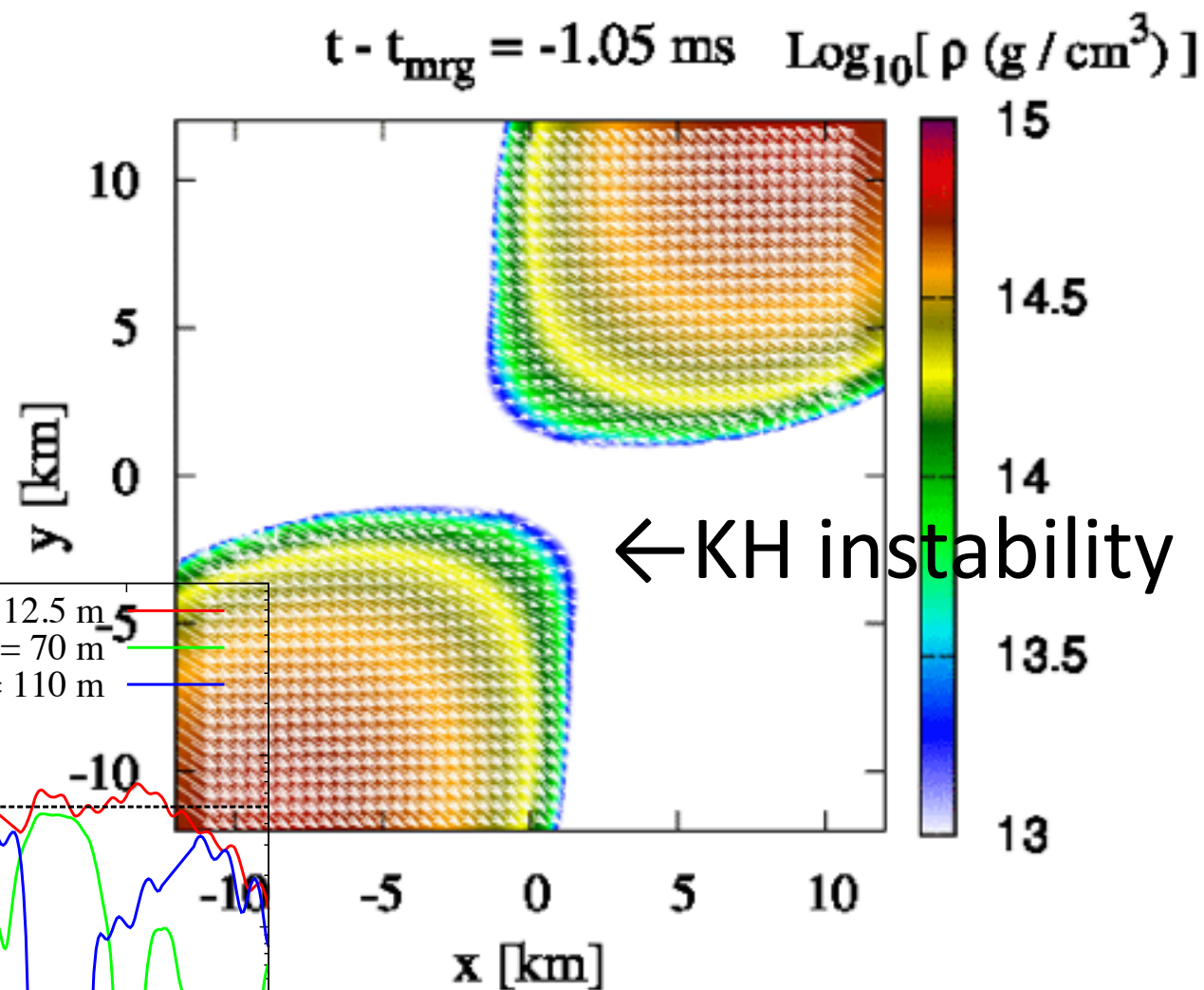
Evolution after the merger



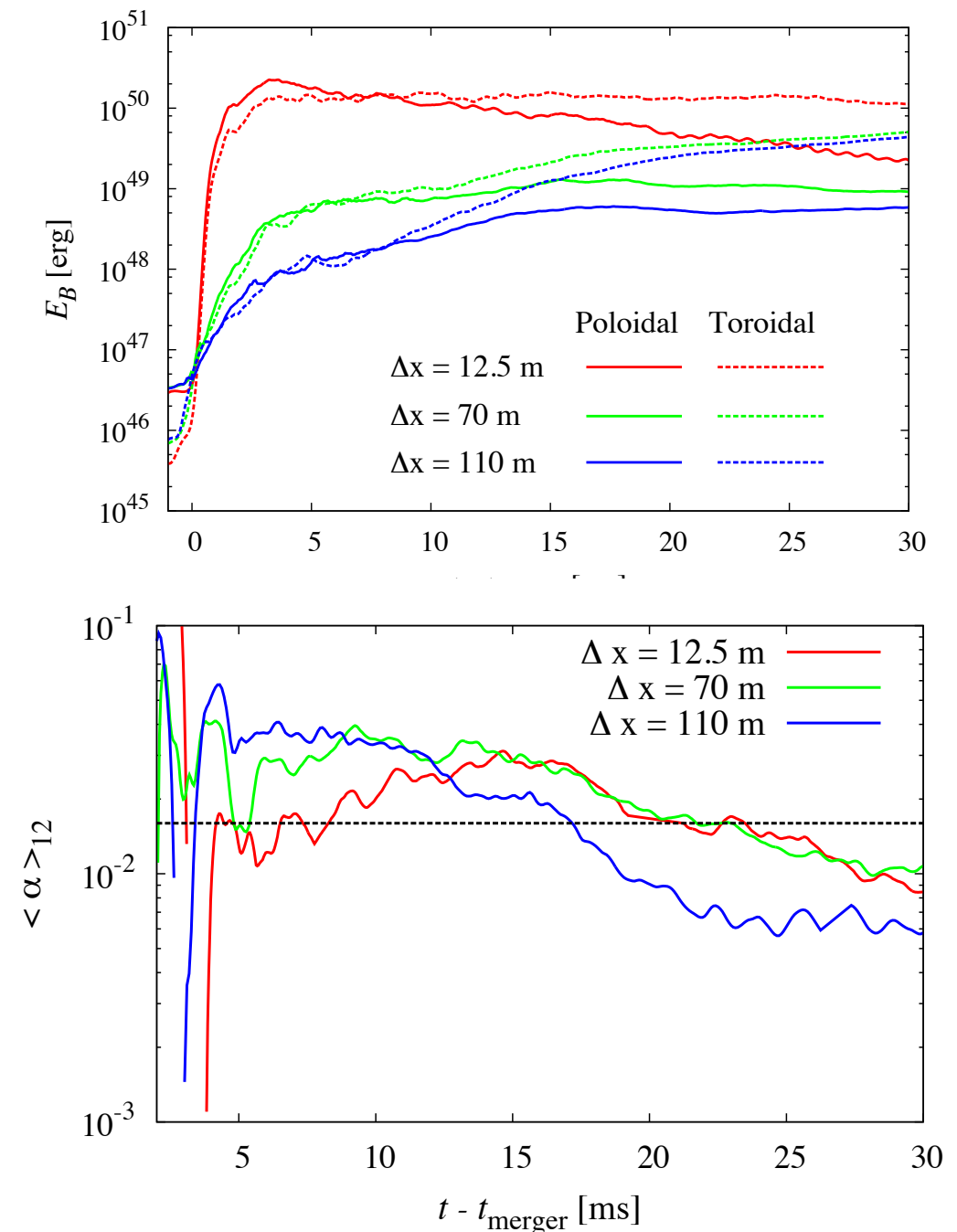
- For $M_{tot} < 2.8 M_{sun}$, NS likely to remain after the merger.
 → neutrino irradiation from the remnant NS would be important

Evolution of Remnant NS & torus: Effective viscosity

Turbulence in the contact surface → amplification of magnetic field
→ effective viscosity would play a role



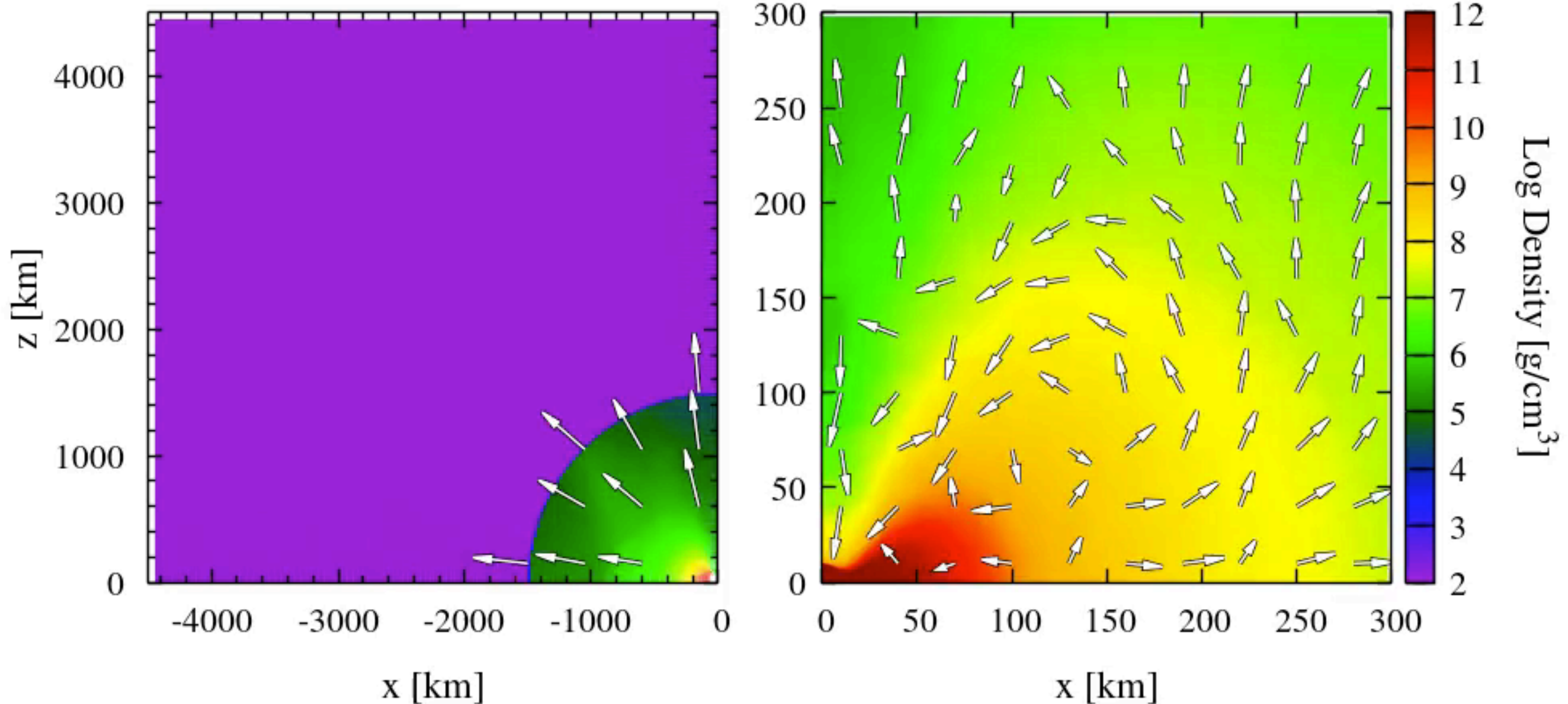
Ref: K. Kiuchi et al. 2015, 2017



Viscous-radiative simulation

Numerical-relativity simulation considering the effects of physical viscosity and neutrino radiation

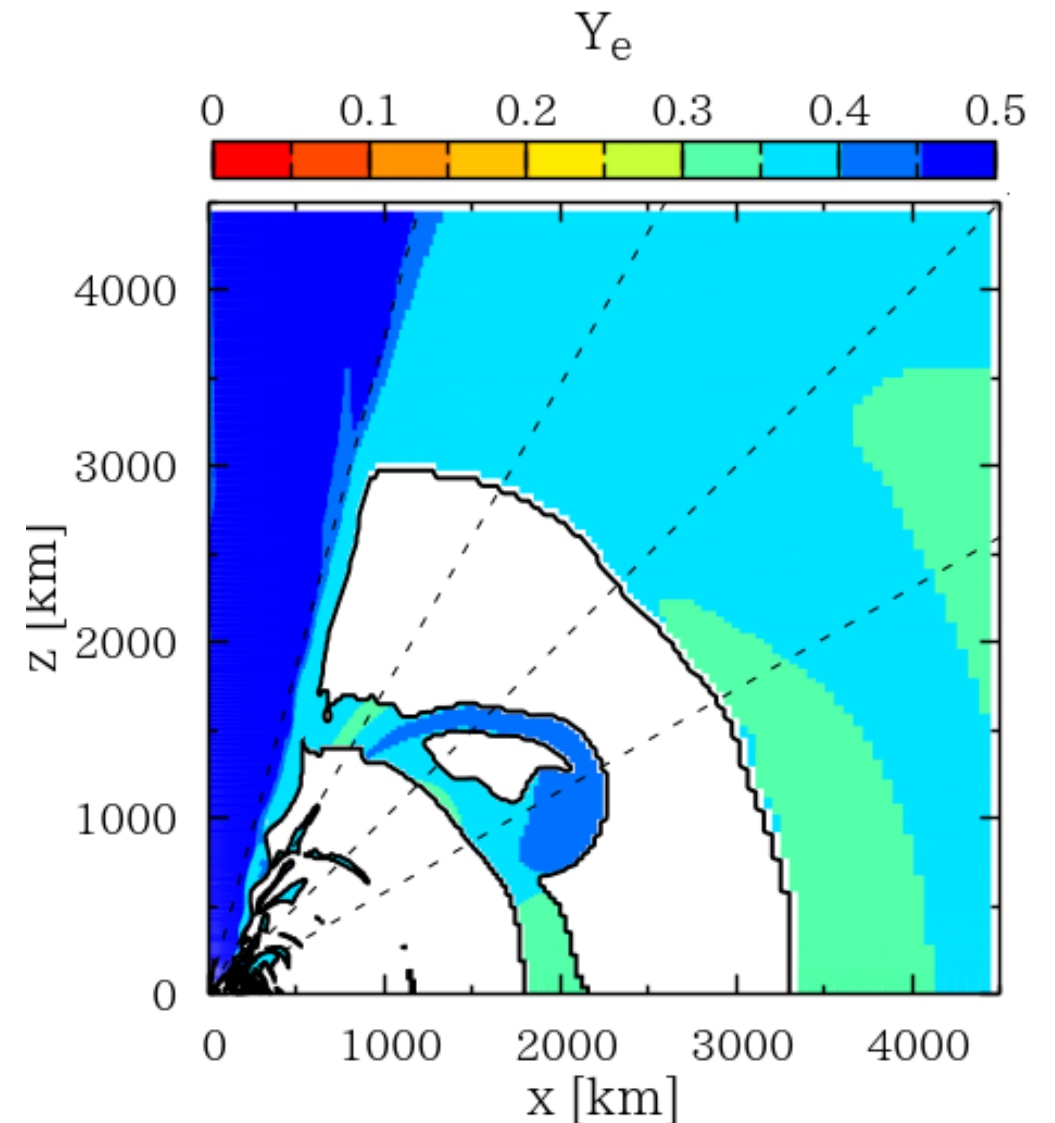
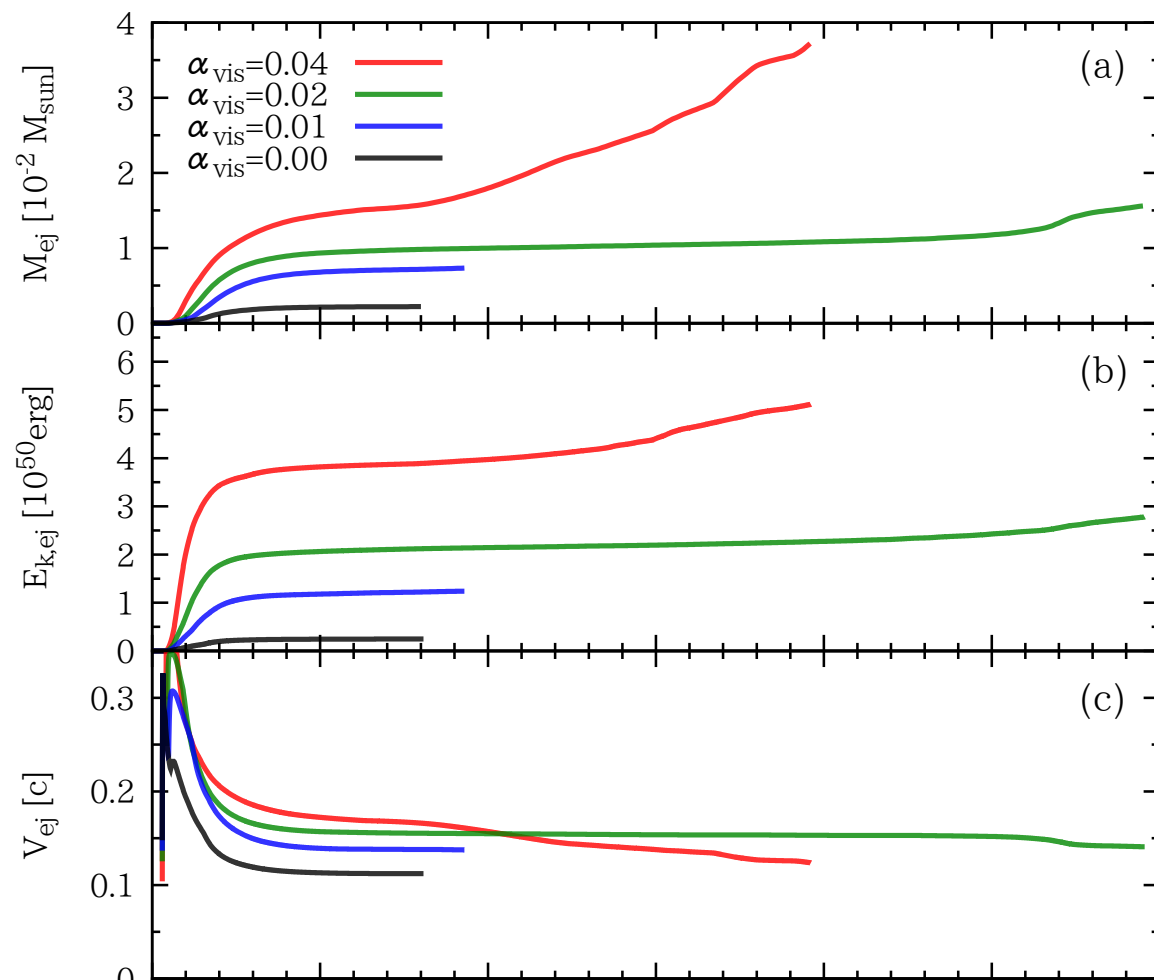
$t = 0.00$ ms



Ref: S. Fujibayashi et al. 2018

Post-merger mass ejection

Ref: S. Fujibayashi et al. 2018

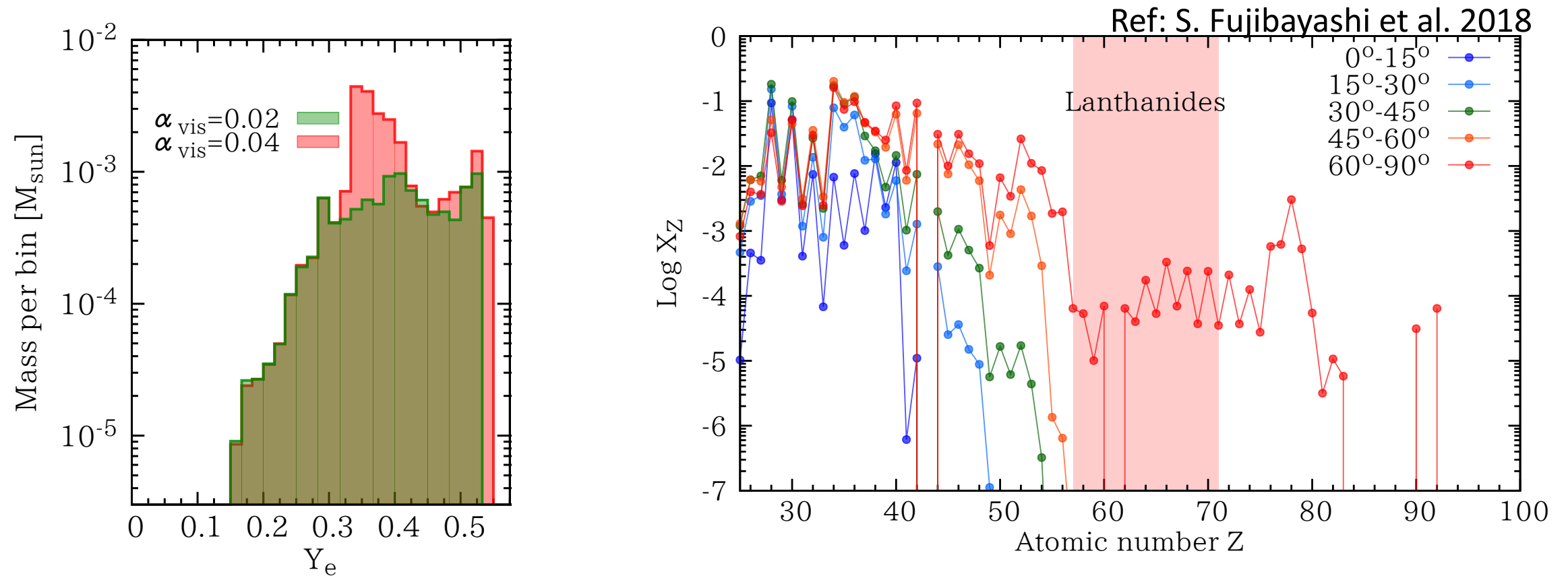


Ejecta mass $\sim 10^{-2} - 10^{-1} M_{\text{sun}}$

Typical velocity $0.03 - 0.15 c$

depending on the viscous parameter and
the lifetime of the remnant NS

Ye distribution



post-merger ejecta typically has $Y_e > 0.25$ due to neutrino irradiation
 \rightarrow lanthanide-free $\rightarrow \kappa \sim 0.1-1 \text{ cm}^2/\text{g}$

$$t_{\text{peak}} \approx 1.5 \text{ days} \left(\frac{M}{0.03 M_\odot} \right)^{1/2} \left(\frac{v}{0.1c} \right)^{-1/2} \left(\frac{\kappa}{0.1 \text{ cm}^2/\text{g}} \right)^{1/2}$$

$$L_{\text{peak}} \approx 4.3 \times 10^{41} \text{ ergs/s} \left(\frac{f}{10^{-6}} \right) \left(\frac{M}{0.03 M_\odot} \right)^{1/2} \left(\frac{v}{0.1c} \right)^{1/2} \left(\frac{\kappa}{0.1 \text{ cm}^2/\text{g}} \right)^{-1/2}$$

$$T_{\text{peak}} \approx 8.0 \times 10^3 \text{ K} \left(\frac{f}{10^{-6}} \right)^{1/4} \left(\frac{M}{0.03 M_\odot} \right)^{-1/8} \left(\frac{v}{0.1c} \right)^{-1/8} \left(\frac{\kappa}{0.1 \text{ cm}^2/\text{g}} \right)^{-3/8}$$

kilonova/macronova for different components

- **Dynamical mass ejection**

$M \sim 0.0001 - 0.01 M_{\text{sun}}$, $v \sim 0.1 - 0.2 c$

$Y_e \sim 0.1 - 0.5$

$\rightarrow t_{\text{peak}} \sim 10$ days,

long-lasting, dim, low temperature

(red) kilonova

- **Post-merger mass ejection**

$M \sim 0.01 - 0.1 M_{\text{sun}}$, $v \sim 0.03 - 0.15 c$

$Y_e \sim 0.3 - 0.4$

$\rightarrow t_{\text{peak}} \sim 1$ days,

short-lasting, bright, high temperature

(blue) kilonova

Dynamical ejecta

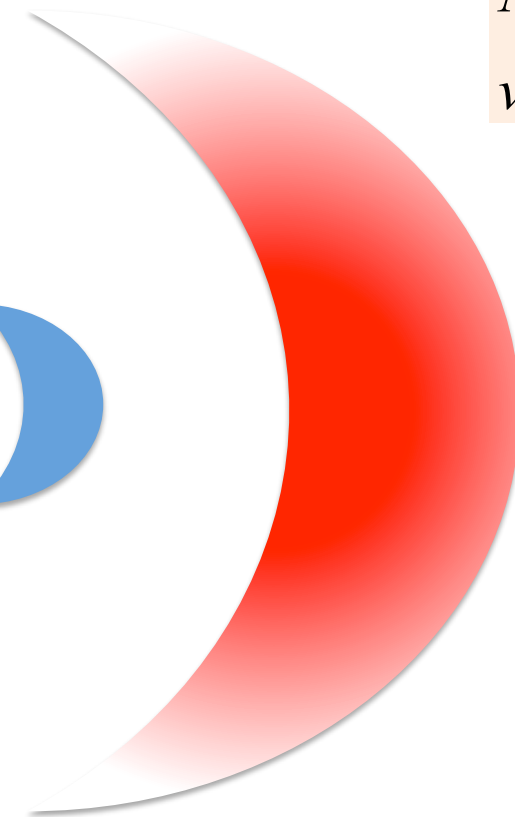
$$Y_e \sim 0.05 - 0.5$$

$$\rightarrow \kappa \sim 10 \text{ cm}^2 / \text{g}$$

$$M \sim 10^{-2} M_{\odot}$$

$$v / c = 0.1 - 0.9$$

Remnant
MNS



Post-merger ejecta

$$Y_e \sim 0.3 - 0.4$$

$$\rightarrow \kappa \sim 0.1 \text{ cm}^2 / \text{g}$$

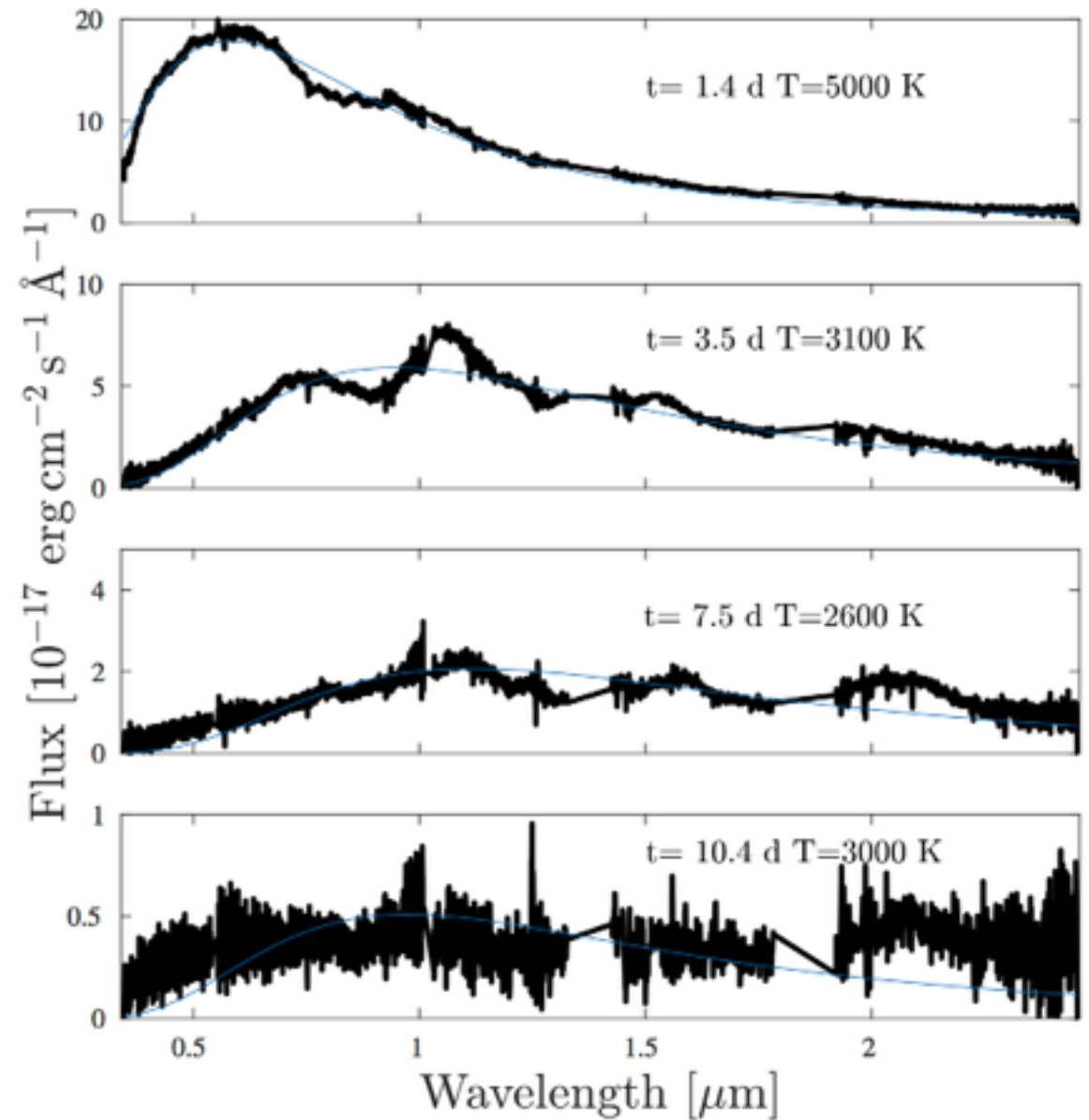
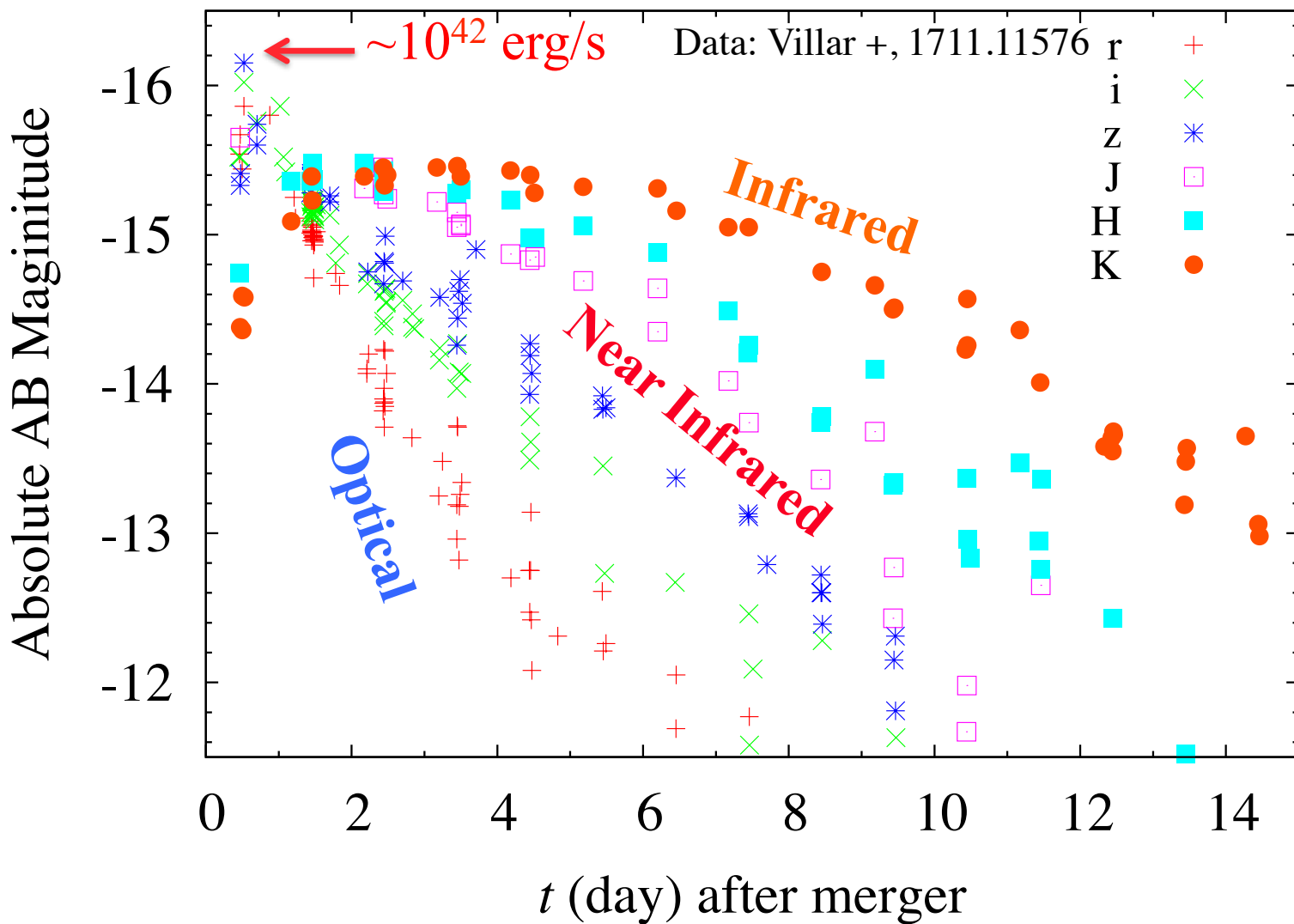
$$M \sim 3 \times 10^{-2} M_{\odot}$$

$$v / c = 0.03 - 0.1$$

SSS17a (GW170817)

Ref: Waxman et al. 2017

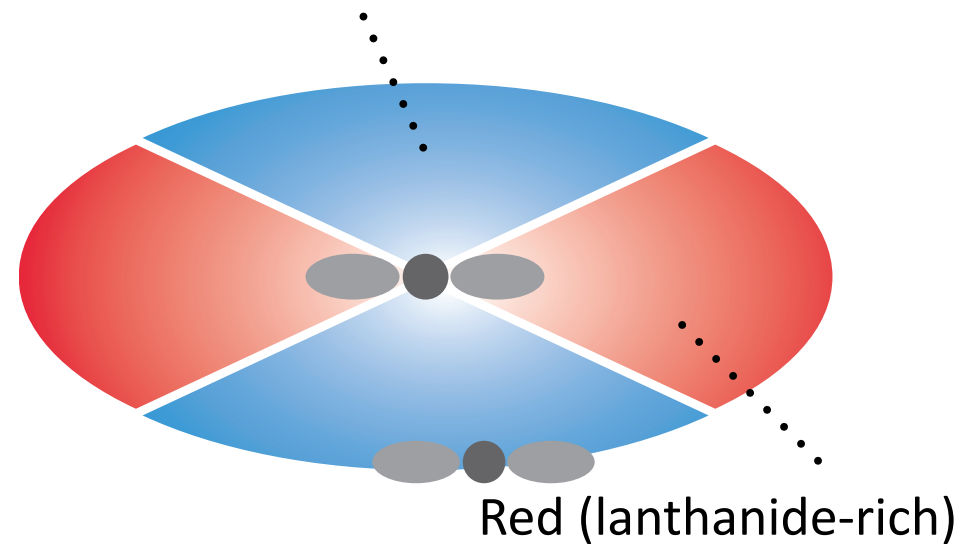
Optical-IR EM counterparts of GW170817



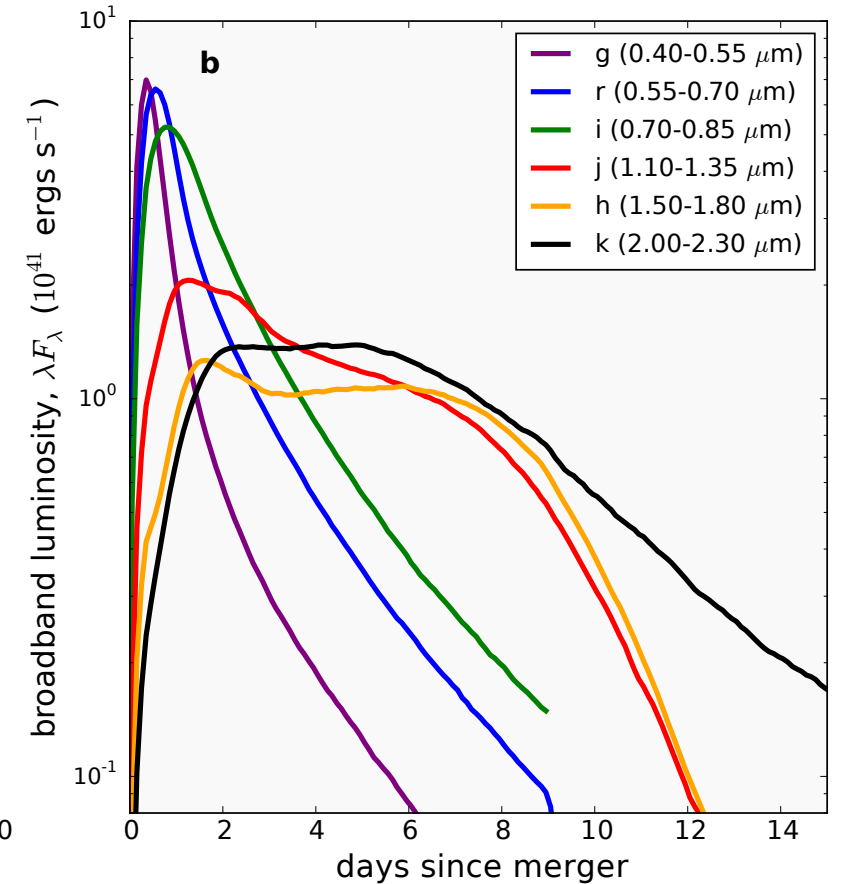
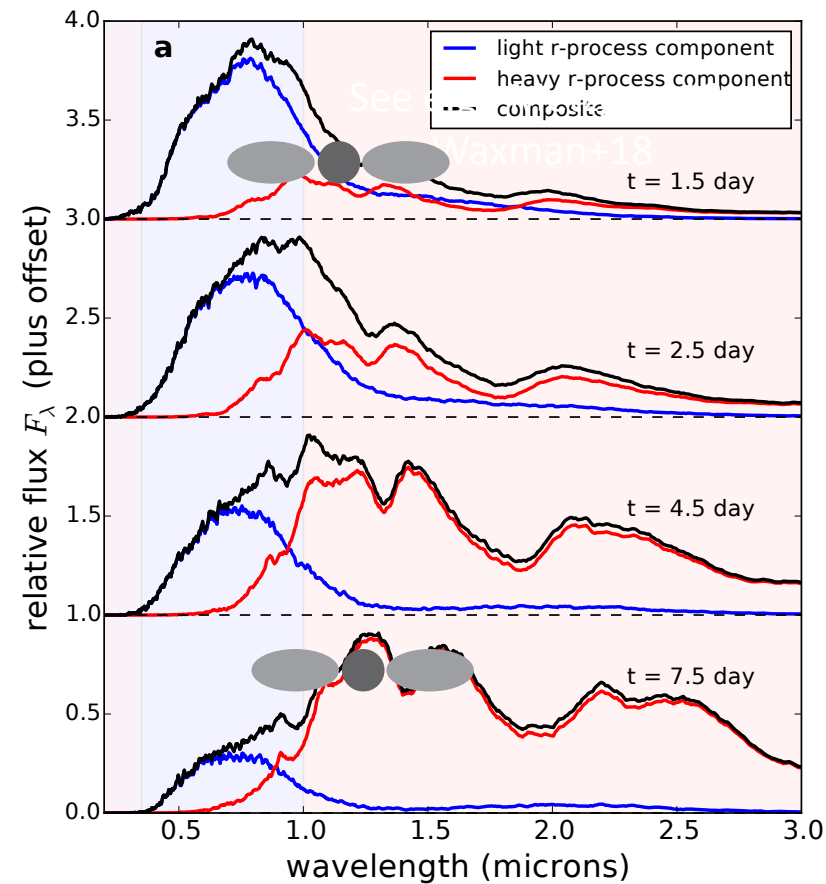
ref) Shibata-san's slide

Multiple component Kilonovae/macronovae

Blue (lanthanide-free)



ref) Tanaka-san's slide



Ref: D. Kasen et al. 2017

- Kilonova/macronova model with multiple components well interprets the observation (see e.g., Kasliwal et al. 2017, Cowperthwaite et al. 2017, Kasen et al. 2017, Villar et al. 2017)
- early-blue component (~ 1 day) from lanthanide-free ejecta
- + long-lasting red component (~ 10 days) from lanthanide-rich ejecta

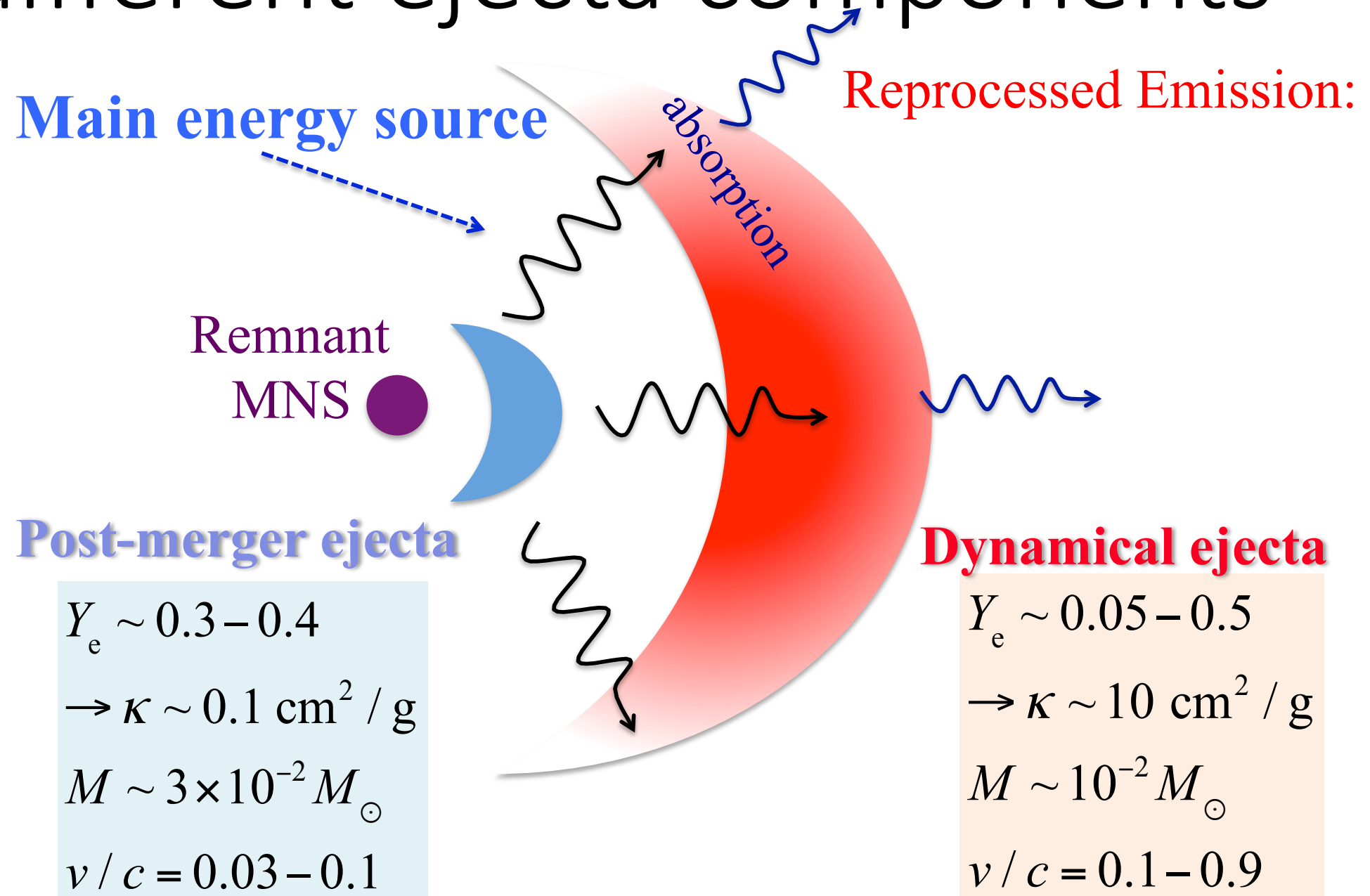
Problems

- Multiple component ejecta kilonova/macronova seem to work, but...

Figure 5 | A unified kilonova model explaining the optical/infrared counterpart of GW170817. The model is the superposition of the emission from two spatially distinct ejecta components: a ‘blue’ kilonova (light r-process ejecta with $M = 0.025M_{\odot}$, $v_k = 0.3c$ and $X_{\text{lan}} = 10^{-4}$) plus a ‘red’ kilonova (heavy r-process ejecta with $M = 0.04M_{\odot}$, $v_k = 0.15c$, and $X_{\text{lan}} = 10^{-1.5}$). **a**, Optical–infrared spectral time series, where the black line is the sum of the light r-process (blue line) and heavy r-process (red line) contributions.

- lanthanide-rich ejecta with $>0.01 M_{\text{sun}}$ seems too large for the dynamical ejecta (typically less than $0.01 M_{\text{sun}}$)
Ref: D. Kasen et al. 2017
- velocity of lanthanide-free ejecta $\sim 0.3 c$ is too high for the post-merger ejecta (typically $\sim 0.05 c$)
- Tension between observed properties and predictions of numerical relativity? (e.g., Waxman et al. 2017, Metzger et al. 2018, Matsumoto et al. 2018)
- **Photon interplay between the dynamical & post-merger ejecta is not taken into account (only simple composition of each lightcurve)**

Radiative transfer between different ejecta components



We perform an axisymmetric radiative transfer simulation for kilonovae/macronovae taking the interplay of multiple ejecta components of non-spherical morphology into account. (KK. et al 2018, see also Perego et al. 2017 for studies with similar setups)

Radiative transfer simulation

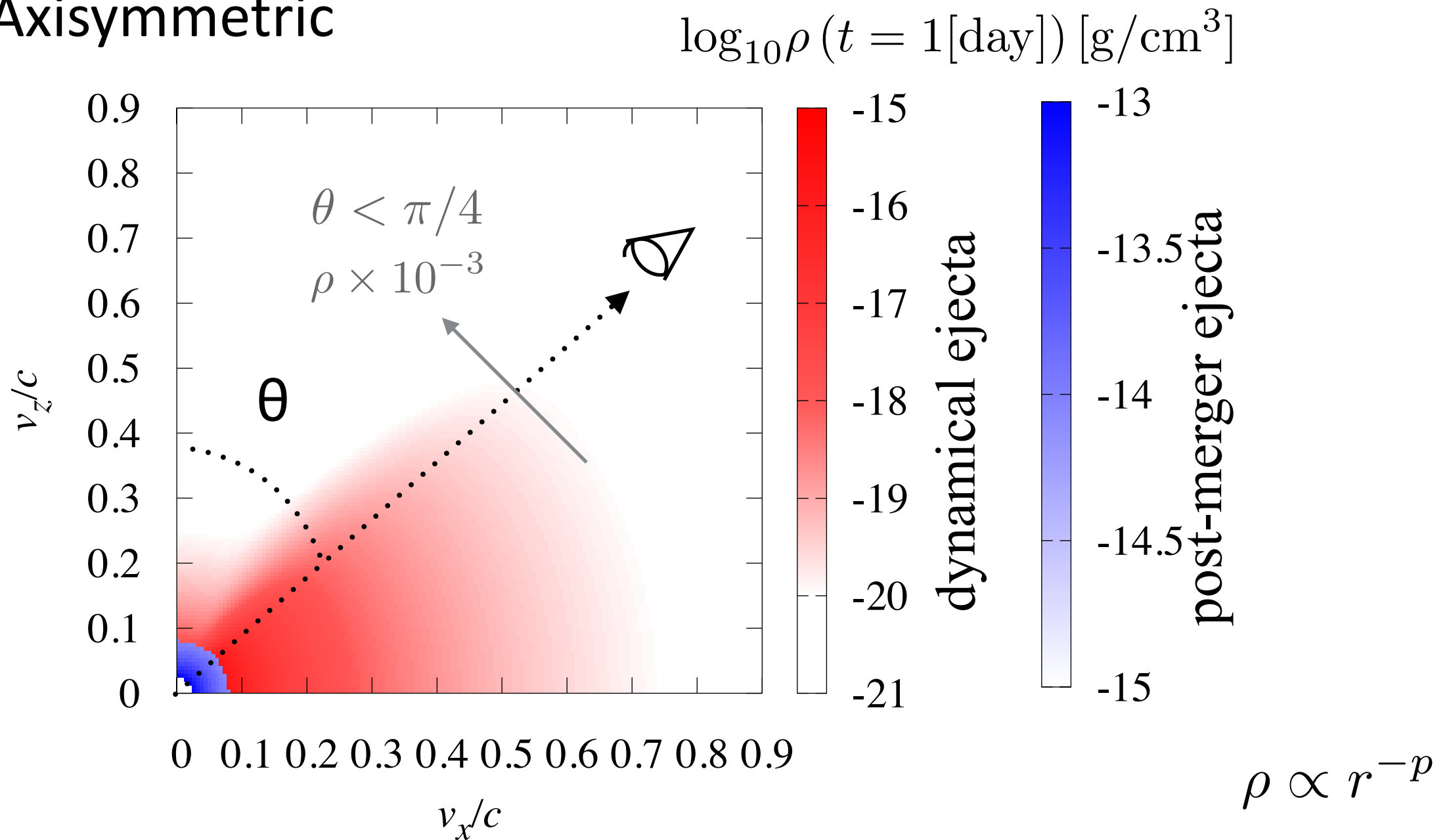
- We employ a wavelength-dependent Monte-Carlo radiative transfer simulation code (M. Tanaka et al. 2013, 2014, 2017)
- The density, velocity, and Ye profiles of ejecta are employed within the range of predictions by numerical-relativity simulations.
(e.g., Dietrich et al. 2016, Hotokezaka et al. 2018, Metzger&Fernandez et al. 2014, Fujibayashi et al. 2018)
- The abundance pattern and nuclear heating rate are given based on r-process nucleosynthesis calculations by (Wanajo et al. 2014)
- Realistic opacity table constructed by the atomic structure calculations (Se, Ru, Te, Nd, and Er)

improved points

- The grid resolution of the simulation is also improved by an order of magnitude from our previous works by imposing axisymmetry.
- special-relativistic effects on photon transfer are fully taken into account

Density distribution

Axisymmetric

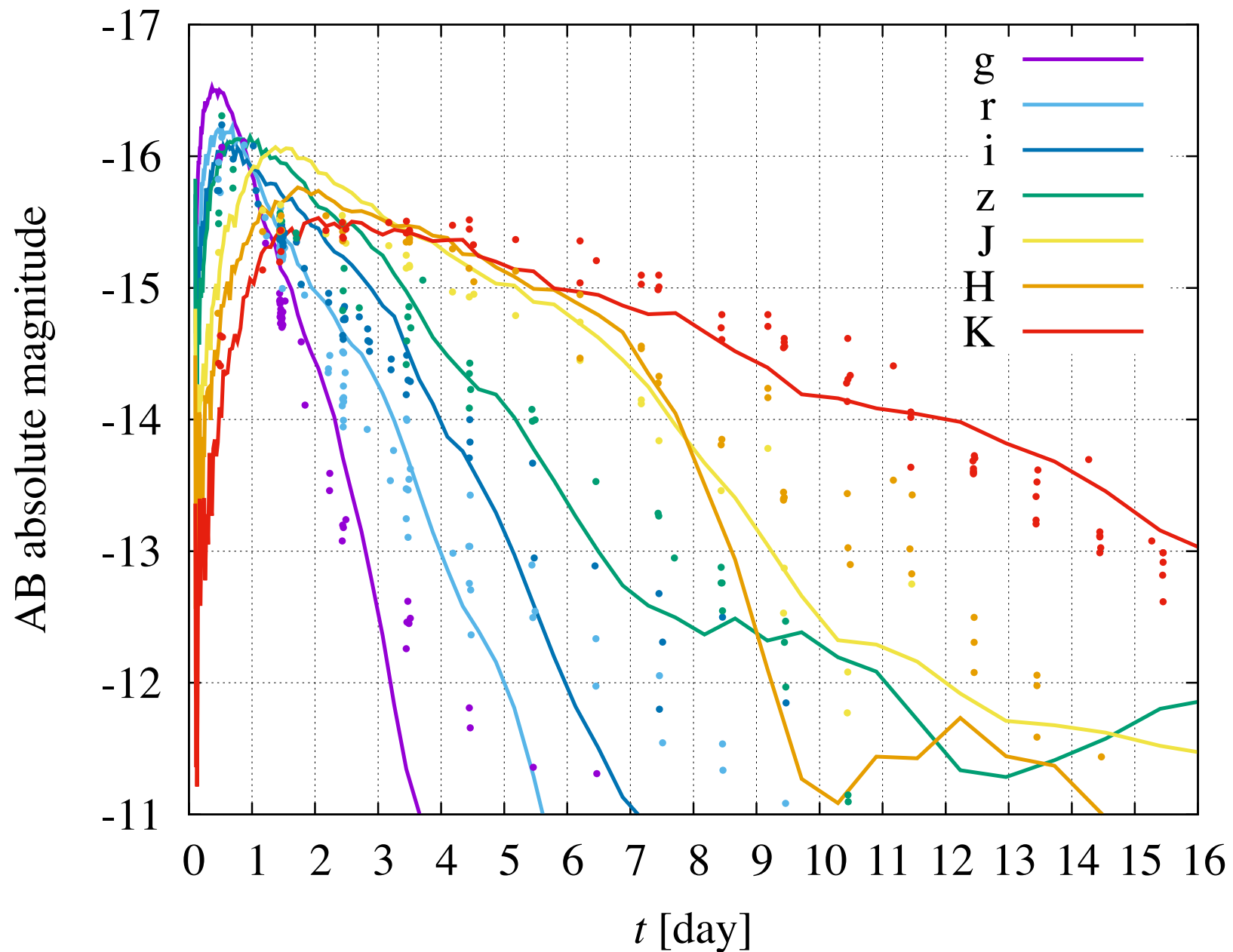


Dynamical ejecta: **0.009 M_sun**, 0.08—0.9 c, $Y_e=0.1-0.4$, $p=-6$

Post-merger ejecta: 0.02 M_sun, **0.025—0.08 c**, $Y_e=0.3-0.4$, $p=-3$

Results: Light curves

D=40 Mpc, $20^\circ \leq \theta < 28^\circ$



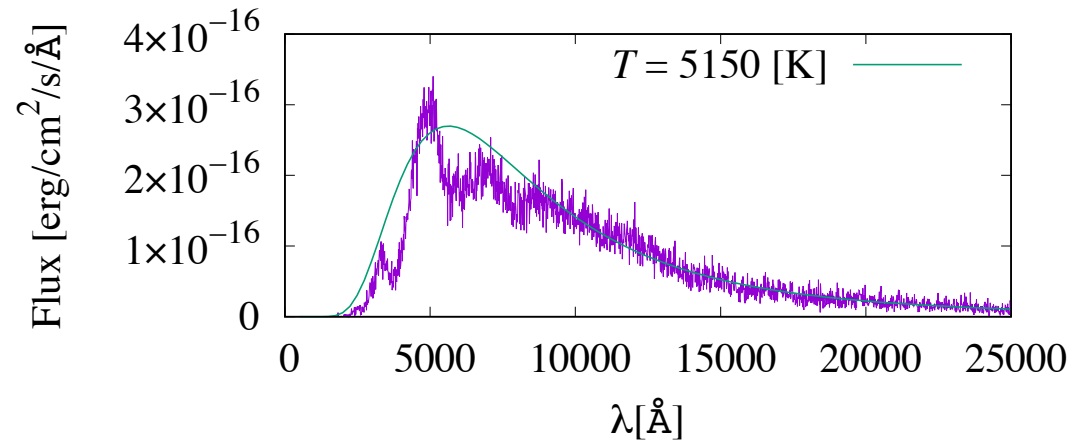
Host galaxy NGC4993: ~ 40 Mpc

GW data analysis gave a constraint on $\theta < \sim 30^\circ$

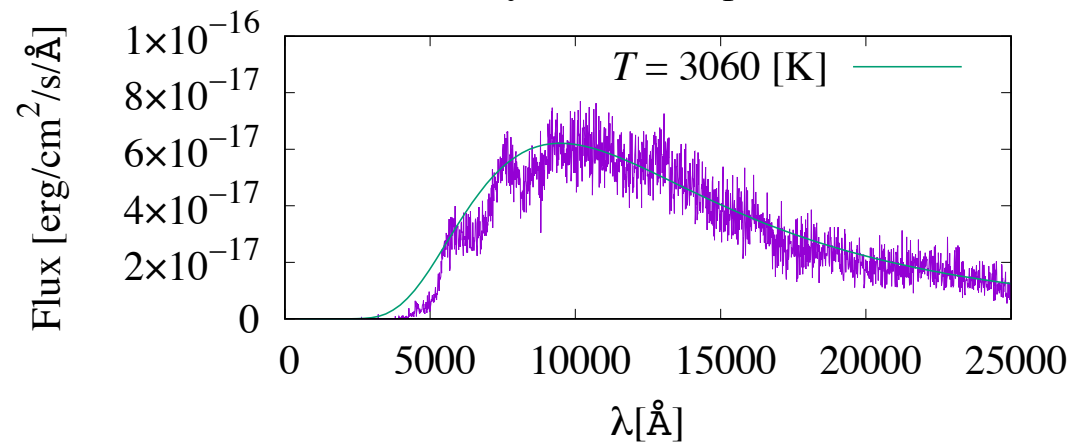
Spectra

Our model

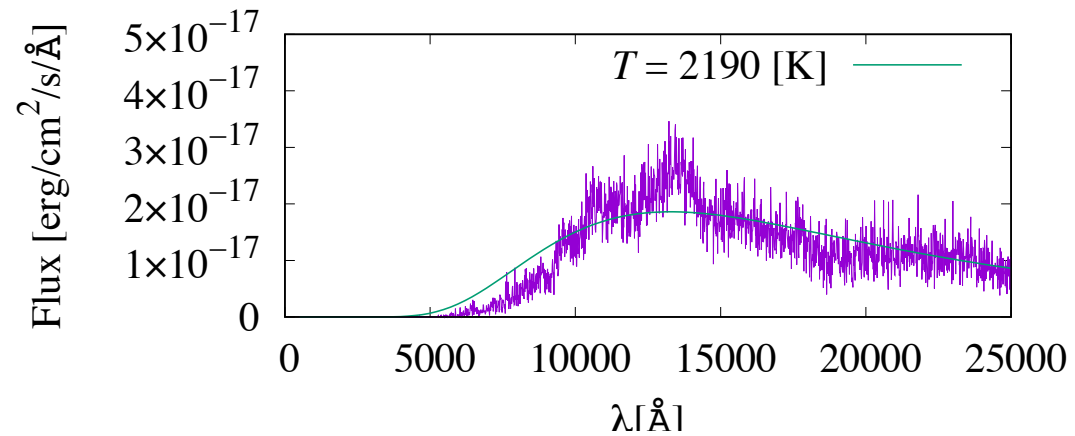
$t = 1.4$ [day], $D = 40$ Mpc, $20^\circ \leq \theta < 28^\circ$



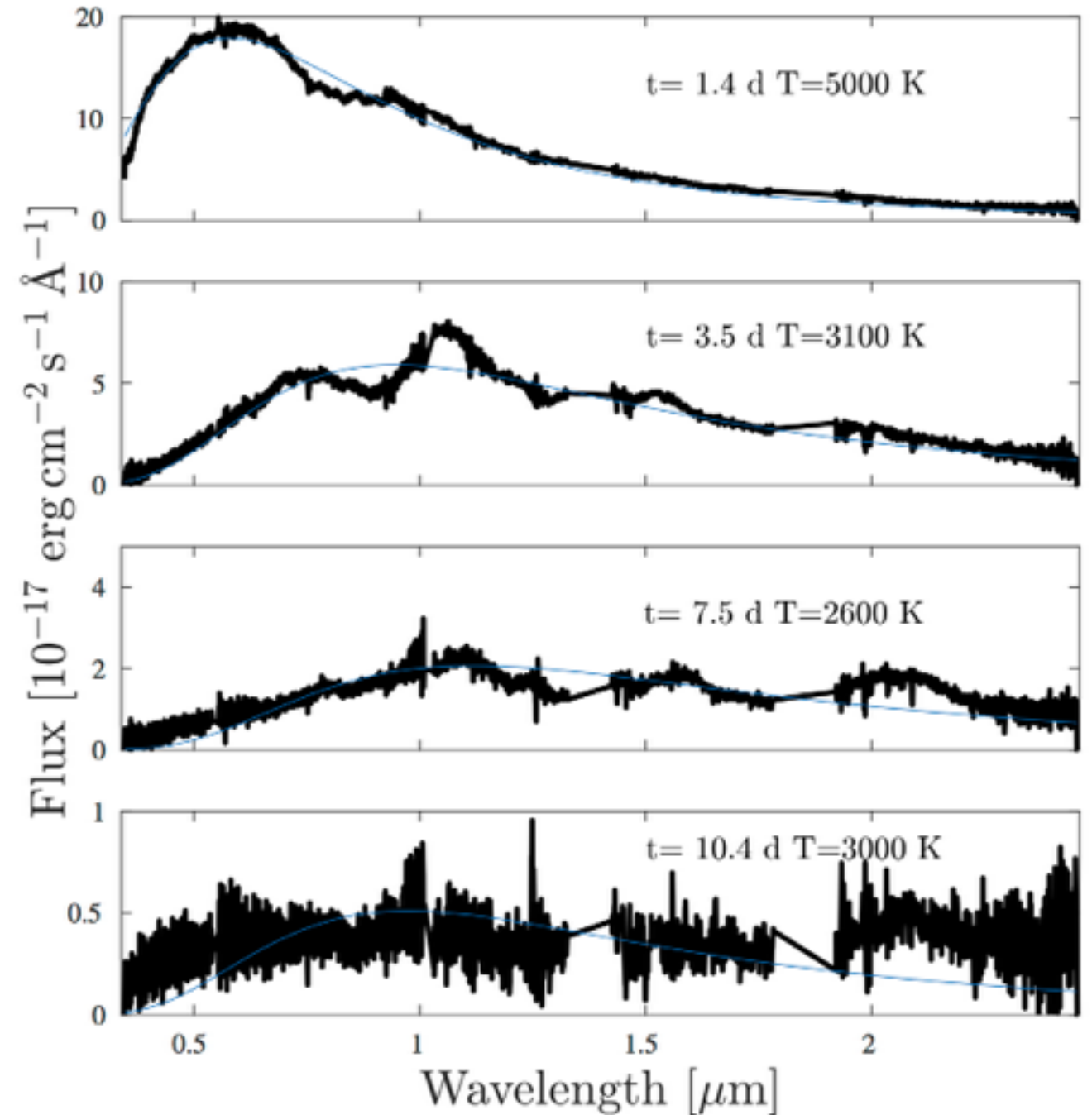
$t = 3.7$ [day], $D = 40$ Mpc, $20^\circ \leq \theta < 28^\circ$



$t = 6.8$ [day], $D = 40$ Mpc, $20^\circ \leq \theta < 28^\circ$

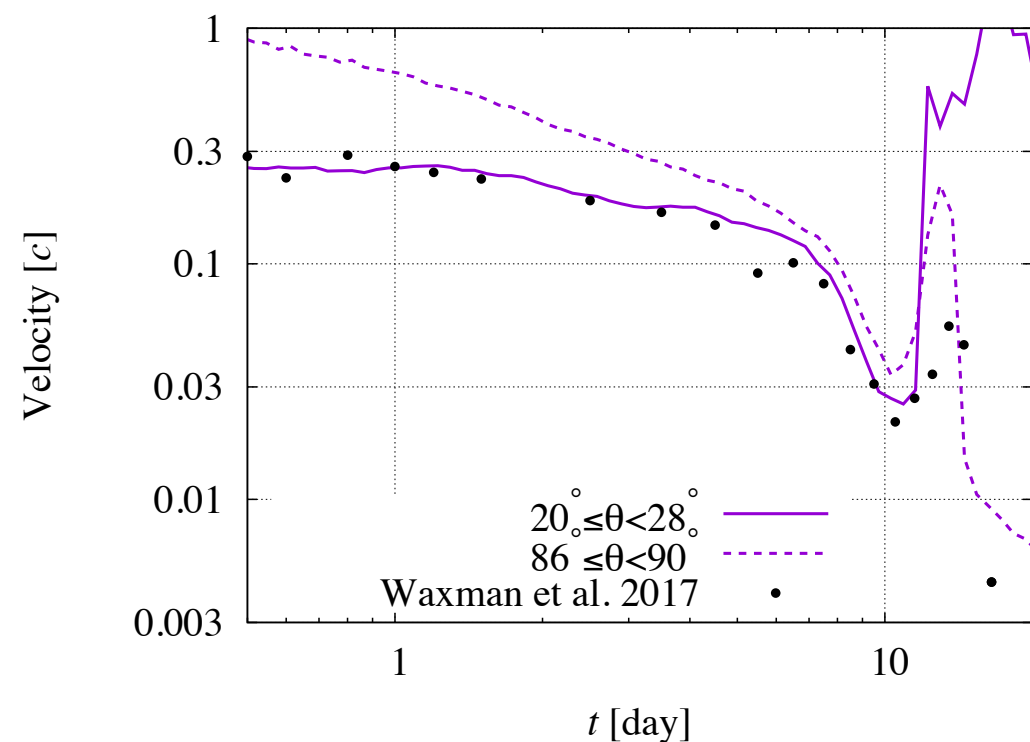
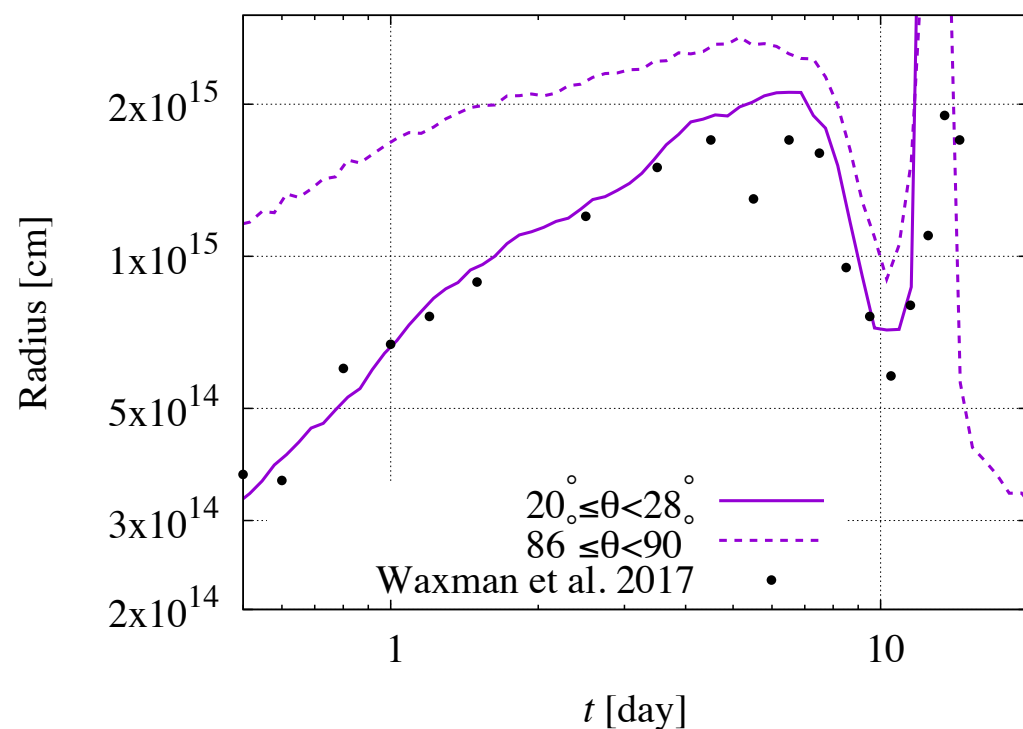
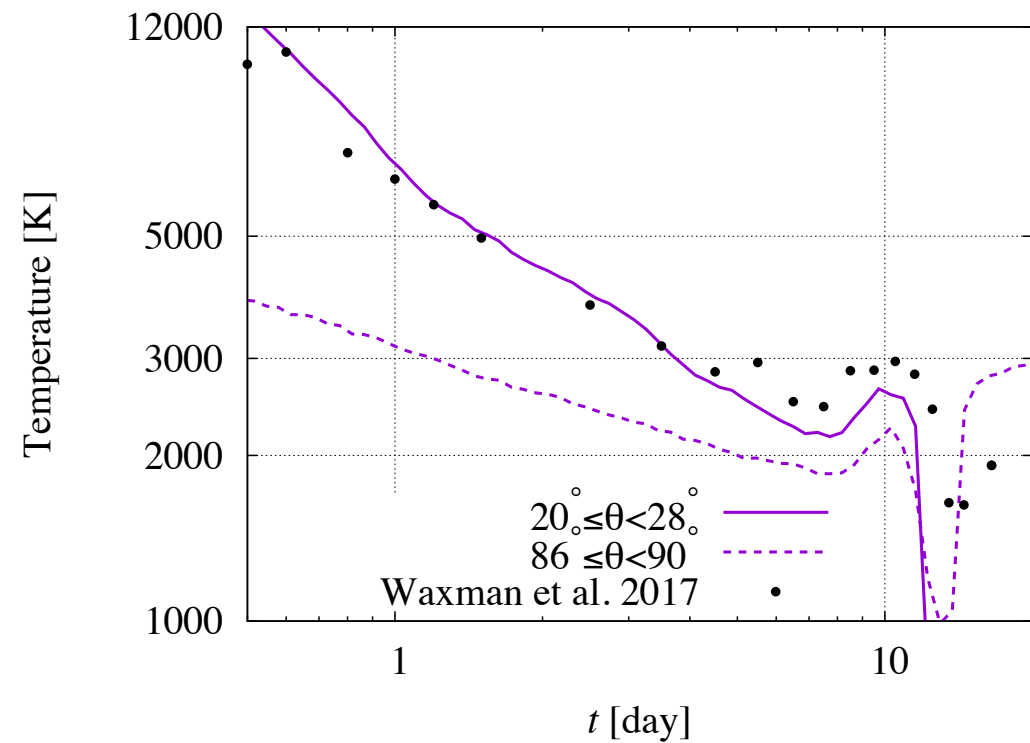
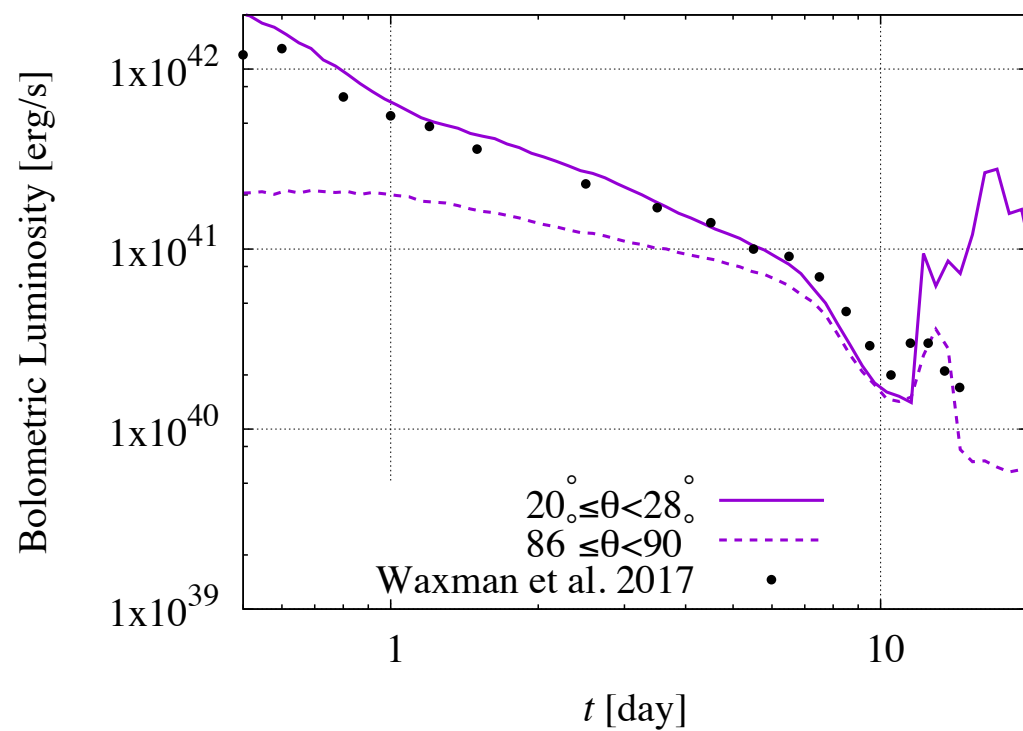


Observation



Photospheric quantities

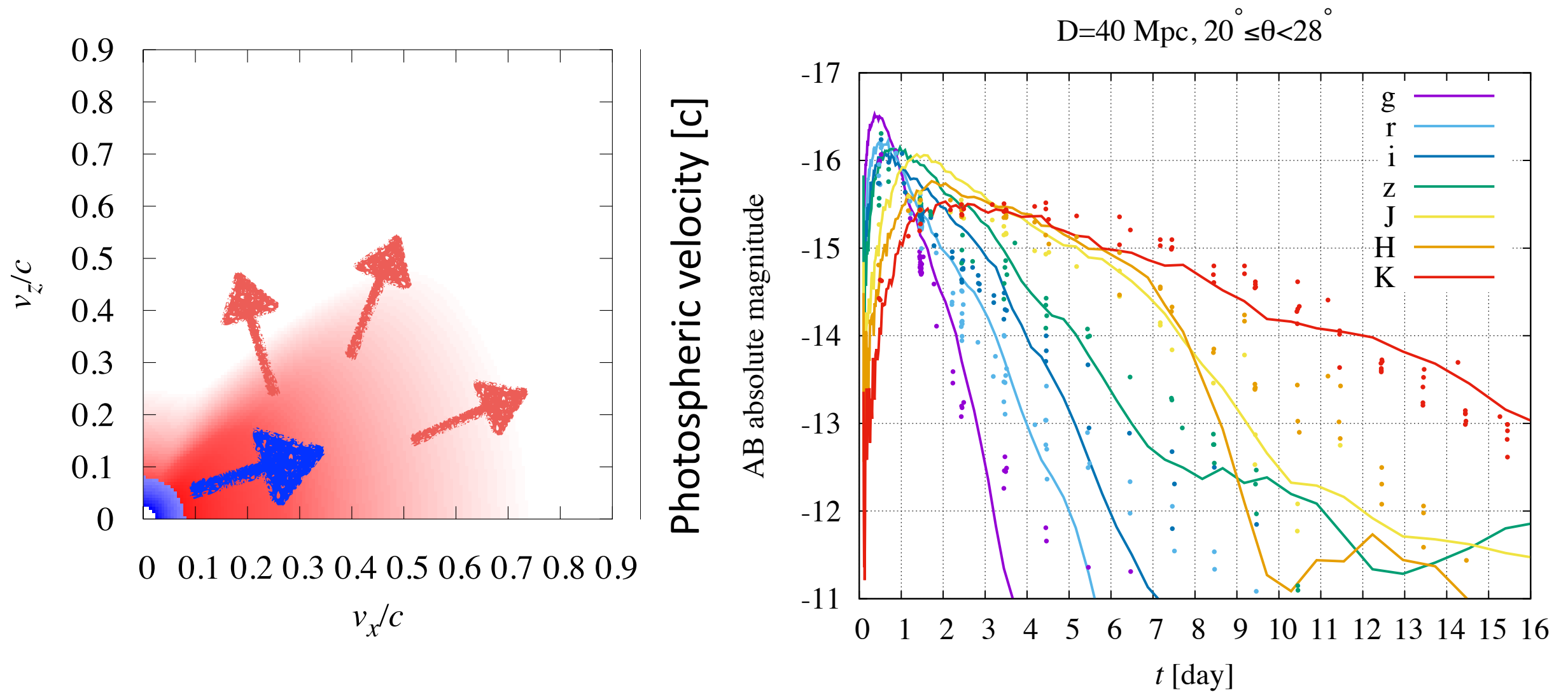
$$L_{\text{bol}} = 4\pi\sigma R_{\text{ph}}^2 T_{\text{ph}}^4 \quad v_{\text{ph}} = R_{\text{ph}}/t$$



Important points

- **A smaller value of mass the dynamical ejecta ($\sim 0.01 M_{\text{sun}}$)** than previous studies is needed for reproducing the observed lightcurves, which agrees with the prediction of NR simulations
- **Velocity of the post-merger ejecta ($\sim 0.05 c$)** also agrees within the prediction of NR simulations
- **The total mass of ejecta is smaller** than the prediction of previous studies ($\sim 0.04-0.08 M_{\text{sun}}$ \rightarrow $\sim 0.03 M_{\text{sun}}$)

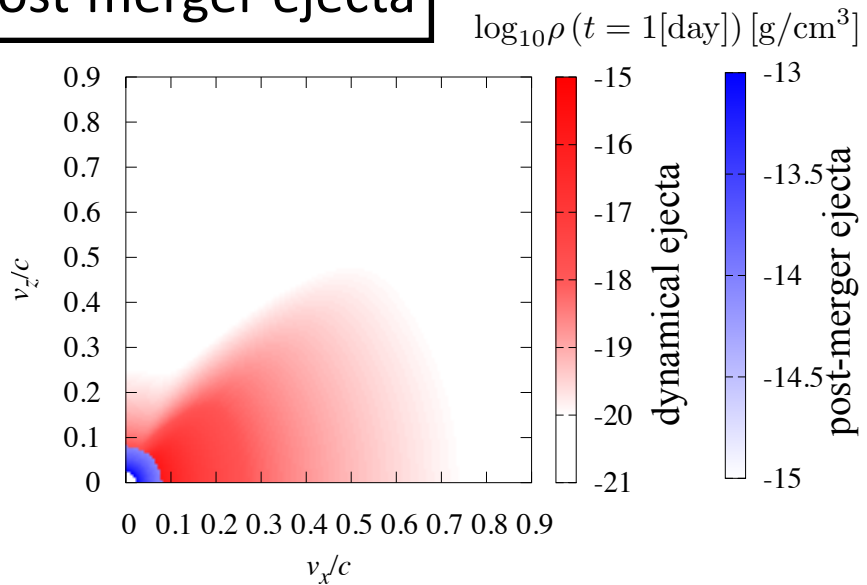
Heating up of dynamical ejecta by post-merger ejecta



- post-merger ejecta irradiate and heat up the dynamical ejecta, and help the long-lasting NIR lightcurves to be reproduced by less massive dynamical ejecta (see also Perego et al. 2017)

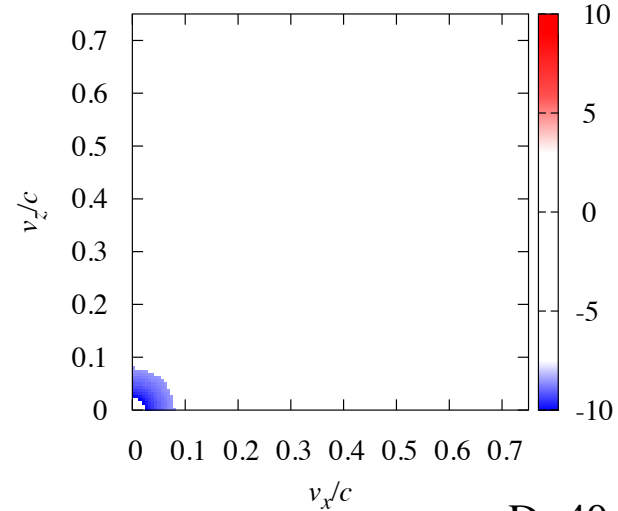
Comparison with composited lightcurves

dynamical
+ post-merger ejecta

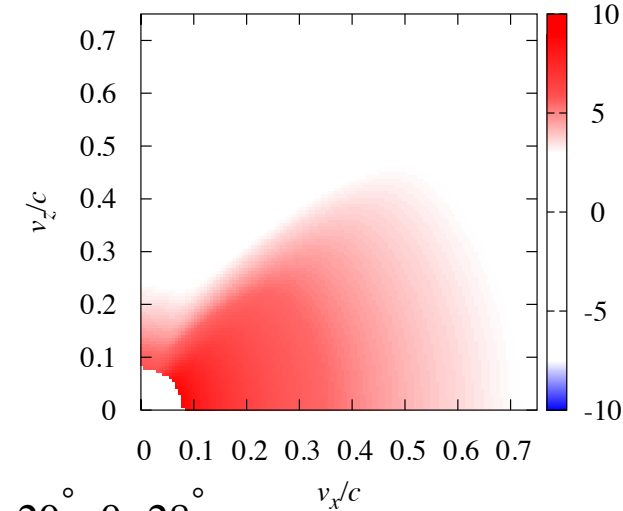


$D=40 \text{ Mpc}, 20^\circ \leq \theta < 28^\circ$

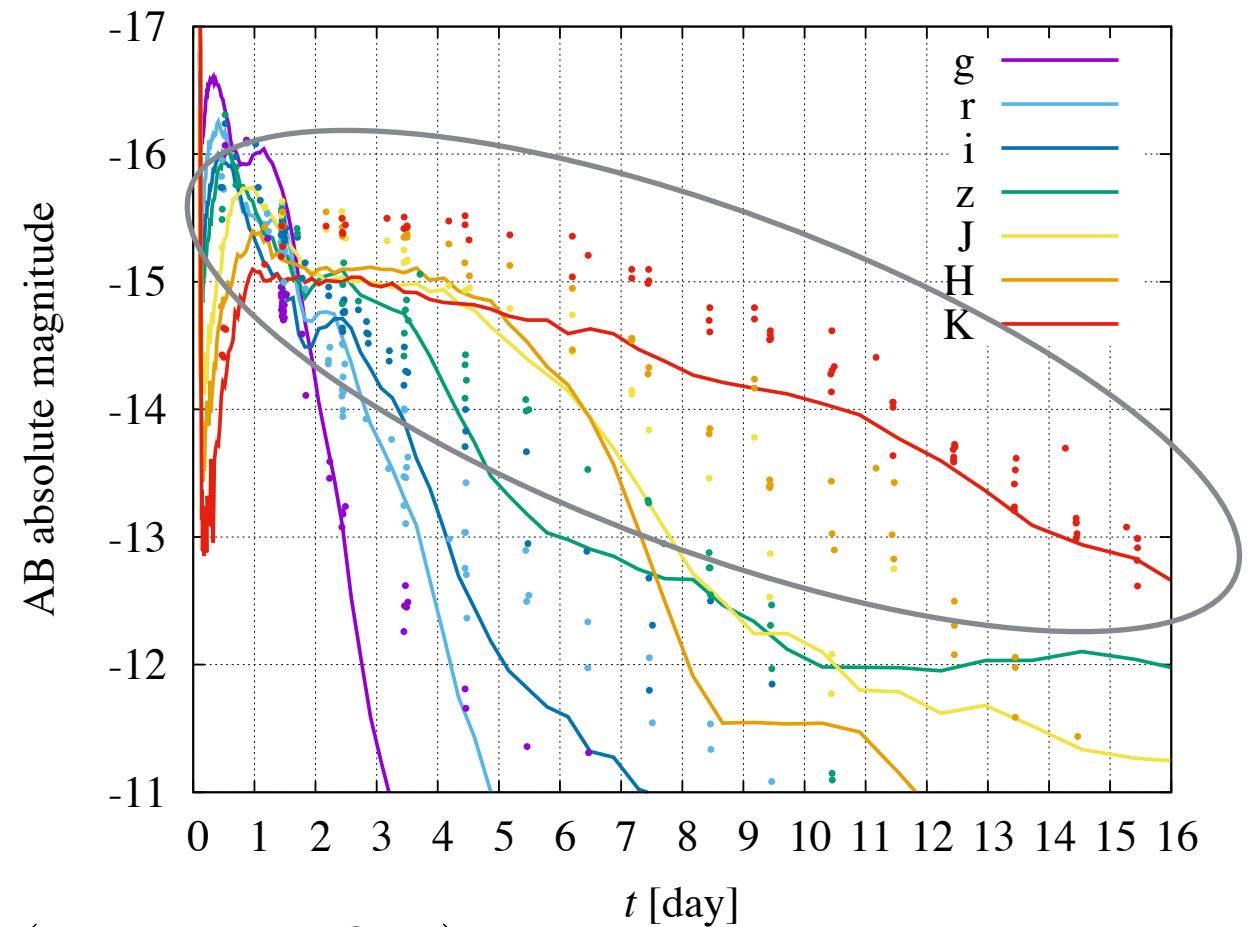
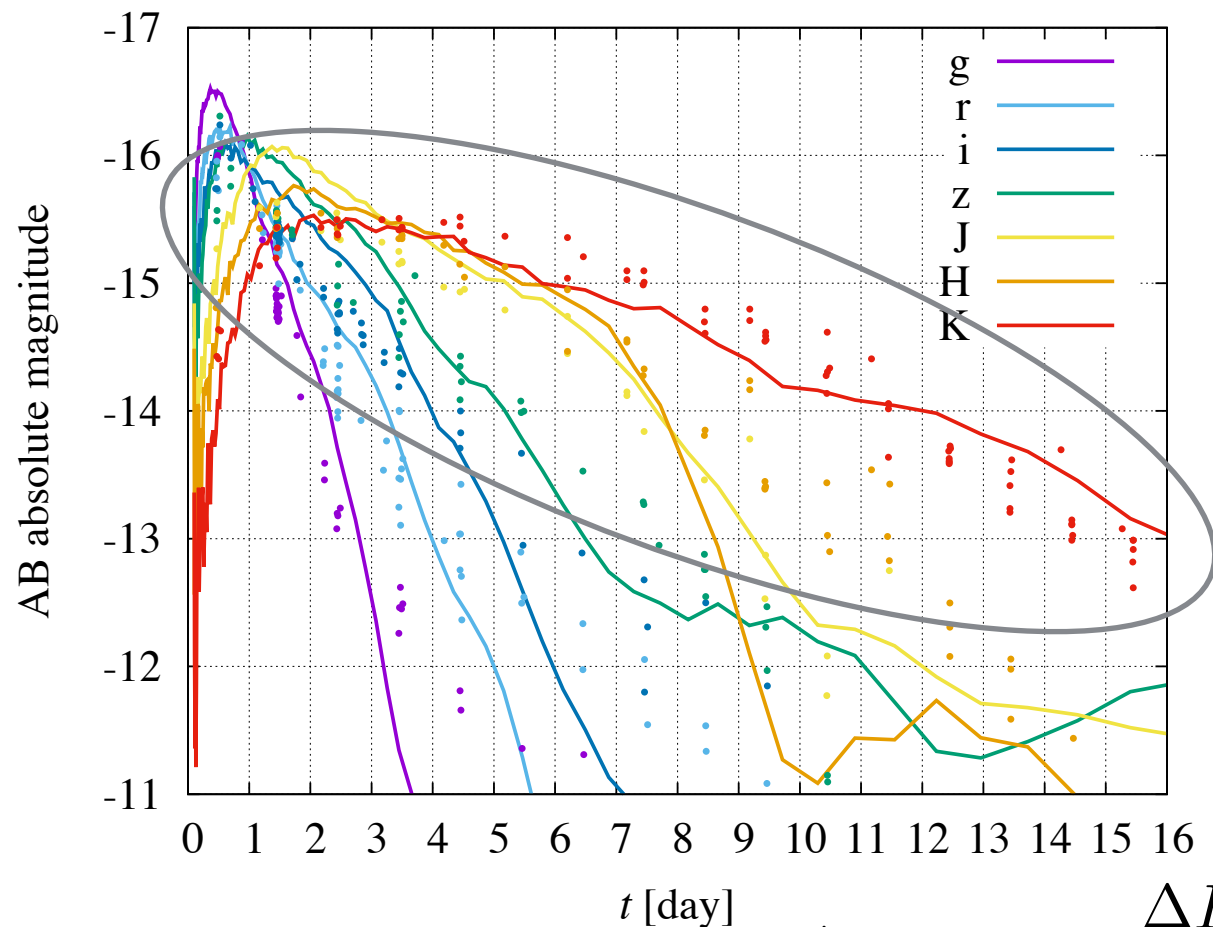
Only post-merger ejecta



Only dynamical ejecta



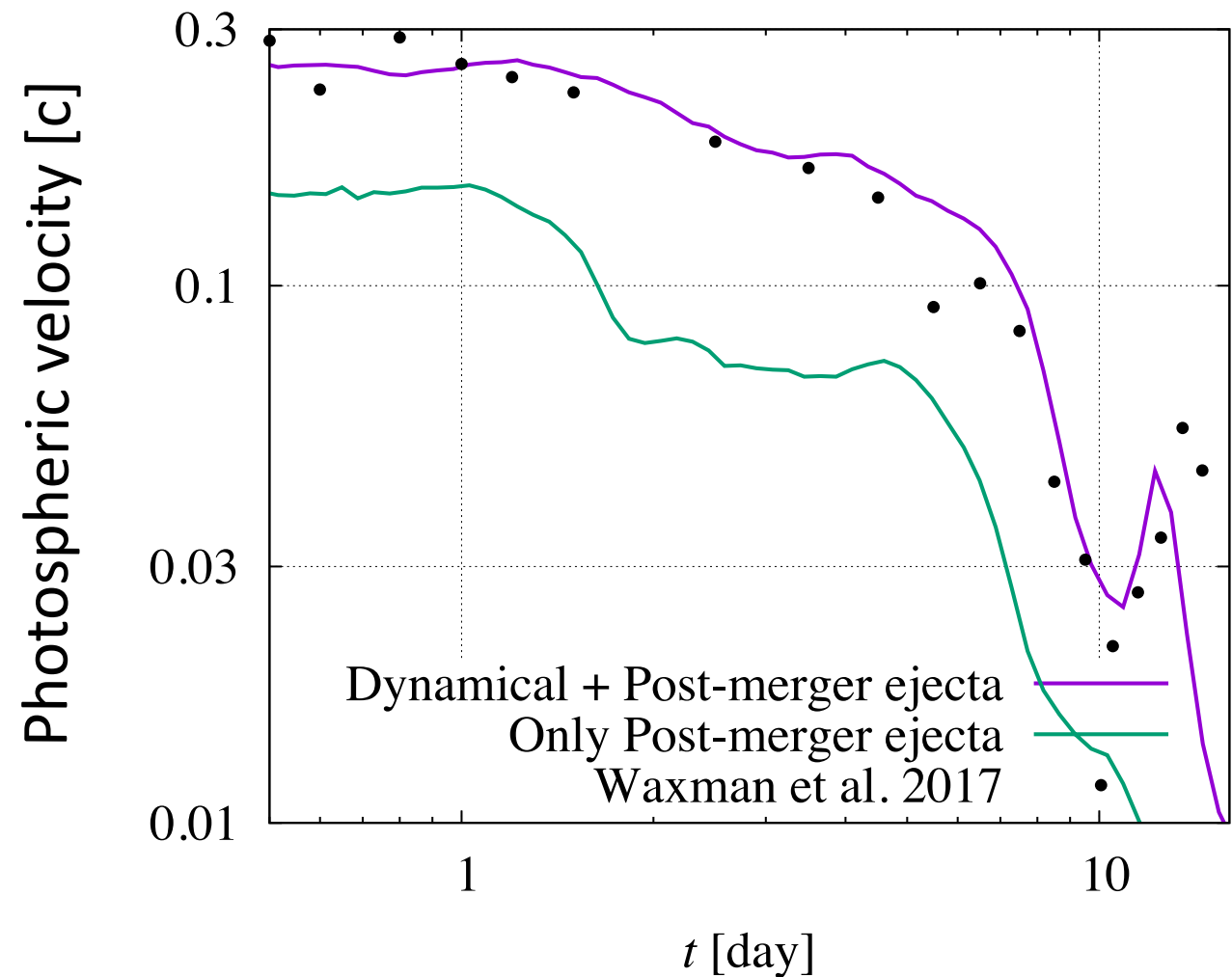
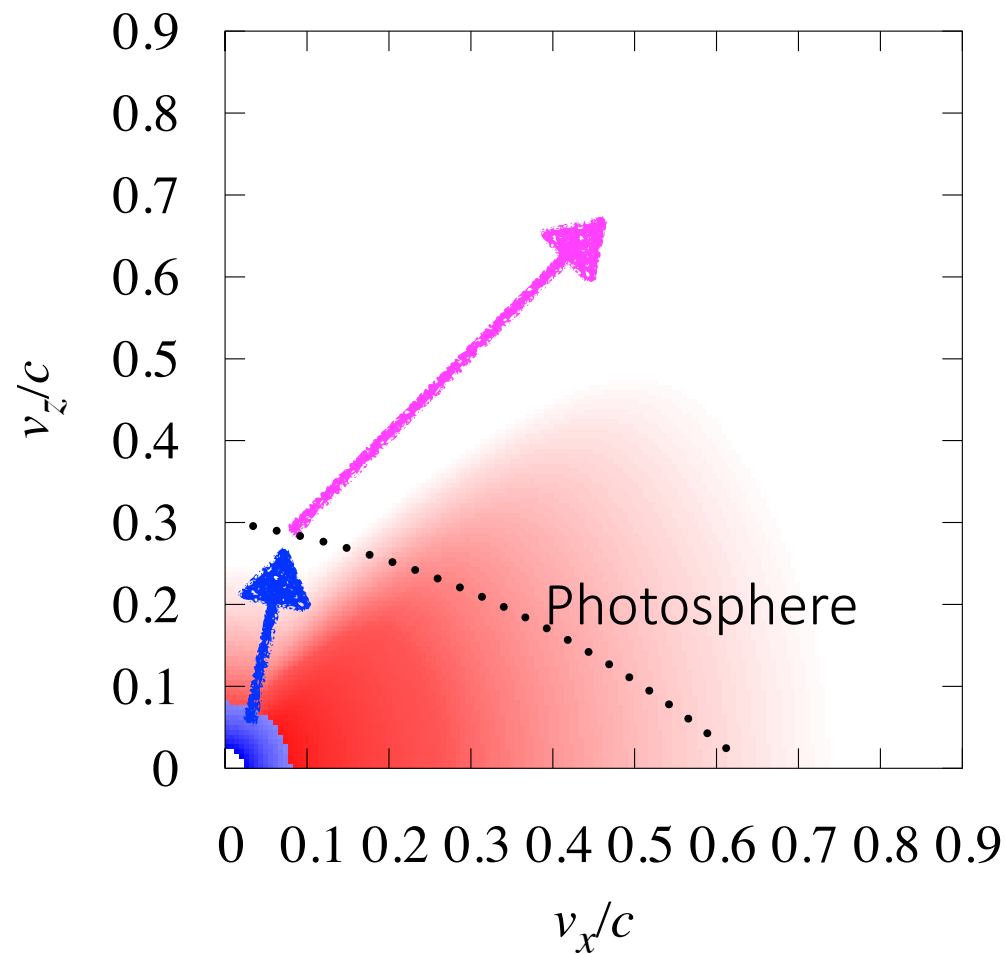
$D=40 \text{ Mpc}, 20^\circ \leq \theta < 28^\circ$



$$\Delta M = 1 \rightarrow \frac{\Delta F}{F} \approx 2.5 \quad (F : \text{energy flux})$$

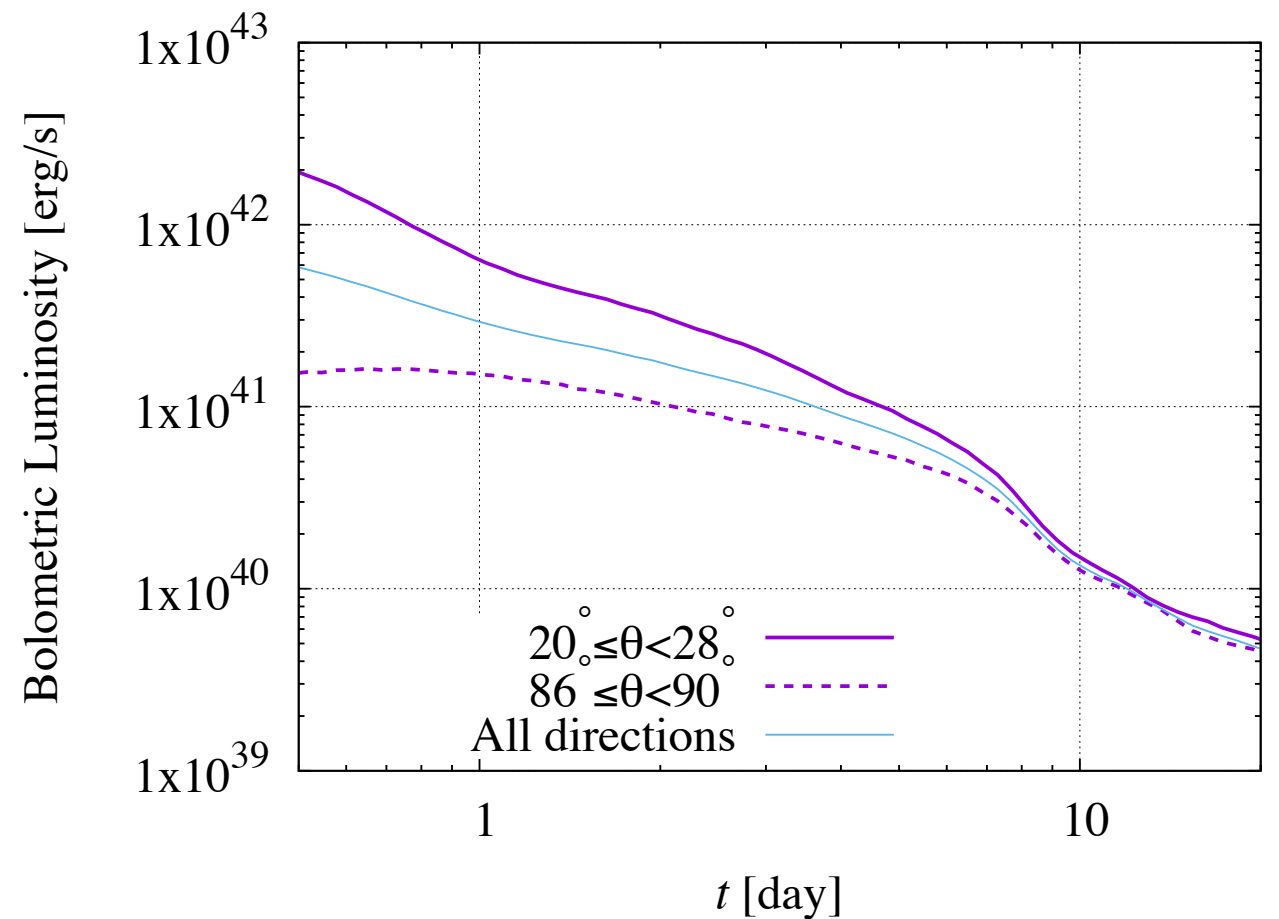
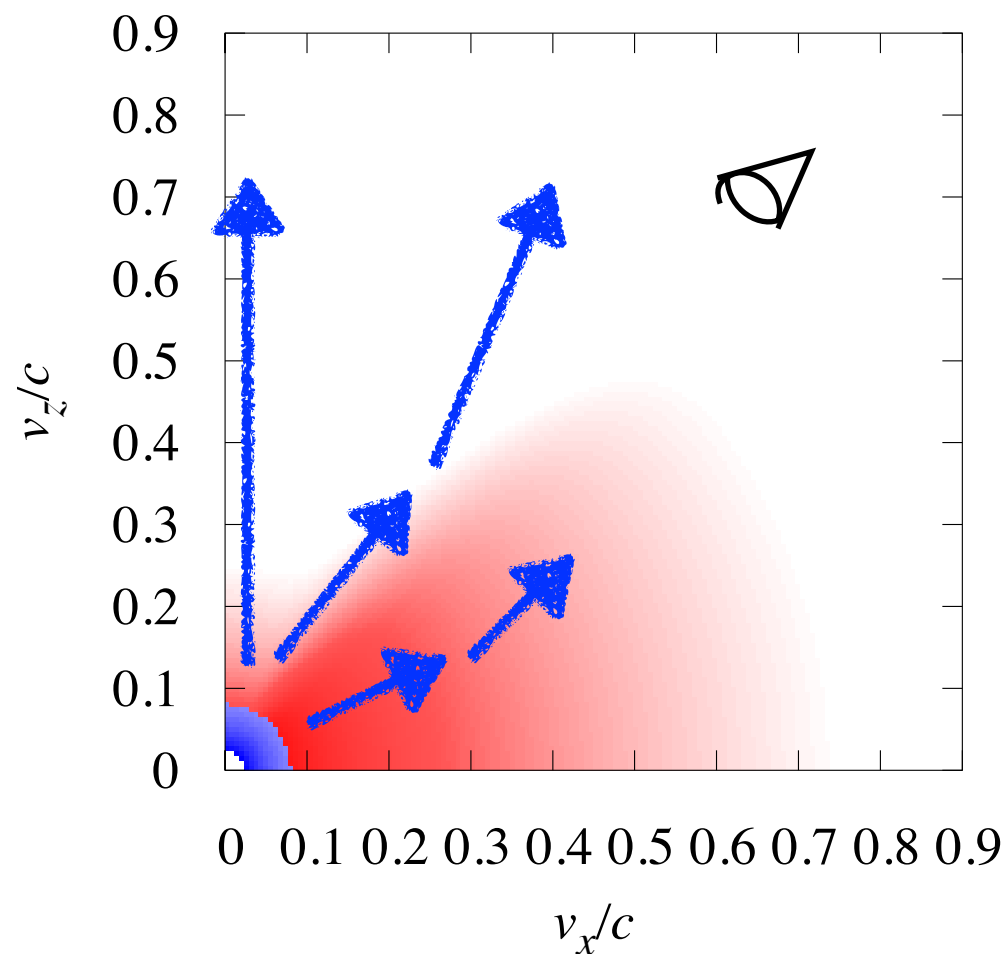
Enhancement of photospheric velocity

$$20^\circ \leq \theta < 28^\circ$$



- The reprocess of photons in the dynamical ejecta helps the photospheric velocity to be enhanced

Angular dependence of photon diffusion



- Photons diffuse preferentially to the polar direction in the presence of the optically thick dynamical ejecta in the equatorial plane, and then, luminosity is effectively enhanced in the polar direction
→ less ejecta mass is required to reproduce observed (isotropic) luminosity

Summary

- We found that the optical and NIR lightcurves as well as photospheric velocity of SSS17a are reproduced by the ejecta model which is within the prediction of NR simulations, and thus, there is no tension between the prediction of numerical-relativity simulations and the observation of SSS17a
- The interplay of the multiple non-spherical ejecta components via photons plays a key role for the kilonova/macronova lightcurves.
- Our model can be examined by the kilonova/macronova observed from different inclination (for BNS with similar total mass)

Future work

- Variations of Kilonova/macronova lightcurves should be studied:
ex) smaller total mass system, a black hole-neutron star merger
- Systematic & Quantitative study varying ejecta parameters, such as the masses and velocity of dynamical and post merger ejecta, are needed to understand the variety of kilonova/macronova lightcurves
- Combined analysis of gravitational waves and kilonova/macronova lightcurves (+other EMs)

Gravitational waves \rightarrow total mass, inclination, tidal deformability

Electromagnetic waves \rightarrow ejecta mass, Y_e (weak process) information

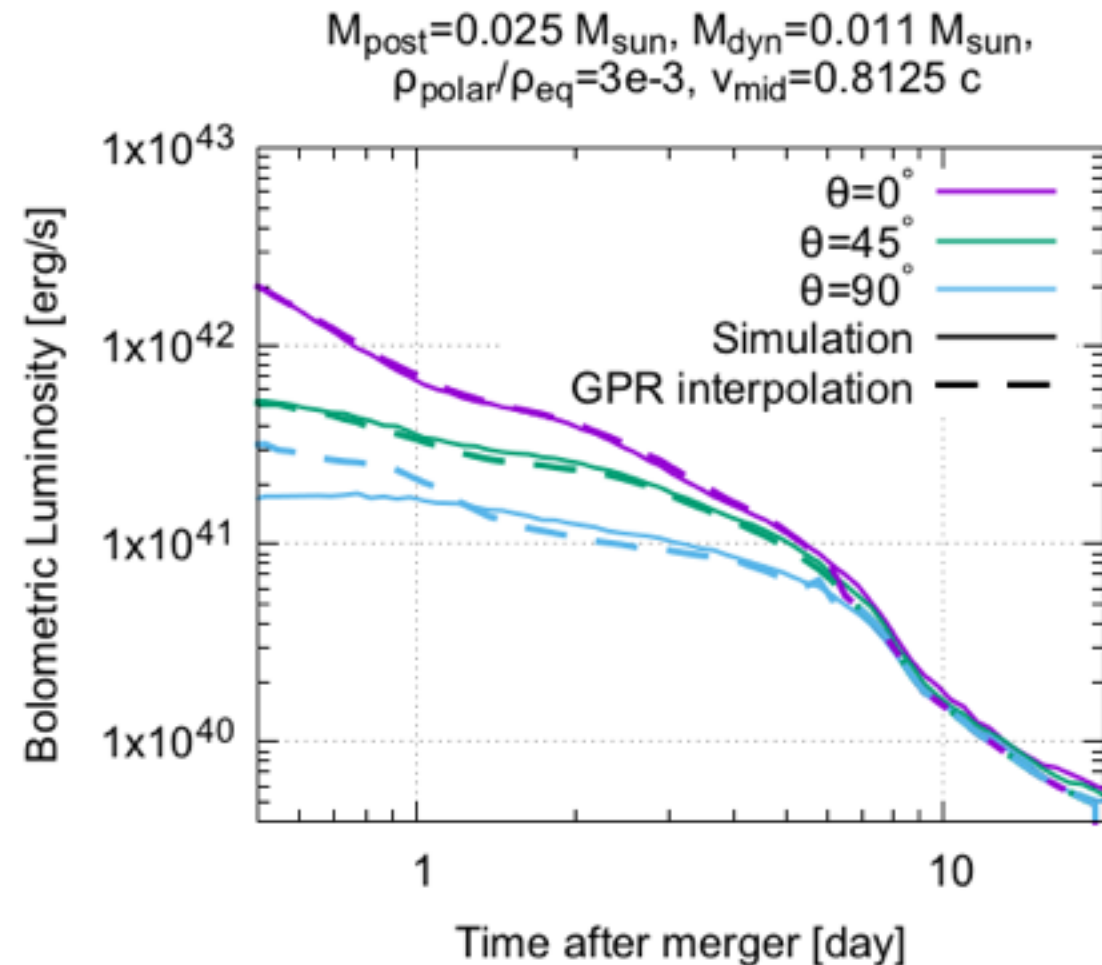
Toward rapid KN prediction: Gaussian Process Regression

RT Data sets ($3 \times 3 \times 3 = 27$ models)

$$M_{\text{post}} = 0.01, 0.03, 0.05 M_{\odot}$$

$$M_{\text{dyn,eq}} = 0.001, 0.005, 0.01 (\times 0.72) M_{\odot}$$

$$M_{\text{dyn,polar}} = 10^{-5}, 5 \times 10^{-5}, 10^{-4} (\times 0.28) M_{\odot}$$

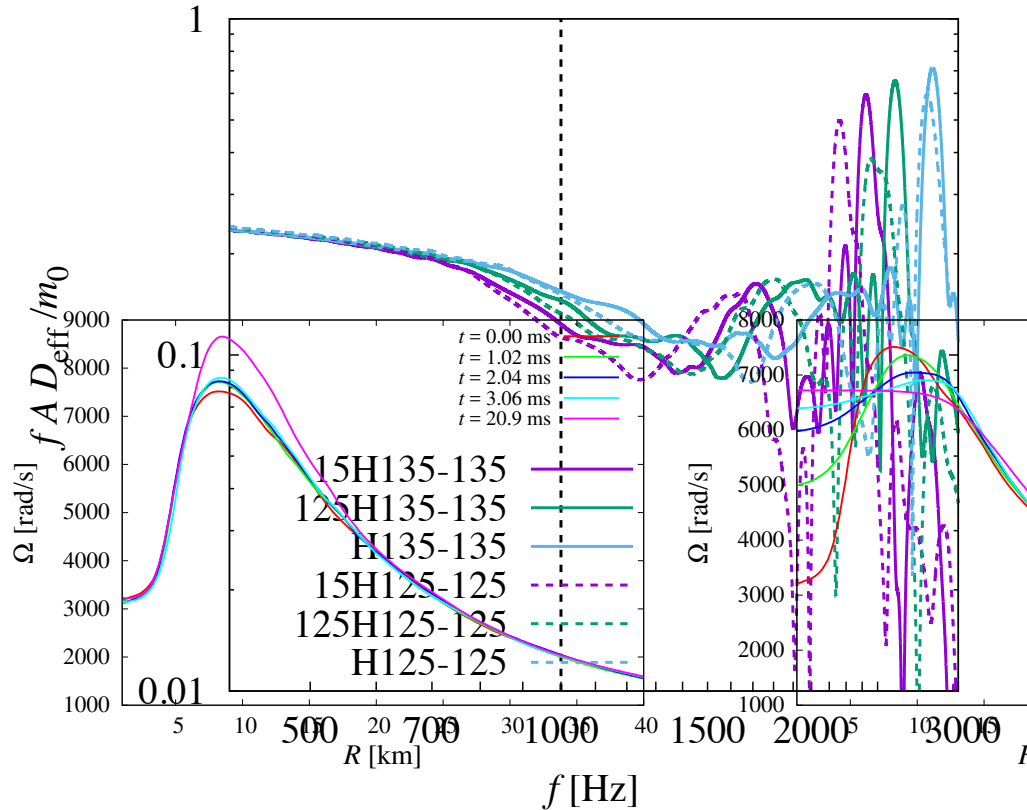


- Gaussian process regression model may be useful to interpolate the data point of RT simulations
- RT simulation ~ 1 Day /model $\rightarrow \sim 1 - 10$ Minutes/model

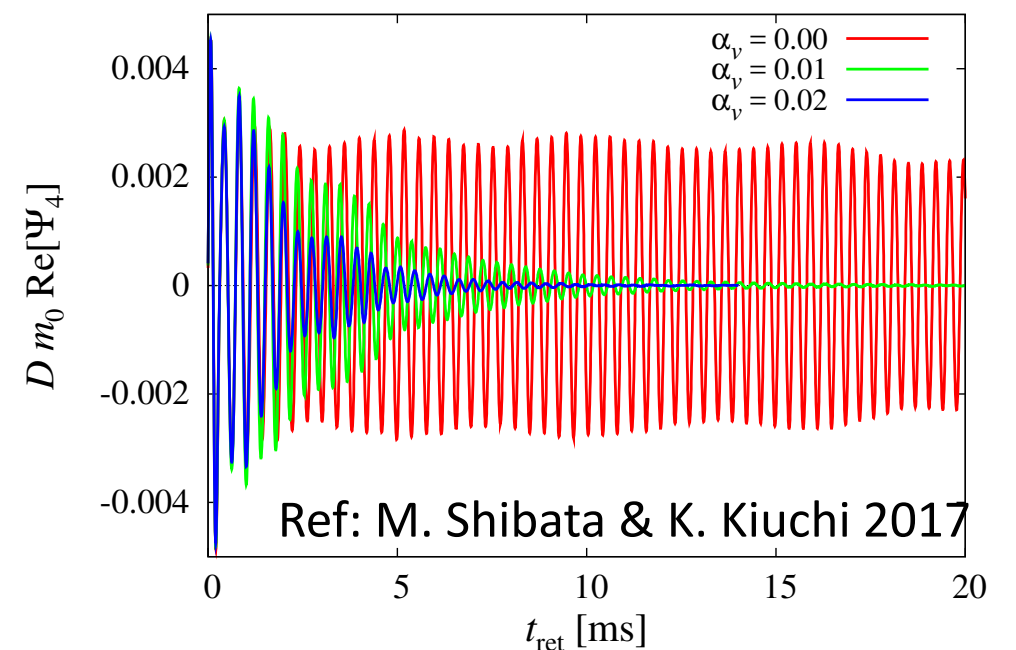
Appendix

Contamination of Post-merger waveforms

- The gravitational-wave spectra for $f > 1000$ Hz would be affected by the post-merger waveforms.
- The post-merger waveforms can be modified by detailed physical effects that are not taken into account for our current numerical-relativity simulations (e.g., M. Shibata et al. 2017)
- we restrict the frequency range of gravitational-wave modelling to 10–1000 Hz to avoid the contamination from the post-merger waveforms



Dependence of the post-merger waveforms on physical viscosity



Set up

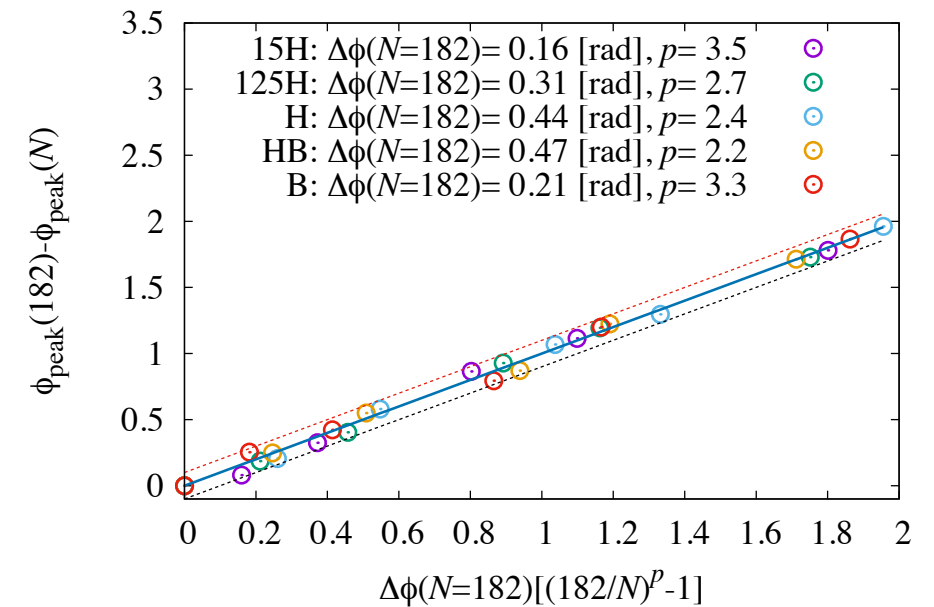
- Binary neutron stars in quasi-circular orbits are numerically derived for the initial conditions of the simulations using a spectral-method library, *LORENE* (<http://www.lorene.obspm.fr/>)
- **small orbital eccentricity $\sim 10^{-3}$** is realized by an eccentricity-reduction procedure described in Kyutoku et al. 2014
- The initial gravitational-wave frequency is ~ 400 Hz, and **~ 30 gravitational cycles (>200 rad)** are obtained before the onset of merger
- Grid resolution of the simulation is improved by **more than a factor of 2**. (With these grid spacing, the semi-major diameter of the neutron stars is covered by about ~ 260 grid points.)
- 540-650k core hours (~ 2 month for 16 core x 32 nodes) for the highest resolution models

Error and Convergence

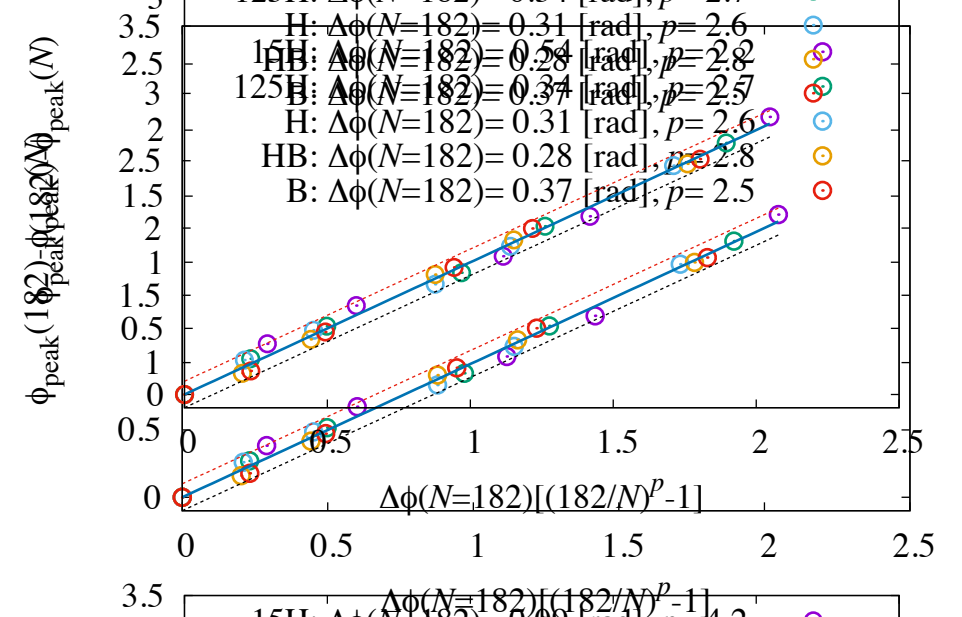
phase at the time of the peak amplitude

1.21-1.51 M_{sun}

- The phase error is dominated by that comes from the finite grid spacing
- We estimate the error of the phase at the time of the peak amplitude by data with 6 different grid-resolutions
- The nearly convergent result is likely to be achieved for all the cases, and the order of the convergence is likely to be about 2-4.
- The error of the peak phase for highest-resolution run due to the finite grid spacing is conservatively about 0.1–0.6 rad.



1.16-1.58 M_{sun}

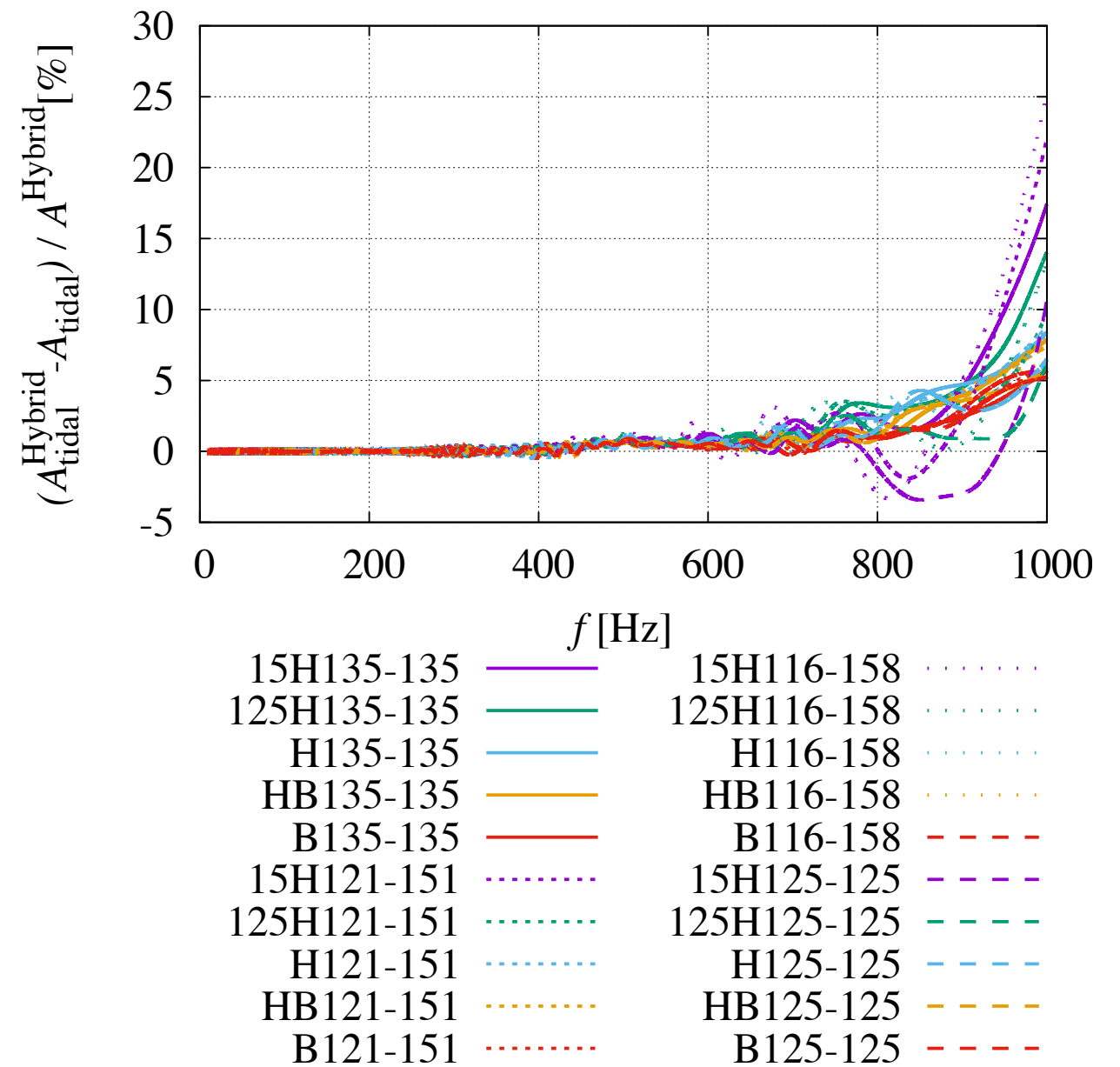


Tidal part amplitude model

- Tidal part amplitude model for the hybrid waveforms is also derived based on 1PN order tidal part formula
- The same hybrid waveform as the tidal part phase model is used for parameter determination (15H125-125)

$$A_{\text{tidal}} = \sqrt{\frac{5\pi\eta}{24} \frac{m_0^2}{D_{\text{eff}}}} \tilde{\Lambda} x^{-7/4} \times \left(-\frac{27}{16} x^5 - \frac{449}{64} x^6 - 4251 x^{7.890} \right)$$

- The relative error of the tidal-part amplitude model is always within 5 % for $f < \sim 900$ Hz, and always within 10 % for $\Lambda \leq 850$ at 1000 Hz



Frequency-domain GW model for inspiralling BNS

- We constructed a frequency-domain gravitational-waveform model for binary neutron stars by employing the tidal-part models and point-particle model
- We employ the phenom-like point-particle model derived by and calibrated to the SEOBNRv2 waveforms

$$\begin{aligned}\tilde{h}_{\text{model}} &= \tilde{h}_{\text{model}} \left(f; \mathcal{M}_c, \eta, \tilde{\Lambda}, \phi_0, t_0, D_{\text{eff}} \right) \\ &= (A_{\text{pp}} + A_{\text{tidal}}) e^{-i(\Psi_{\text{pp}} + \Psi_{\text{tidal}})}.\end{aligned}$$

$$\begin{aligned}\Psi_{\text{tidal}} &= \frac{3}{128\eta} \left[-\frac{39}{2} \tilde{\Lambda} \left(1 + 12.55 \tilde{\Lambda}^{2/3} x^{4.240} \right) \right] x^{5/2} & A_{\text{tidal}} &= \sqrt{\frac{5\pi\eta}{24} \frac{m_0^2}{D_{\text{eff}}}} \tilde{\Lambda} x^{-7/4} \\ &\times \left(1 + \frac{3115}{1248} x - \pi x^{3/2} + \frac{28024205}{3302208} x^2 - \frac{4283}{1092} \pi x^{5/2} \right) & &\times \left(-\frac{27}{16} x^5 - \frac{449}{64} x^6 - 4251 x^{7.890} \right)\end{aligned}$$

- We check the validity of our waveform model by comparing our waveform model and the hybrid waveforms supposing advanced LIGO as a fiducial detector.

Tidal part phase model

- The 2.5 PN order (equal-mass) tidal-part phase (Damour et al. 2012)

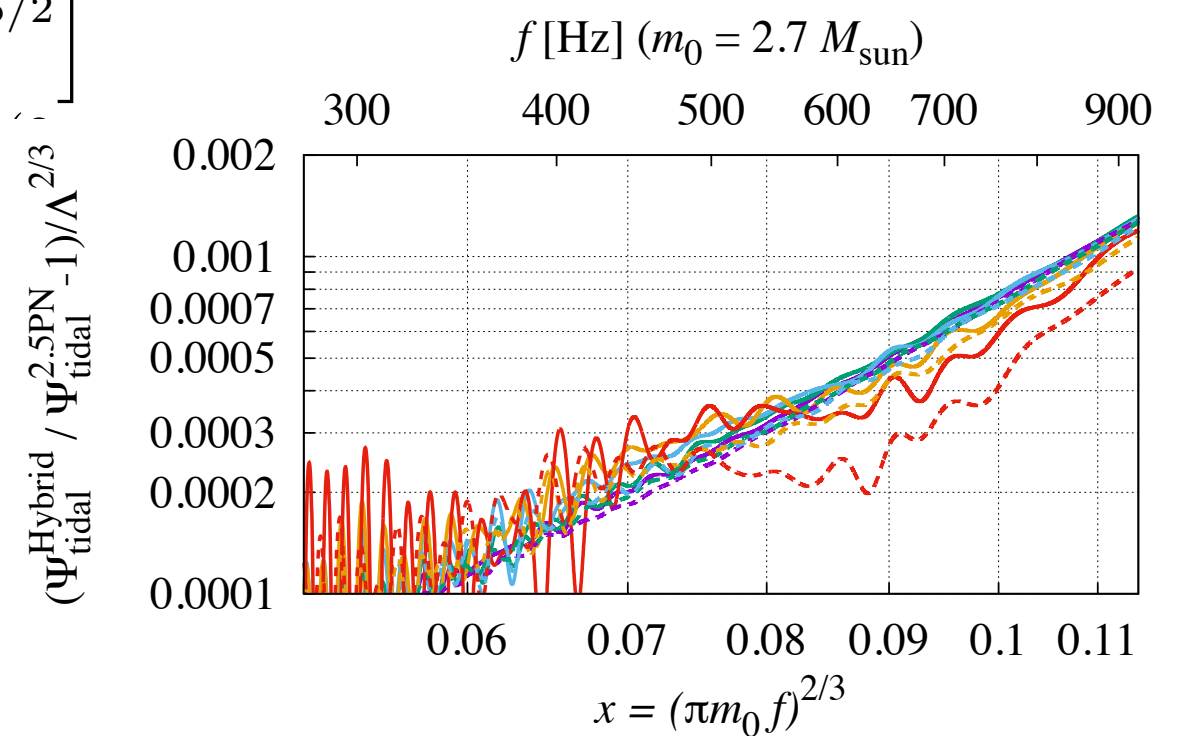
$$\Psi_{\text{tidal}}^{2.5\text{PN}} = \frac{3}{32} \left(-\frac{39}{2} \Lambda \right) x^{5/2} \times \left[1 + \frac{3115}{1248} x - \pi x^{3/2} + \frac{28024205}{3302208} x^2 - \frac{4283}{1092} \pi x^{5/2} \right]$$

The relative deviation of the tidal-part phase

$$\frac{\Psi_{\text{tidal}}^{\text{Hybrid}} - \Psi_{\text{tidal}}^{2.5\text{PN}}}{\Psi_{\text{tidal}}^{2.5\text{PN}}}$$

- We find that the relative deviation can be well approximated by a power law in the PN parameter, x
- Furthermore, we find that the relative deviation is approximately proportional to $\Lambda^{2/3}$

$$\Psi_{\text{tidal}}^{\text{em}} = \frac{3}{32} \left[-\frac{39}{2} \Lambda \left(1 + a \Lambda^{2/3} x^p \right) \right] x^{5/2} \times \left[1 + \frac{3115}{1248} x - \pi x^{3/2} + \frac{28024205}{3302208} x^2 - \frac{4283}{1092} \pi x^{5/2} \right]$$



15H135-135	—	15H125-125	- - -
125H135-135	—	125H125-125	- - -
H135-135	—	H125-125	- - -
HB135-135	—	HB125-125	- - -
B135-135	—	B125-125	- - -

$m_0 = m_1 + m_2$: total mass of binary

$x := (\pi m_0 f)^{2/3}$: PN parameter

Mismatch (2.5 PN tidal)

2.5 PNtidal: same as our model
but with 2.5 PN tidal phase formula
(and 1PN tidal amplitude formula)

$$\Psi_{\text{tidal}}^{2.5\text{PN}'} = \frac{3}{128\eta} \left(-\frac{39}{2}\tilde{\Lambda} \right) x^{5/2} \\ \times \left[1 + \frac{3115}{1248}x - \pi x^{3/2} + \frac{28024205}{3302208}x^2 - \frac{4283}{1092}\pi x^{5/2} \right]$$

$$A_{\text{tidal}}^{1\text{PN}'} = \sqrt{\frac{5\pi\eta}{24}} \frac{m_0^2}{D_{\text{eff}}} \tilde{\Lambda} x^{-7/4} \left(-\frac{27}{16}x^5 - \frac{449}{64}x^6 \right)$$

Ref. Vines et al. 2011, Damour et al. 2012,
Hotokezaka et al. 2016

Model	$\tilde{\Lambda}$	our waveform model	2.5PNtidal
15H135-135	1211	4.1×10^{-6}	1.4×10^{-3}
125H135-135	863	4.0×10^{-6}	5.6×10^{-4}
H135-135	607	2.9×10^{-6}	1.8×10^{-4}
HB135-135	422	2.6×10^{-6}	5.0×10^{-5}
B135-135	289	2.0×10^{-6}	1.3×10^{-5}
15H121-151	1198	6.3×10^{-6}	1.6×10^{-3}
125H121-151	856	2.5×10^{-6}	5.7×10^{-4}
H121-151	604	2.8×10^{-6}	1.8×10^{-4}
HB121-151	422	3.0×10^{-6}	5.2×10^{-5}
B121-151	290	3.1×10^{-6}	1.1×10^{-5}
15H116-158	1185	1.1×10^{-5}	1.7×10^{-3}
125H116-158	848	3.8×10^{-6}	6.3×10^{-4}
H116-158	601	3.0×10^{-6}	1.9×10^{-4}
HB116-158	421	4.0×10^{-6}	5.1×10^{-5}
B116-158	291	5.0×10^{-6}	1.0×10^{-5}
15H125-125	1875	1.6×10^{-6}	2.5×10^{-3}
125H125-125	1352	1.6×10^{-6}	1.1×10^{-3}
H125-125	966	3.5×10^{-6}	3.7×10^{-4}
HB125-125	683	5.0×10^{-6}	1.0×10^{-4}
B125-125	476	8.3×10^{-6}	1.8×10^{-5}

- Large values of mismatch ($10^{-3} - 10^{-4}$) between the 2.5 PN tidal waveforms

Systematic error (2.5 PN tidal)

- We found that Λ can be overestimated by the order of 100 for $\Lambda \sim 600$ when employing PN tidal formulas (assuming the hybrid waveforms are the realistic signal)
- In the absence of the non-linear enhancement of Λ , spuriously larger values of Λ are needed for 2.5PN tidal formula to complement the enhancement of tidal effects.

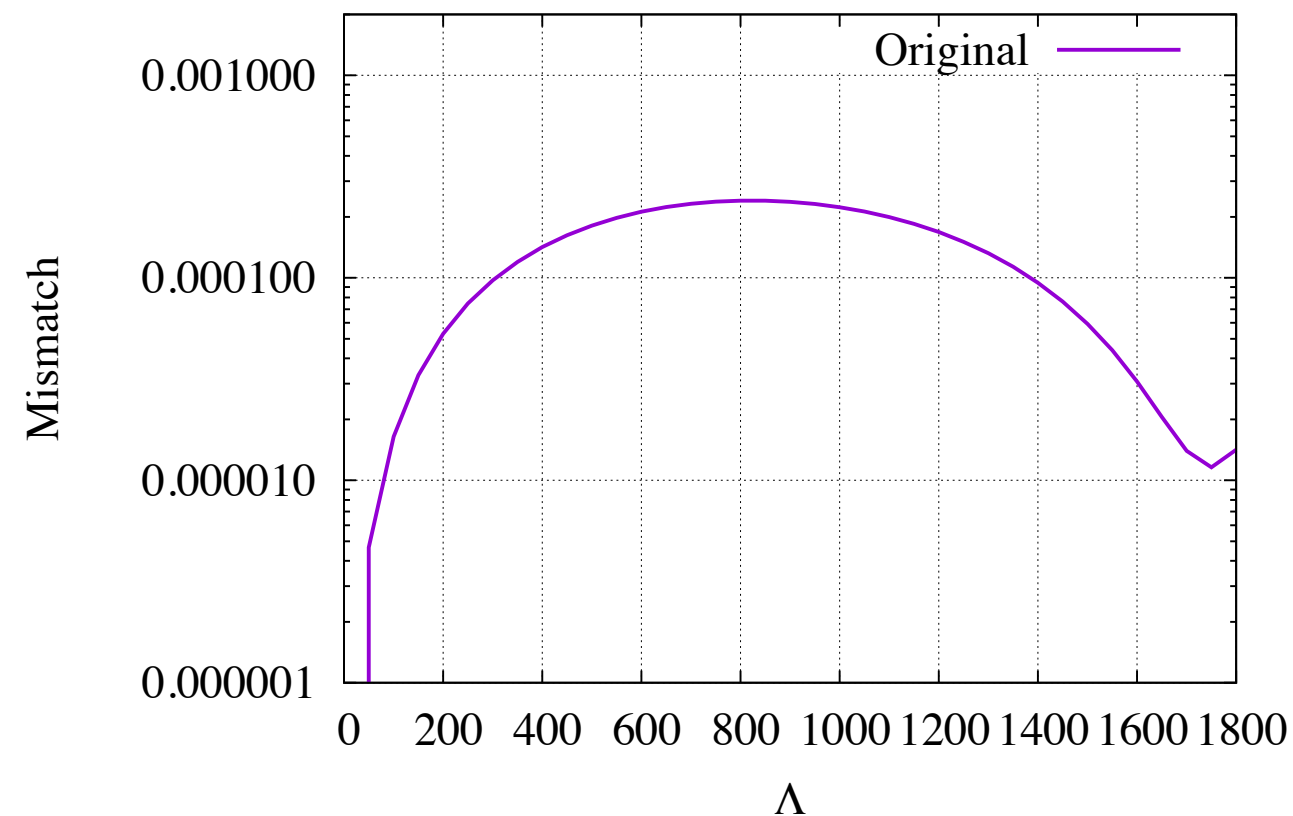
Model	$\tilde{\Lambda}$	2.5PNtidal		
		$\Delta\mathcal{M}_c [M_\odot]$	$\Delta\eta$	$\Delta\tilde{\Lambda}$
15H135-135	1211	3.8×10^{-6}	3.1×10^{-4}	250
125H135-135	863	3.1×10^{-6}	2.5×10^{-4}	177
H135-135	607	2.0×10^{-6}	1.6×10^{-4}	105
HB135-135	422	1.4×10^{-6}	1.0×10^{-4}	59
B135-135	289	7.8×10^{-7}	5.5×10^{-5}	28.9
15H121-151	1198	3.9×10^{-6}	3.1×10^{-4}	245
125H121-151	856	3.2×10^{-6}	2.5×10^{-4}	175
H121-151	604	2.1×10^{-6}	1.6×10^{-4}	105
HB121-151	422	1.4×10^{-6}	1.0×10^{-4}	59
B121-151	290	8.0×10^{-7}	5.5×10^{-5}	27
15H116-158	1185	4.0×10^{-6}	3.2×10^{-4}	243
125H116-158	848	3.4×10^{-6}	2.6×10^{-4}	176
H116-158	601	2.2×10^{-6}	1.6×10^{-4}	105
HB116-158	421	1.5×10^{-6}	1.0×10^{-4}	58
B116-158	291	7.7×10^{-7}	5.2×10^{-5}	24
15H125-125	1875	2.5×10^{-6}	2.6×10^{-4}	296
125H125-125	1352	3.2×10^{-6}	3.0×10^{-4}	265
H125-125	966	2.2×10^{-6}	2.0×10^{-4}	168
HB125-125	683	1.4×10^{-6}	1.2×10^{-4}	93
B125-125	476	7.8×10^{-7}	6.2×10^{-5}	39

Comparison with Dietrich et al. 2017

- A BNS GW model is also derived in Dietrich et al. 2017 based on NR waveforms
- Different NS waveforms and the TidalEOB waveforms used for the model calibration
- The waveform model is derived in the time domain, and then, is transformed to a frequency-domain waveform model employing the stationary-phase approximation
- While their model and our model agrees quite well, some difference is found for a large value of Λ due to the difference that the non-linear tidal correction

Comparison with Dietrich+17

$$f_{\min} = 10 \text{ Hz}, f_{\max} = 1000 \text{ Hz}, \\ m_1 = m_2 = 1.35 M_{\text{sun}}$$



$$\Psi_T^{\text{NRP}} = -\kappa_2^T \frac{\tilde{c}_{\text{Newt}}}{X_A X_B} x^{5/2} \times \\ \frac{1 + \tilde{n}_1 x + \tilde{n}_{3/2} x^{3/2} + \tilde{n}_2 x^2 + \tilde{n}_{5/2} x^{5/2}}{1 + \tilde{d}_1 x + \tilde{d}_{3/2} x^{3/2}}$$

Ref: Dietrich et al. 2017

Radiative transfer simulation

- We employ a wavelength-dependent radiative transfer simulation code (M. Tanaka et al. 2013, 2014, 2017)
- The density, velocity, and Ye profiles of ejecta are employed within the range of predictions by numerical-relativity simulations. (e.g., Dietrich et al. 2016, Hotokezaka et al. 2018, Metzger&Fernandez et al. 2014, Fujibayashi et al. 2018)
- The abundance pattern and nuclear heating rate are given based on r-process nucleosynthesis calculations by (Wanajo et al. 2014)
- Realistic opacity table constructed by the atomic structure calculations (Se, Ru, Te, Nd, and Er)

improved points

- The grid resolution of the simulation is also improved by an order of magnitude from our previous works by imposing axisymmetry.
- special-relativistic effects on photon transfer are fully taken into account

R-process nucleosynthesis

Credit) Sho Fujibayashi:

